T.C.
DOKUZ EYLUL UNIVERSITY
IZMIR INTERNATIONAL
BIOMEDICINE AND GENOME INSTITUTE

GENERATION OF CRISPR/CAS9-BASED DISEASE MODELS AND INVESTIGATION OF THE MOLECULAR MECHANISMS OF REGENERATION IN ZEBRAFISH

Ramazan Uğur Bora

MOLECULAR BIOLOGY AND GENETICS

PhD Dissertation

Thesis Code: DEU.IBG.PhD-2018850027

İZMİR-2024

T.C.
DOKUZ EYLUL UNIVERSITY
IZMIR INTERNATIONAL
BIOMEDICINE AND GENOME INSTITUTE

GENERATION OF CRISPR/CAS9-BASED DISEASE MODELS AND INVESTIGATION OF THE MOLECULAR MECHANISMS OF REGENERATION IN ZEBRAFISH

MOLECULAR BIOLOGY AND GENETICS

Ph.D. Dissertation

Ramazan Uğur Bora

Supervisor: Prof. Dr. Güneş Özhan

(This thesis is supported by TUBITAK BIDEB 2211-C National PhD Scholarship Program in the Priority Fields in Science and Technology program and Council of Higher Education (CoHE) of Turkey 100/2000 Doctoral Scholarship in Gene and Genome Research)

Thesis Code: DEU.IBG.PhD-2018850027

T.C.
DOKUZ EYLÜL ÜNİVERSİTESİ

İZMİR ULUSLARARASI BİYOTIP VE GENOM ENSTİTÜSÜ

DOKTORA TEZ SAVUNMA SINAVI TUTANAĞI

Dokuz Eylül Üniversitesi İzmir Uluslararası Biyotıp ve Genom Enstitüsü Genom Bilimleri ve Moleküler Biyoteknoloji Anabilim Dalı Moleküler Biyoloji ve Genetik Doktora Programı 2018850027 numaralı öğrencisi Ramazan Uğur Bora, "Generation of CRISPR/Cas9-based disease models and investigation of the molecular mechanisms of regeneration in zebrafish" konulu Doktora tezini 10.07.2024 tarihinde yapılan savunma sınavı sonucunda başarılı / ~~başarısız~~ olmuştur.

BAŞK
Prof. Dr. Güneş ÖZHAN

JÜRİ ÜYES
Prof. Dr. Pınar

JÜRİ ÜYESİ
Dr. Öğr. Üyesi Yavuz Oktay

JÜRİ ÜYESİ
Prof. Dr. Volkan Seyrantepe

JÜRİ ÜYESİ
Dr. Öğr. Üyesi Ayşe Banu Demir

ACKNOWLEDGEMENT

First and foremost, I would like to express my deepest gratitude to my supervisor Prof. Dr. Güneş Özhan for guiding me in this journey. Walking together in this road with ups and downs, she always supported me with her intelligence, enthusiasm and dedication. I am grateful to her to giving me opportunity to become a part of the Ozhan lab.

I would like to thank our past and present lab members for their support, sharing everyday together with a cup coffee, undertaking struggles together has been a pleasure.

I would like to thank my committee members Prof. Dr. Pınar Akan, Asst. Prof. Yavuz Oktay, Asst. Prof. Ayşe Banu Demir and Prof. Dr. Volkan Seyrantepe for their valuable time.

I would like to thank my dearest friends, Aykut Kuruoğlu, Onur Önder, Yavuz Mercan, Ekin Azbazdar, Burcu Ekinci-Görgün, Tutku Yaraş, Başar Koç and Enrico Mingardo for their support and friendship. A special thanks to Burcu Açıkgöz for always being there for me, supporting me endlessly and overcoming every challenge together. One more thanks to my lovely cat, Felis for endless purrs.

I wish to thank Federation of European Biochemical Society (FEBS) for their fellowship grant, providing me opportunity extend my research on international level.

I would like to express my deepest gratitude my mother Melek Bora, my father Hasan Bora and my brother Ufuk Bora for always supporting me in every way possible and their unconditional love.

Lastly, I would like to thank The Council of Higher Education (CoHE) (YÖK 100/2000) and the Scientific and Technological Research Council of Turkey (TUBITAK)-BIDEB 2211-C National PhD Scholarship Program providing financial support for my doctoral research.

TABLE OF CONTENTS

Figure Index

Table Index

ABBREVIATIONS

Alzheimer's Disease : AD

Amyotrophic Lateral Sclerosis: ALS

Cancer Stem Cells: CSS

Cerebroventricular Microinjection: CVMI

Clustered Regularly Interspaced Short Palindromic Repeats: CRISPR

Complementary DNA: cDNA

Days post injection: DPI

Genome-wide association studies: GWAS

Glial Fibrillary Acidic Protein: GFAP

Green Fluorescent Protein: GFP

Left Ventricular Noncompaction: LVNC

Lysophosphatidylcholine : LPC

Multiple Sclerosis: MS

Myelin Basic Protein: MBP

Myelin Protein Zero: MPZ

Neurodegenerative Disease :ND

Next-generation sequencing: NGS

Oligodendrocyte Lineage: OL

Parkinson’s Disease: PD

Peripheral Nervous System: PNS

Ribonucleoprotein: RNP

Single nucleotide polymorphisms: SNPs

Single-guide RNA: sgRNA

Spinal Cord Injury: SCI

Whole genome sequencing: WGS

Whole-mount *in-situ* hybridization: WMISH

GENERATION OF CRISPR/CAS9-BASED DISEASE MODELS AND INVESTIGATION OF THE MOLECULAR MECHANISMS OF REGENERATION IN ZEBRAFISH

R. Uğur Bora, Izmir International Biomedicine and Genome Institute

ABSTRACT

Human diseases, especially nervous system disorders or damage affects millions of people. Central nervous system regeneration has limited capacity in mammals. However, zebrafish has extensive tissue regeneration capabilities. Comparison of the regenerative and non-regenerative organisms on molecular level may help discoveries of potential therapeutic approaches. Zebrafish emerges as pivotal model organism due to its significant functional and sequential homology with mammals, extensive regenerative abilities, accessibility of diverse transgenic lines, and various manipulation tools. This study introduces three distinct approaches for human disease modeling.

Firstly, an adult zebrafish brain demyelination model was developed to investigate remyelination mechanisms. For this purpose, we generated LPC-induced adult zebrafish brain demyelination model. Furthermore, we aimed to Wnt signaling pathway's role in the remyelination. Inhibition of Wnt signaling resulted altered remyelination. Proteomic analysis revealed lack of Wnt signaling causes increased immune response and altered lipid metabolism.

Secondly, we explored parallels between cancer and regeneration mechanisms in early stages, hypothesizing that insights into these processes could unveil novel therapeutic avenues. For this reason, we used genetic glioma model of the zebrafish and applied RNA-sequencing to investigate differentially expressed genes.

Thirdly, we used CRISPR/Cas9 genome editing to investigate identified novel missense mutation on the myh7 gene causing left ventricular non-compaction. Myh7 mutant fish showed disorganized s-loop formation causing altered heart development and altered cardiac related gene expression These approaches collectively aim to deepen our understanding from molecular mechanisms to organism-level effects, contributing to the disease research and therapeutic innovation.

Keywords: zebrafish, human diseases, myelination, oligodendrocytes, proteomic, glioma, CRISPR/Cas9, Wnt signaling

CRISPR/CAS9 TABANLI HASTALIK MODELLERİNİN ÜRETİLMESİ VE ZEBRA BALIKLARINDA REJENERASYONUN MOLEKÜLER MEKANİZMALARININ ARAŞTIRILMASI

R. Uğur Bora, İzmir Uluslararası Biyotıp ve Genom Enstitisü

ÖZET

İnsan hastalıkları, özellikle sinir sistemi bozuklukları veya hasarları milyonlarca insanı etkilemektedir. Memelilerde merkezi sinir sistemi rejenerasyonunun kapasitesi sınırlıdır. Ancak zebra balığının kapsamlı doku yenileme yetenekleri vardır. Rejeneratif ve rejeneratif olmayan organizmaların moleküler düzeyde karşılaştırılması potansiyel terapötik yaklaşımların keşfedilmesine yardımcı olabilir. Zebra balığı, memelilerle, yüksek oranda fonksiyonel ve gen dizisi homolojisine, kapsamlı rejeneratif yeteneklere, çeşitli transgenik hatlara ve çeşitli manipülasyon araçlarının mevcut olması nedeniyle önemli bir model organizma olarak ortaya çıkmaktadır. Bu çalışma, insan hastalıklarının modellenmesi için üç farklı yaklaşım sunmaktadır.

İlk olarak, remiyelinizasyon mekanizmalarını araştırmak için yetişkin bir zebra balığı beyin demiyelinizasyon modeli geliştirdik. Bu amaçla LPC kullanarak yetişkin zebra balığı beyninde demiyelinizasyon modelini oluşturduk. Ayrıca Wnt sinyal yolağının remiyelinizasyondaki rolü araştırmayı hedefledik. Wnt sinyalinin baskılanması, remiyelinizasyonun bozulmasına neden oldu. Proteomik analizlerimiz sonucunda, Wnt sinyallemesinin eksikliğinin, immün yanıtın artmasına ve lipid metabolizmasının bozulmasına neden olduğunu ortaya çıkardı.

İkinci olarak, erken aşamalarda benzerlik gösteren doku yenilenmesi ve kanser ilişkisinin ileri safhalarda farklılaşmasından dolayı bu iki olay arasındaki moleküler benzerlik ve farklılıkları araştırmayı hedefledik. Bu nedenle zebra balığının genetik glioma modeli kullanarak, RNA dizileme yöntemiyle diferansiyel olarak eksprese edilen genleri araştırdık.

Üçüncü olarak, sol ventriküler nonkompaksiyona neden olan, *myh7* geninde tanımlanmış, yanlış anlamlı mutasyonun etkilerini araştırmak için CRISPR/Cas9 genom düzenleme tekniğini kullandık. *Myh7* mutant balıklarda, s-döngü oluşumunda bozulma sonucu, kalp gelişimi bozukluklarına ve kalple ilgili gen ifadelerinin değişimini saptatık. Bu çalışma ile bütüncül olarak, hastalıkların moleküler mekanizmalardan organizma düzeyindeki etkilere kadar anlayışımızı derinleştirmeyi, insan hastalık araştırmalarının ve yeni terapötik yaklaşımlara katkıda bulunmayı amaçlamaktadır.

Anahtar Kelimeler: zebra balığı, insan hastalıkları, miyelinizasyon, oligodendrositler, proteomik, glioma, CRISPR/Cas9, Wnt sinyal yolağı

1 INTRODUCTION AND AIM

Human diseases, particularly neurodegenerative conditions and damage to the nervous system, impose significant burden to societies. Therefore, understanding disease mechanisms and devising therapeutic approaches centred on tissue regeneration is crucial. The comparative analysis of mammals and animals exhibiting superior regenerative capacities such as zebrafish serves as a functional approach to uncover similarities and distinctions, thereby facilitating the development of novel treatment modalities. Zebrafish has emerged as a significant model organism due to its substantial functional and sequential homology with mammals, extensive regenerative capabilities, the accessibility of numerous transgenic lines, and the availability of various manipulation tools. Consequently, it facilitates the development and investigation of human disease models through diverse approaches.

In the present study, three distinct approaches were developed to probe human disease modelling,

i) Adult zebrafish brain demyelination model to investigate remyelination mechanisms. Myelination plays important role in brain homeostasis and associated with neurodegenerative diseases. In Multiple Sclerosis, Leukodystrophy, Huntington's disease, myelination directly affected. Moreover, neurodevelopmental and psychiatric disorders highlight disrupted myelination. However, demyelination/remyelination studies often underlines immune reactions rather than remyelination. To study remyelination, damage induction method should be reversable. Therefore, we utilized LPC-based demyelination model in adult zebrafish telencephalon. Furthermore, we investigated role of the Wnt signaling pathway, a controversial mechanism in remyelination.

ii) Cancer and regeneration show similar mechanisms in early states, however, while regeneration mechanisms terminate proliferation in tightly controlled manner, in cancer aberrant proliferation occurs and creates its own microenvironment. Thus, we hypothesize that investigating early and late mechanisms of cancer and tissue regeneration would lead to novel cues for therapeutic approaches. Our laboratory, previously published investigating brain regeneration in different time points on molecular level. In this study, we utilized transgenic glioma model and applied bulk RNA sequencing.

iii) Advancing gene and genome sequencing technologies yields identification of many mutations and associates genes and diseases. To better understand functions of variants, we are in need of *in-vivo* models to investigate its effect molecular to organism level. In the study, a novel missense mutation determined on *myh7* gene, causing left ventricular non-compaction. To study of the effects of the identified mutation, we exploited CRISPR/Cas9 genome editing on zebrafish.

2 LITERATURE REVIEW

2.1 Neurodegenerative Diseases

Neurodegenerative diseases (NDs) are characterized by neural cell disfunction, axonal damage, demyelination and ultimately neuronal loss caused by abnormal protein accumulation, genetic or environmental factors, autoimmune response. Consequently, loss or distortion of coordinated movement, cognitive abilities, other neurological and psychological impairments become distinctive features, eventually leads to death (Martin, 1999; Wilson et al., 2023). Alzheimer's Disease (AD), Parkinson's Disease (PD), Amyotrophic Lateral Sclerosis (ALS), Multiple Sclerosis (MS) and brain cancer can be categorized as chronic diseases since defects and cellular death occur over prolonged period. Due to progressive nature of chronic degenerative diseases, clinical onset usually occurs in the late adulthood. Furthermore, chronic state of degeneration causes widespread effects. Chronic degeneration frequently but not exclusively affects, cortex and hippocampus in AD, Substantia Nigra in PD, basal ganglia, brain stem and myelin rich areas in MS, and subcortical areas depending on the subtype of the glioma (Figure 1) (Matilla-Dueñas et al., 2017). On the other hand, Spinal Cord Injury (SCI) and Ischemia categorized as acute degeneration, often restricted to limited area and time. (Hussain et al., 2018; Mirahmadi et al., 2016).

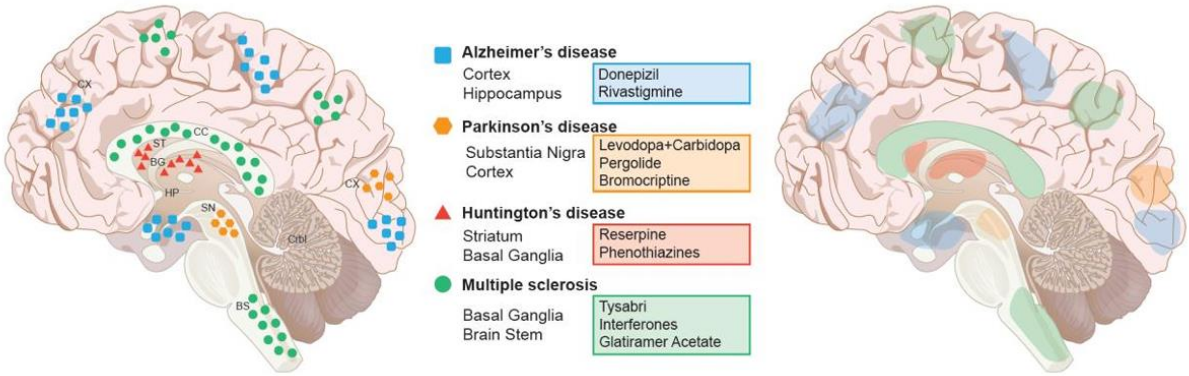

Figure 1: Neurodegenerative diseases and effected regions (Hussain et al., 2018).

Genetic elements play pivotal role neurodegenerative diseases. The majority of these conditions root from genetic pathological mutations, in some cases, exposure to mutagens or substances during pregnancy or in early in life. More than 50% of the 7000 rare monogenic diseases have been identified in the last 30 years. (Matilla-Dueñas et al., 2017). Collectively, protein misfolding and aggregation, extreme accumulation of reactive oxygen species, aberrant inflammation in nervous system are the main cellular events causing neurodegenerative disorders. However, there are still handful treatments available and better understanding of etiology needs to be addressed.

2.2 Chapter 1: Oligodendrocytes and Myelination

In vertebrates, subclass of glia, **oligodendrocytes (OL)**, are the cells responsible for myelination in the central nervous system, play a crucial role in facilitating rapid action potential conduction and providing vital trophic support for CNS homeostasis. OLs differentiate from oligodendrocyte progenitor cells (OPCs) which widely distributed throughout the adult brain, serving as a permanent cellular reservoir for replacing oligodendrocytes and remyelination (Ettle et al., 2016). In developmental stages, subventricular stem cells form committed OPCs which divide and migrate through brain and spinal cord. In mammals, oligodendrocyte development occurs in three waves. First wave OPCs arise from ventral regions of neural tube, however, these cells mostly replaced by dorsal derived OPC at later stages (Emery, 2010). OPC development is tightly regulated multistep process. Following specification from multipotent stem cells, OPCs migrate through their destination and either stays dormant until needed or starts maturation program, contact axonal cues and become myelinating oligodendrocytes (Cristobal & Lee, 2022). Moreover, OPCs have shown presenting distinct populations, one having higher degrees of calcium signaling and forming networks, however, rarely differentiates. While other subgroup more active in proliferation but less active in calcium dependent signaling (Marisca et al., 2020).

Oligodendrocyte differentiation and maturation stages can be defined as **1)** Oligodendrocyte precursor cells **2)** Pre-myelinating oligodendrocytes **3)** Myelinating oligodendrocytes (Figure 2). Multiple molecular mechanisms involved between interplay of OL fate changes (Masson & Nait-Oumesmar, 2023). Olig1/2 are major transcription factors involved in OL fate. Motor neurons and oligodendrocytes share same ascendent stem cells and Olig2 and Sox10 transcription factors controls precursor fate switch at the stages of lineage specification. Further differentiation into pre-

myelinating oligodendrocytes, the transcriptional regulation of cellular fate change is managed through a balance of different factors. While, Sox9, Hes5, Tcf7l2, Gpr17 enhances proliferation and suppress differentiation, Myrf, Zfp488, Nkx2.2, Zeb2 promotes differentiation and maturation (Cristobal & Lee, 2022).

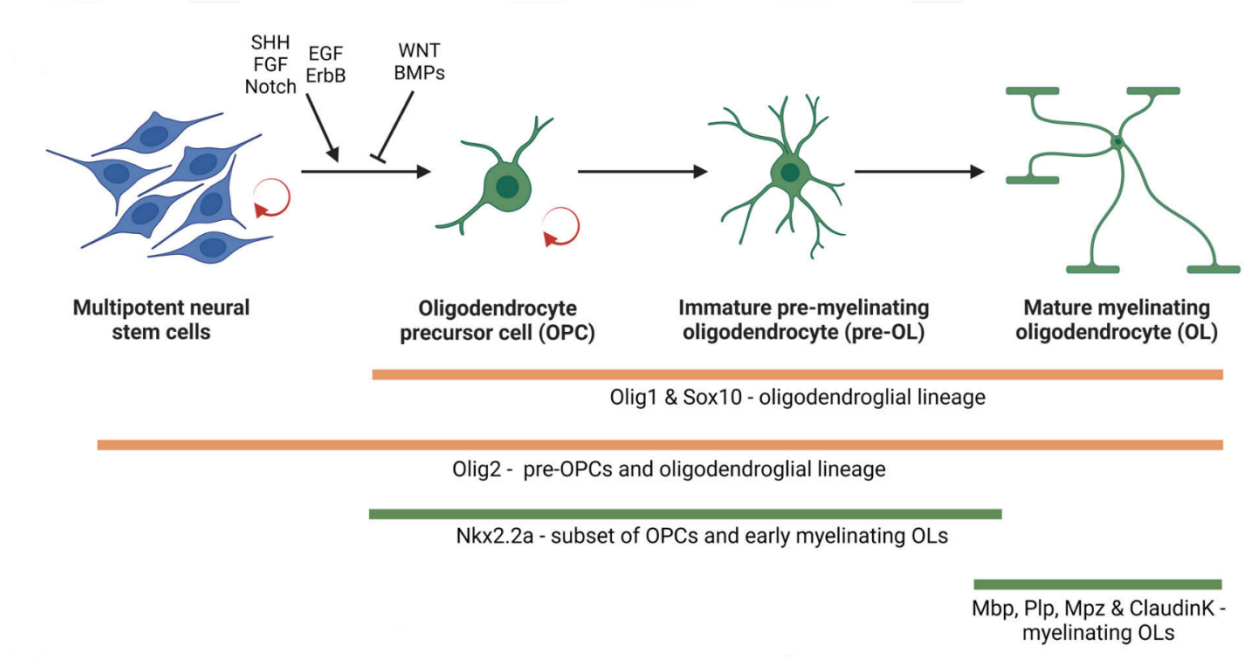

Figure 2: Developmental stages of oligodendrocyte lineage cells and stage specific markers (Masson & Nait-Oumesmar, 2023)

Moreover, oligodendrocyte development governed by interaction of several signaling pathways such as Wnt, BMP, Shh, Notch. However, pathways show opposing actions depending on the stage, environmental signals or presence of damage/disease. Thus, timing and proper interaction of gene expression programs crucial for oligodendrocyte development and myelination (Elbaz & Popko, 2019).

Myelin structure (myelin sheat) is the extension of the membrane of mature oligodendrocytes wrapped around the axons, first named by Virchow (Virchow, 1854). Three important functions have been described for myelin (Zalc, 2016):

- Protection of the axons
- Acceleration of nerve influx
- Trophic and structural support

Disruption in myelin structure, causes impaired nerve conduction, failure in support of neurons and other glia, axonal degeneration and eventually, neuronal death. Oligodendrocyte lineage cells functions is not limited to myelination. It has been shown that OPCs and neurons form active synapses, furthermore, take a significant roles in various neural processes such as phagocytosis, immune reaction and axonal remodeling (Bergles & Richardson, 2016; Xiao et al., 2022; Xiao & Czopka, 2023). On the other hand, intrinsic and extrinsic pathways are activated upon insult to the brain, therefore OPCs contribute to regenerative mechanisms (Sanchez-Gonzalez et al., 2022). Overall, OPCs and Oligodendrocytes not only orchestrates myelination, also plays crucial role in brain homeostasis and response to the injuries.

“Demyelination” and **“Dismyelination”** represent two important aspects of myelinopathy. Demyelination means loss or damage to the myelin structure, which often caused by autoimmune reactions, infections or toxic exposure. Dismyelination can be described by abnormalities of the formation or maintenance of myelin structure, usually due to genetic mutations in myelin-related genes. (Duncan et al., 2015; Powezka et al., 2020).

Multiple Sclerosis (MS), CNS injuries including stroke or trauma, leukodystrophy, neuropsychiatric diseases including autism and schizophrenia have been associated with demyelination (Gorter & Baron, 2022). Remyelination process consist of three major steps (i) activation and proliferation of OPCs, (ii) migration to the lesion site (iii) differentiation to the mature oligodendrocytes (Franklin et al., 2021). OPCs are the largest proliferative cell population in the adult CNS, however, they have slow division rates and not actively proliferating cells.

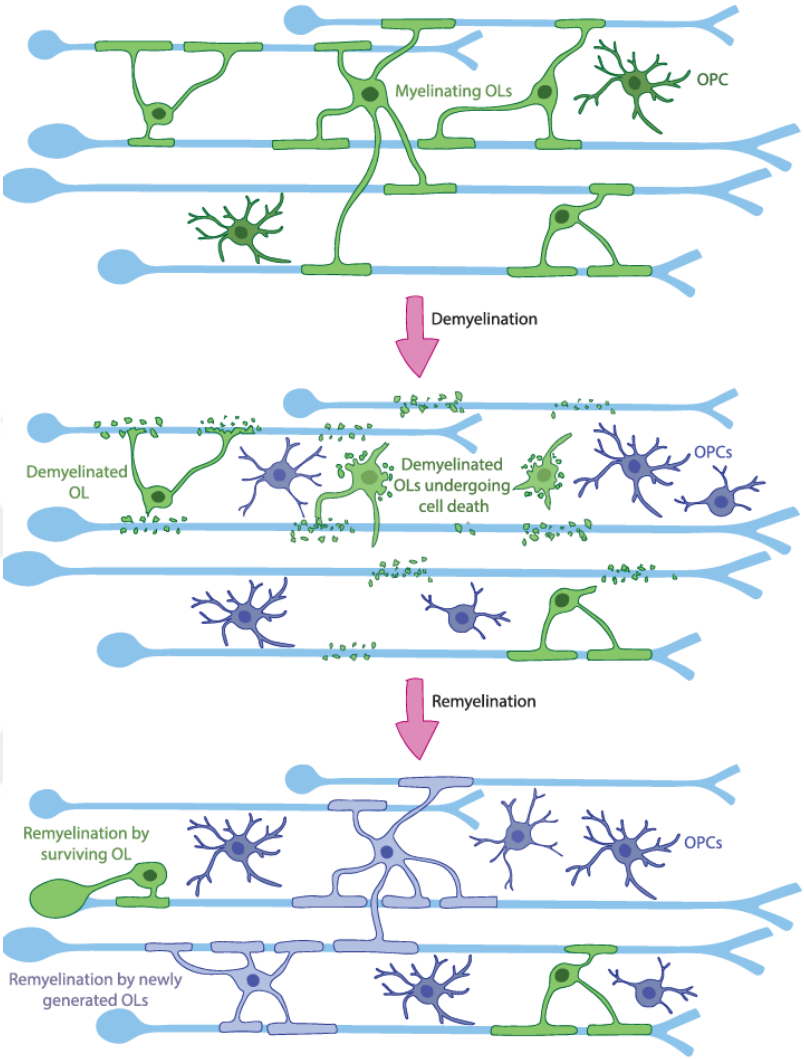

Figure 3: Representative image of remyelination.

Top shows regular myelinating oligodendrocytes and OPCs. Middle, demyelination presence leads to lose of myelin and OL death, consequently OPCs activation. Bottom, activated OPCs differentiate and starts myelinating axons, some of the surviving OLs contribute to remyelination to some extent (Franklin et al., 2021).

OPCs presence and remyelination have been identified in patients suffer from demyelinating diseases to some extent, despite that remyelinated axons were decreased and newly formed myelin were thinner and shorter than the original (Goldschmidt et al., 2009; Patani et al., 2007; Polito &

Reynolds, 2005). Therefore, it is important to perceive OPC behavior and molecular mechanisms behind it to develop new therapeutic approaches.

2.3 Chapter 2: Tissue Regeneration and Cancer

Tissues can be damaged due to reasons such as disease, aging, injury, and genetic anomalies. Tissue regeneration is a very important and tightly controlled phenomenon that consists of many interconnected stages. Despite variations in the regeneration process across different organisms, it fundamentally involves the stages of cell proliferation, migration, differentiating into specified cells and renewal of functional tissue. Among these phenomena, particularly cellular proliferation has been associated with cancer as well as regeneration (Beachy et al., 2004). Proliferation during tissue regeneration, deliberately terminated in tightly controlled mechanisms. This regulation ensures that regeneration activity finalized without excessive formation of cellular masses caused by abnormal cellular proliferation. Studies had shown that disturbance of the regeneration mechanism can lead to chronic inflammatory response, hypoxia, repeated damage due to failure of termination of regeneration, similar hallmarks observed in cancer. These fundings highlights the importance of proper termination of regeneration is pivotal for prevention of the pathological consequences (Greten & Grivennikov, 2019; Oviedo & Beane, 2009; Verkhratsky & Butt, 2013).

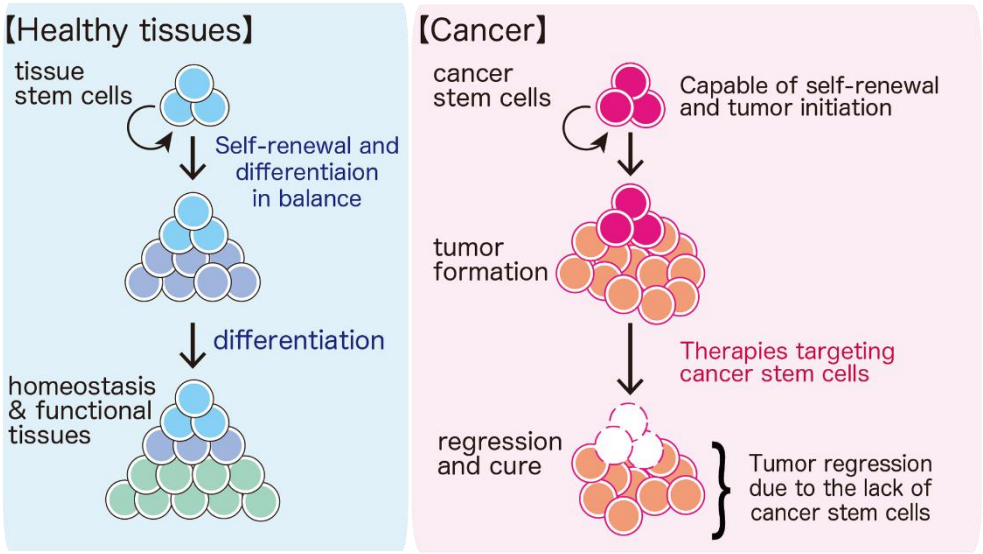

Figure 4: Demonstration of how stemcells in regeneration and cancer (Ito Lab, https://cellfate.infront.kyoto-u.ac.jp/research/).

Therefore, it is crucial to deciphering these mechanisms to develop therapeutic approaches against cancer. From this perspective, cancer can be described as regenerating tissue that has impaired regulation in terms of proliferation, leading to abnormal cellular aggregation and tumor formation. This perspective highlights deflection of normal physiological can lead to transformation of pathological nature of cancer. The hypothesis regarding the relationship of excessive cell proliferation with cancer and tissue regeneration was first proposed by Waddington in the 1930s, and there have been many studies focusing on this issue over time (Stern, 2000; Waddington, 1935).

Glioblastoma, the most prevalent brain cancer affecting both the brain and spinal cord, uncontrolled proliferation of glial cells, creating its microenvironment, sometimes having its own differentiated cells and has one of the highest mortality rates in cancer types. Despite the use of combinatorial use of surgical intervention, radiotherapy and chemotherapy, recurrence persist at elevated levels. Presence of the cancer stem cells (CSS) is one of the major factors that favors higher recurrence rates (Sundar et al., 2014). Cancer stem cells exhibit similar characteristics to developing or regenerating tissue. CSS, as in regenerating tissue, proliferate, migrate and differentiate, thereby, creates and contributes tumor formation. In the mammalian brain, two primary neural stem cell reservoirs exist: the subventricular zone and the dentate gyrus. Studies suggest that brain tumors may originate from these areas (Altmann et al., 2019; Lee et al., 2018). Given this context, investigating the similarities and differences between glioma and brain regeneration is of paramount importance.

2.4 Chapter 3: Disease Modelling and Zebrafish

According to research published at The Lancet Neurology almost 1/3 of the people all around the world living with form of neurological disorder including stroke, brain injury, dementia, forms of nerve damage, brain and spinal cord cancers, psychiatric and developmental disorders (Steinmetz et al., 2024). There are around 600 identified neurological conditions have been present, furthermore, it is estimated that number of rare diseases are 10000 (Smith et al., 2022).

Developing a treatment for diseases have been a significant challenge trough the dawn of times. However, modern advancements provide immersive collection of information and tools to decipher disease mechanisms, evaluate and test therapeutic approaches, translate data to clinical practice. To enhance our understanding the nature of the disease pathology, innumerable models have been

generated to mimic conditions. This progress bridges the gap between laboratory research and patient care.

The zebrafish (Danio rerio) and human brains exhibit similarities in neuroanatomical, neurochemical, and behavioral aspects (Mueller & Wullimann, 2009; Shenoy et al., 2022; Valente et al., 2012). With over 80% of human genes having at least one zebrafish ortholog, and with orthologs of genes mutated in neurodegenerative diseases, the zebrafish has emerged as a unique complementary model for studying these conditions across its embryonic, larval, and adult stages. This relevance is further enhanced by the observable behavioral patterns exhibited by zebrafish. (Chia et al., 2022; Wang & Cao, 2021).

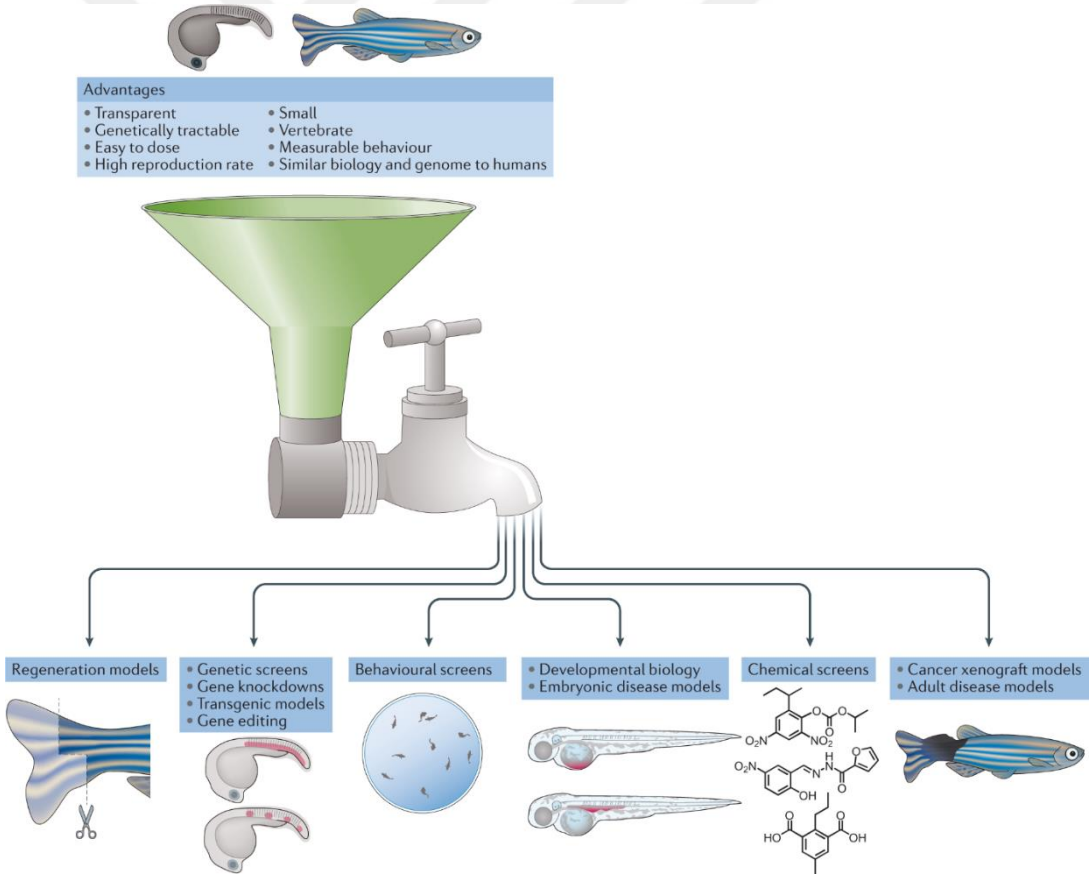

Figure 5: Schematic representation of zebrafish disease models its role in medicine (Patton et al., 2021)

Notably, zebrafish possess the remarkable ability to regenerate critical tissues, such as the heart, muscle, liver, and nervous system, following injury. This regenerative capability is particularly notable in comparison to mammals, where the central nervous system demonstrates limited regenerative capacity, where neurogenesis is restricted mainly to two neural stem cell niches in the subgranular zone of the dentate gyrus and the subventricular zone of the lateral ventricles, the zebrafish brain contains sixteen distinct regions harboring neural stem/progenitor cells, demonstrating a significant regenerative capacity (Kroehne et al., 2011). This exceptional regenerative potential has positioned zebrafish as a significant model organism in biomedical research.

Furthermore, zebrafish are invaluable for cancer research due to their capacity to model various types of cancer. Through the application of mutagens or the overexpression of oncogenes, facilitated by advanced transgene tools, researchers can induce and study cancer within zebrafish models (Peng & Peng, 2015). These models benefit from the evolutionary conservation of oncogenes and tumor suppressor genes between humans and zebrafish, which exhibit similar patterns of gene expression. This genetic similarity enhances the relevance of zebrafish in understanding cancer biology and the molecular mechanisms underpinning tumor development and progression.

Given these attributes, zebrafish emerge as an exemplary model organism for studies in both regenerative biology and oncology. Their unique regenerative abilities and the capacity to accurately model human cancers provide a robust platform for investigating the processes of tissue repair and cancer pathogenesis. As such, zebrafish not only advance our fundamental understanding of these biological phenomena but also hold potential for translating research findings into therapeutic strategies.

The advanced imaging techniques applicable to zebrafish, combined with their suitability for high-throughput screening and their similarities to human physiology, render zebrafish highly advantageous for functional and neurophysiological analyses, as well as for the screening of neurospecific compounds. These characteristics underscore the zebrafish as an efficient, high-resolution, and cost-effective model for the study of human neurodegenerative diseases.

Overall, the zebrafish model stands out with fully sequenced genome, high degree of sequence and functional homology with mammals, observable behavior, regenerative capabilities. Furthermore, having prolific offspring production, transparent embryonic and larval development, relatively easy and cost-effective housing, application of forward and reverse genetic approaches and live imaging techniques making it an invaluable tool in the modeling and understanding of neurodegenerative diseases. This model facilitates high-resolution insights into disease mechanisms and the development of therapeutic strategies, reinforcing its utility in neuroscientific research.

3 MATERIALS AND METHODS

3.1 Type of Research

Present study was experimental research.

3.2 Location and Time Frame of Research

The research designed and conducted between August 2019 and May 2024 at Izmir Biomedicine and Genome Center.

3.3 Research Materials

Tg(mbp:EGFP-caax), Tg(7xTCF-Xla.siam:mCherry), Tg(6XTCF:dGFP), Tg(zic4:GAL4TA4,UAS:mCherry) and AB wildtype fish lines obtained from Ozhan Lab Stocks. All fish raised and housed according to Izmir Biomedicine and Genome Center Zebrafish Core Facility guidelines.

3.4 Research Variables

LPC, IWR-1 treatments, plasmid or RNP complex injections and duration of treatment are independent variables, changes in cellular events such as proliferation, differentiation, inflammation, apoptosis as well as aberrant tissue development such as cancer or developmental defects are dependent variables.

3.5 Data Collection Tools

3.5.1 Devices

Laboratory equipment used in this study are shown below (Table 1).

Table 1: List of the devices

Instruments	Vendor
Vortex	Thermo Fisher Scientific
Microwave Oven	Beko
Borosilicate Glass Capillary	World Precision Instrument
7500 Fast Real-Time PCR System	Applied Biosystem
Cryostat	LEICA

LSM880 Laser Scanning Confocal Microscopy	ZEISS
Nanodrop 2000 Spectrophotometer	Thermo Fisher Scientific
pH meter	Mettler Toledo
Thermal Cycler	Thermo Fisher Scientific
mySPIN 6 Mini Centrifuge	Thermo Fisher Scientific
2100 Bioanalyzer	Agilent Technologies
Water bath	Nüve NB9
-80°C Freezer	Thermo Scientific
Microplate Reader	Thermo Varioskan® Flash
Stemi 305 Compact Stereo Microscope	Zeiss
SZX2 Series Stereo Microscope	Olympus
Flaming/Brown Micropipette Puller	Sutter Instrument

3.5.2 Commercial Kits

Commercially available kits used in this study are shown below (Table 2).

Table 2: List of the commercial kits.

Kit	Vendor
GoTaq qPCR Master Mix	Promega
miRNeasy Micro Kit	Qiagen
iScript™ cDNA Synthesis Kit	Bio-Rad
Phusion High-Fidelity DNA Polymerase	Thermo Fisher Scientific
HiScribe™ T7 High Yield RNA Synthesis Kit	NEB
RNA Clean & Concentrator-25	Zymo Research
DIG RNA Labeling Mixture	Roche
NucleoSpin Gel and PCR Clean-up	Macherey-Nagel

3.5.3 Chemicals

Chemicals used in this study are shown below (Table 3).

Table 3: List of the chemicals

Chemical	Vendor
Lysophosphatidylcholine (LPC)	Sigma-Aldrich
Dimethyl Sulfoxide (DMSO)	Sigma-Aldrich
Ethanol Absolute	Merck
Ethylenediaminetetraacetic acid (EDTA)	Sigma-Aldrich
Gelatin	Merck
Glycerol	Amresco
IWR-1	Sigma-Aldrich
Methanol	Sigma-Aldrich
Paraformaldehyde	Sigma-Aldrich
Potassium Chloride	Sigma-Aldrich
Sodium Chloride	Sigma-Aldrich
Sodium Phosphate dibasic	Sigma-Aldrich
Sodium Phosphate monobasic	Sigma-Aldrich
Sucrose	Sigma-Aldrich
Tissue-Tek O.C.T	SAKURA
Tricaine	Sigma-Aldrich
Tris	Sigma-Aldrich
Triton X-100	Sigma Aldrich
Chloroform	Merck

3.5.4 Consumables

Consumables used in this study are shown below (Table 4).

Table 4: List of the consumables

Needle 30G 0,3x13 mm
Disposable plastic pipette tips
Disposable filter plastic pipette tips
Disposable scalpel
Disposable microtome blades
1,5 mL Eppendorf tubes
2 mL Eppendorf tubes
15 mL centrifuge tubes
50 mL centrifuge tubes
96 well plate
Coplin staining jar
Embedding Molds
Borosilicate glass capillary

3.5.5 Primers

The primers used in this study designed with The NCBI Primer Designing Tool (https://www.ncbi.nlm.nih.gov/tools/primer-blast/) and ordered from Oligomer Biotechnology in Ankara, Turkey. Primers received in lyophilized form and dissolved in nuclease free water (NFW). List of the primer sequences shown below.

3.5.6 Methods

3.5.6.1 Demyelination/Remyelination Model

3.5.6.1.1 Validation of the LPC-induced Myelin Damage

To induce demyelination Lysophosphatidylcholine (Sigma-Aldrich, St Louis, MO, USA) were used. LPC dissolved in saline (0,9 NaCl solution) and aliquoted by 1%, 5µL and stored in -20°C. In order to observe demyelinating effect of LPC, Tg(mbp:EGFP-caax) transgenic myelin reporter line were used. Following mating, eggs collected in E3 medium (5 mM NaCl; 0.17 mM KCl; 0.33 mM MgSO4; 0.33 mM CaCl2; pH 7.5 in ddH2O) kept in 37°C incubator. 1 day-post-fertilization eggs are bleached and dechorionated then kept in 1-phenyl 2-thiourea (PTU) containing E3

medium to inhibit pigmentation. To test LPC-induced demyelination, 4dpf fish were anesthetized with (Tricaine methanesulfonate, MS-222, Sigma-Aldrich). Spinal cord injection performed between somite 13-16, following, fish were transferred in PTU containing E3 medium(Cunha et al., 2020; Morris & Kucenas, 2021). 1 days-post-injection (dpi) fish were anesthetized and mounted with low melting agarose to perform live-imaging.

3.5.6.1.2 Establishment of Demyelination Model of Adult Brain

To induce demyelination in the adult brain, CVMI (Cerebroventricular Microinjection) method were used. Adult fish were anesthetized and placed onto injection platform. To create small incision, 30-gauge insulin needle were used. 0,5 µL injection mixture (1% LPC + DiL) injected slowly to prevent physical damage. Control injections performed with 0,5 µL saline. Then fish were transferred clean water, immediately. Fish water changed daily. Following sacrificing fish, dispersion of the injection mix checked by fluorescence microscope, failed fish excluded from the experiments.

3.5.6.1.3 Validation and Characterization of Demyelination and Remyelination

To validate demyelination and remyelination, LPC injected fish were sacrificed at 1-, 3-, and 7dpi. 1st and 3rd day described as early demyelination and demyelination stages, respectively. 7th day described as remyelination stage. Stages confirmed by myelin related gene expression levels and immunofluorescence staining. To visualize myelin structure in adult telencephalon Tg(mbp:EGFP-caax) transgenic reporter line were used. To validate and characterize demyelination/remyelination, myelin structure, oligodendrocyte lineage, immune response, glial response, and proliferation related changes were evaluated.

3.5.6.1.4 IWR-1 treatment

To inhibit Wnt signalling activity IWR-1-endo (Selleck Chemicals, USA) applied. IWR-1 enhances axin2 protein levels and facilitates β-catenin phosphorylation by stabilizing Axin-scaffolded destruction complexes. Starting a day before LPC injection, IWR-1 applied at 10 µM concentration (Demirci et al., 2020).

3.5.6.1.5 RNA isolation, cDNA Synthesis and Quantitative Real-time PCR

To isolate RNA, RNeasy Micro Kit (QIAGEN) were used according to manufacturer's guidelines. Briefly, telencephalons were dissected and transferred into 1.5 mL sterile tubes on ice. 50 µL QIAzol Lysis Reagent (QIAGEN) added, and brain tissue mechanically homogenized with RNase-free pestles. Then, final volume adjusted to 700 µL and thoroughly pipetted for homogenous mixture. 140 µL chloroform added and tubes were shaken vigorously for proper phase separation and placed bench top for 3 minutes. Then, centrifuged for 12.000g for 15 minutes at 4°C. Proper separation yields 3 phases, upper (clear) phase transferred into a clean tube. 525 µL absolute ethanol were added and mixed well. Mixture loaded into spin columns and centrifuged for 15 seconds at 8000g at room temperature. Flow-through discarded and 700 RWT buffer loaded and centrifuged at 8000g for 15 minutes. Flow-through discarded and washed 3 times with 500 µL RPE buffer 15 seconds at 8000g. 500µl 80% ethanol in NFW added and centrifuged for 2 minutes at 8000g. Flow-through discarded and to clear ethanol and dry the membrane spin columns centrifuged 5 minutes at full speed. Spin columns transferred into clean tube, 15 µL NFW added and placed onto bench for 3 minutes for full immersion. Then, centrifuged for 2 minutes to isolate RNAs. RNA concentration was quantified with Nanodrop 2000 Spectrophotometer. To synthesize cDNA, BIORAD iScript™ cDNA Synthesis Kit was used according to manufacturer's specifications. 100 ng RNA was used for each reaction. qRT-PCR reactions implemented with Applied Biosystem 7500 Fast Real-Time PCR. Relative fold change of gene expressions was calculated by $2^{-\Delta\Delta CT}$ method, RPL13a was used as housekeeping gene for normalization, each run was performed with three technical replications.

3.5.6.1.6 Histological Preparation and Immunofluorescence Staining

Fish were sacrificed with ice water. Top of the skull was opened and telencephalon were exposed, then heads were separated and placed into ice-cold 4% PFA and incubated at +4°C for 2 days. Following fixation with PFA, telencephalons were isolated from rest of the head and placed into 30% Sucrose for cryopreservation for 2 days. Tissues were embedded with OCT in the hand-made molds and stored in the -80°C. 10 µm sections were taken with cryostat (Leica) and incubated at 65°C overnight, then stored at -20°C until further use.

Slides were kept on bench top at room temperature for 30 minutes before staining procedure. Then, washed twice for ten minutes with PBSTx for permeabilization and rinsed with PBS afterwards. Slides were incubated with 10 mM Sodium Citrate Buffer (pH:6) for 15 minutes (pre-heated to 85°C) for antigen retrieval. Then, washed with PBS (2x5min) and PBSTx (2x10min), respectively. Sections were blocked with 10% donkey serum in PBSTx for 30 minutes and primary antibodies applied. Slides were incubated with primary antibodies overnight at +4°C. Next morning, slides were rinsed with PBSTx, secondary antibodies applied for 2 hours in room temperature. DAPI applied at last 10 minutes for nuclear staining. Slides were washed with PBS and mounted with 70% Glycerol in PBS. Primary and secondary antibodies were diluted in 10% donkey serum in PBSTx according to manufacturer's instructions. Samples were imaged by using an LSM 880 laser scanning confocal microscope (Carl Zeiss AG, Oberkochen, Germany).

3.5.6.1.7 Protein Isolation and Proteomics Analysis

Dissected brains were transferred into 1.5 mL tubes on ice and immediately flash freezed with liquid nitrogen to preserve proteins effectively. To stabilize the proteins, RIPA buffer was prepared and supplemented with protease and phosphatase inhibitors before protein isolation. 120 µL RIPA buffer was added to each tube to increase protein concentration. Tissue was homogenized with sterile pestles on ice, then vortexed every 5 minutes for 30-45 minutes. Afterwards, the mixture was passed through insulin syringe 10 times to break down mucous structure. Then samples centrifuged for 30 minutes at +4°C. Supernatant were transferred into sterile 1.5 mL tubes on ice and BCA Assay (Thermo Fisher Scientific) were performed according to manufacturer's instruction to determine concentrations. 50 µg were aliquoted for proteomic analysis and rest were aliquoted 20 µg for western blotting. All samples stored at -80°C until further use.

For the MS-based quantitative proteomics, proteins derived from telencephalons were detected via nano-LCMS/MS (nanoscale liquid chromatography-mass spectrometry/mass spectrometry) coupled with fragment-ion analysis methodology. Protein mixtures were digested to generate tryptic peptides using filter-aided sample preparation (FASP). The resulting peptides were separated by reversed-phase chromatography and analyzed in the nLC-MS/MS Orbitrap mass spectrometry system.

Raw LC-MS/MS data of tryptic peptides obtained from the mass spectrometry device were run with MaxQuant (ver 2.1) software. As the target database, the reference proteome file in FASTA format containing 46696 proteins that belong to the most recent zf (Danio rerio) organism in UniProt were downloaded. The software was enabled protein level identifications and determination of quantitative changes between the control and treatment groups, at least 2 biological/technical replicates were performed in each group. The statistical distribution between groups were visualized by principal component analysis (PCA). All groups were transformed by log2. Proteins with altered expression were classified using the MaxLFQ quantitative values, and the rates of change between groups (Fold-Change) and statistical test values (P-Value) were compared with R (ver 4.1) Limma package. Those with FDR values below 5% were determined by the Benjamini-Hochberg procedure. Proteins with a minimum corrected FDR-value less than 0.05 and a group variation rate greater than 33% will be visualized by Volcano plot.

The identified differentially expressed proteins (i.e Ctrl vs Damage, Damage vs IWR) were further analyzed to associate with the network of biological classes, i.e. biological process, molecular function, and cellular component, will be examined using the RPage 11 of 30 gprofiler2 package on the Gene Ontology (GO) database. For proteins that do not reveal any functional association, human or mouse orthologs will be determined with the R babelgene package and the same procedures will be repeated. Matching pathways will be determined by performing analyses on Stringdb, KEGG, Reaktome, and Wikipathways databases. Visualization of GO terms with pathways and network analysis will be performed by using Bioconductor compatible R packages.

3.5.6.2 CRISPR/Cas9-based Human Disease Modelling

3.5.6.2.1 Single Guide RNA (sgRNA) Design and Synthesis

Target sequence of myh7 gene were selected via online cloud-based informatics tool “Benchling” (https://benchling.com). GRCz11 genome dataset were selected for target and guanine nucleotide added 5’ of the target sequence to improve in vitro transcriptrion. Template for single guide RNA synthesis was generated by PCR based approach (Phusion High-Fidelity DNA Polymerase, Thermo Fisher Scientific) with forward primer containing T7 promoter and targeted gRNA sequence and reverse primer encoding standard chimeric sgRNA scaffold (ref?:) (Table 1). Oligonucleotides were obtained from Oligomer. NucleoSpin Gel and PCR Clean-up Kit (Macherey-Nagel) was used

to purify the DNA template and HiScribe™ T7 High Yield RNA Synthesis Kit (New England Biolabs) was used for in vitro transcription (IVT) as manufacturers guidelines. IVT products were purified by RNA Clean & Concentrator-25 (Zymo Research) as manufacturer's instructions. RNA quantity was determined by NanoDrop™ (Thermo Fischer Scientific).

3.5.6.2.2 Ribonucleoprotein (RNP) Complex Preparation and Microinjection

sgRNA and recombinant Cas9 protein (Guide-it™ Recombinant Cas9, Takara Bio) was mixed 1:1 (500/500 ng/µL) and incubated at room temperature for 5 minutes to generate RNP complex and 0.05% phenol red was added to the mixture for visualization of injections. 1-1.5 nL of solution was injected into 1-cell stage embryos in the yolk close to the cell or directly into the cytoplasm.

3.5.6.2.3 DNA Extraction and Sequencing

Embryos injected with RNPs at 5 dpi were used for genotyping. 10 individual larvae were transferred to 1.5 mL tubes in 50 µL DNA Extraction Buffer (10 mM Tris HCl pH:8.0, 50 mM KCI, 0.3 % Tween 20, 1 mM EDTA) and incubated at 98°C for 10 minutes. 3 µl proteinase K (5mg/mL; Sigma Aldrich) solution was added to each tube and incubated at 55 °C overnight. Samples were incubated at 98°C for 10 minutes to inactivate proteinase K and centrifuged tube at 14.000 rpm for 4 minutes. Supernatants transferred into new tubes. 50 µL ddH2O, 10 µL 3M sodium acetate, 180 µl isopropanol were added onto supernatant and vortexed then kept on ice for 10 minutes. Samples were centrifuged at 14,000 rpm for 15 minutes at 4°C. Supernatants were discarded and remaining pellet was washed with cold 70% ethanol and left air dry for 15 minutes. Pellets were resuspended in 10 µL nuclease-free water. Genomic DNA quantity was determined by NanoDrop™ (Thermo Scientific™ 840274200).

Targeted myh7 loci were amplified with PCR used for Sanger Sequencing. Genomic DNA was used as template at 100 ng/µL concentration and CloneAmp HiFi PCR Premix (Takara Bio, Cat. No. 639298). Primers was designed to contain mutation area (F: 5' - TAAATTAGCCACGCTGGCAC - 3'; R: 5'- TCTAAGAATGGAAAGTGTTGCTGT -3'). Final volume was adjusted with nuclease-free water to 25 µL. PCR was performed in SimpliAmp Thermal Cycler (Thermo Fischer Scientific) using the following conditions: 98°C for 1 min; 35 cycles of 98°C for 30 s, 62°C for 30s, and 72°C for 20s; followed by 72°C for 10 min. 1µL of each sample were loaded into %1 agarose gel and electrophoresed. PCR products was cleaned up with

PCR clean up and gel extraction (Macherey-Nagel) as manufacturer suggestions. Quantification of products was determined by NanoDrop™ (Thermo Scientific™ 840274200).

3.5.6.2.4 Whole Mount in Situ Hybridization (WMISH)

Embryos were collected at 3 dpi and 5dpi and fixed with 4% PFA for 48 hours. WMISH performed for *Myh7, Myh7l* and *Mylk3* antisense RNA probes as described in (Ozgun, 2020; Thisse and Thisse, 2007).

3.5.6.2.5 In Vivo Imaging of Zebrafish

In vivo phenotypic evaluation of embryos implemented with Olympus SZX2-ILLB stereomicroscope (Olympus Microscopes) and images were captured with Olympos SC50 microscope camera (Olympus Microscopes).

3.5.6.3 Glioma Model

3.5.6.3.1 Generation Of Glioma Developing Zebrafish

Tol2 Transposase system were used to create the zebrafish glioma model. The Tol2 transposase system is based on the principle of injecting the plasmid containing Tol2 enzyme cutting sites and Tol2 mRNA into the embryo at the single-cell stage. In this way, the plasmid is cut from the tol2 cutting sites and integrated into the fish genome through recognition sites. The first line obtained is called F0 and the expression of the transgene is mosaic. For this reason, the F0 line is brought to adulthood and mated with the wild type to obtain the F1 line with stable transgene expression (Kwan et al., 2007; Suster et al., 2009).

To create the glioma model, the mutant rasG12V gene, an oncogene were expressed under the glial fibrillary acidic protein (GFAP) promoter expressed in mammalian astroglia and neural stem cells, as well as in radial glia cells in zebrafish. The designed plasmid has the GFAP:eGFP- rasG12V map. Thus, by ensuring the expression of green fluorescent protein in radial glial cells, examination with a fluorescent microscope were possible. After microinjection, the larvae were examined under a fluorescent microscope on the 5th day, when the nervous system development is mostly completed, and larvae that emit strong fluorescent light in the brain and spinal cord were selected and raised. In this way, it is aimed to increase the possibility of transferring the transgene to the next generation when the F1 line is crossed with the wild type to be grown.

Additionally, Gal4-UAS system used to generate another transgenic glioma line (Mayrhofer et al., 2017). This sequence encodes a codon-optimized variant of the transcription factor Gal4, regulated by the zic4 enhancer, specifically in the proliferative regions of the developing central nervous system. To generate, somatic glioma line UAS:GFP-HRASV^{12} plasmid combined with tol2 RNA and were injected into single-cell stage fish. F0 fish raised to adulthood for further analysis.

3.5.6.3.2 RNA-Seq Sample Preparation

RNA samples were collected from 3 months old control or f0 fish according to section 3.5.6.1 and aliquoted by 20 µg/uL. 4 control and 4 injected fish randomly selected. RNA samples delivered to GenEra LifeSciences for further quality control and bulk RNA sequencing.

3.6 Research Plan and Timeline

Generation of the Glioma Model	09/2019-06/2021
Generation of the *myh7*KO Model	03/2020-09/2021
Validation and Characterization *myh7* KO	09/2021-03/2022
Generation of the Myelin Damage Model	01/2022-01/2023
Validation and Characterization of the Myelin Damage Model	01/2023-10-2023
RNA-Seq Samples for Glioma and Analysis	10/2023-02/2024
Proteomic Samples for Myelin Damage and Analysis	10/2023-06/2024

3.7 Data Analysis

Image J, GraphPad Prism8 and Student's T Test were used for statistical analysis. Experiments performed in triplicate. Statistical significance is represented as *p<0.05; **p<0.01; ***p<0.001.

3.8 Limitations of research

Further validation and comparison from mammalian models and/or human data would enhance the validity of the human disease models established in this study.

3.9 Ethical committee approval

Animal experiments were approved by the Animal Experiments Local Ethics Committee of Izmir Biomedicine and Genome Center (IBG-AELEC) (See Appendix).

4 RESULTS

4.1 Chapter 1: Role of the Wnt Pathway in Remyelination

4.1.1 Verification of the LPC-induced Demyelination

Lysophosphatidylcholine (LPC) is a well-established myelinotoxic agent frequently employed to induce focal demyelination in vertebrate models. Typically, a 1% LPC injection is administered to elicit myelin damage, although the specifics can vary depending on the model organism, targeted tissue, and application methodology. The onset of demyelination is observable within 6 hours to 1-day post-injection (1 dpi). Subsequently, remyelination processes can be detected within 7 to 10 days. This temporal framework allows for a detailed investigation of both the mechanisms underlying demyelination and the subsequent regenerative processes, providing valuable insights into potential therapeutic approaches for demyelinating diseases (Cunha et al., 2020; Morris et al., 2020; Münzel et al., 2014; Nyamoya et al., 2019)

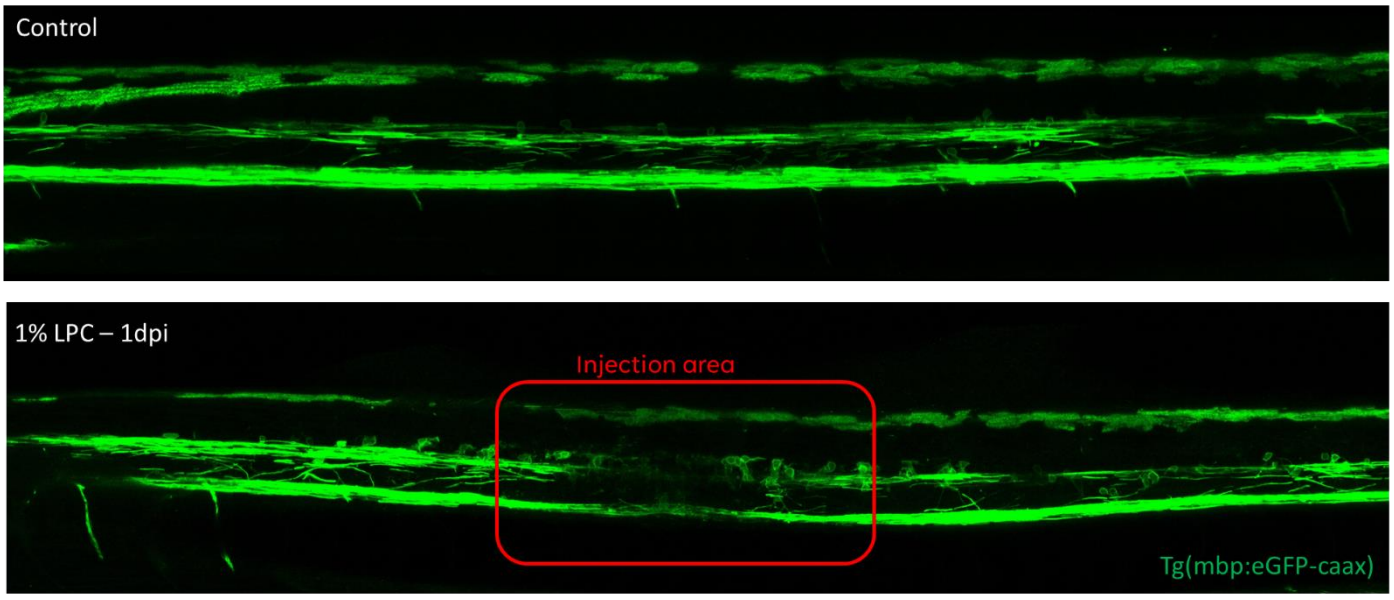

Figure 6: Characterization of LPC-based myelin damage in zebrafish larvae

Herein, we first confirmed LPC induced myelin damage with zebrafish larvae. Transparent larvae offer significant benefits for live imaging. Furthermore, another advantage of the zebrafish is availability of the numerous transgenic strains. Therefore, we have exploited Tg(mbp:EGFP-caax) transgenic line to visualize myelin structure. 1% LPC injection performed between somite 13-16 in the spinal cord. 1dpi myelin structure were disrupted, vucuolisation of the membrane present and cell bodies were intact (Figure 6).

4.1.2 Verification Adult Demyelination Model

To develop demyelination in adult brain of zebrafish, cerebroventricular microinjection (CVMI) method was combined with LPC. CVMI approach depends on the dispersion of the administered liquid within the cerebroventricular fluid and its subsequent absorption by cells proximal to the ventricle.

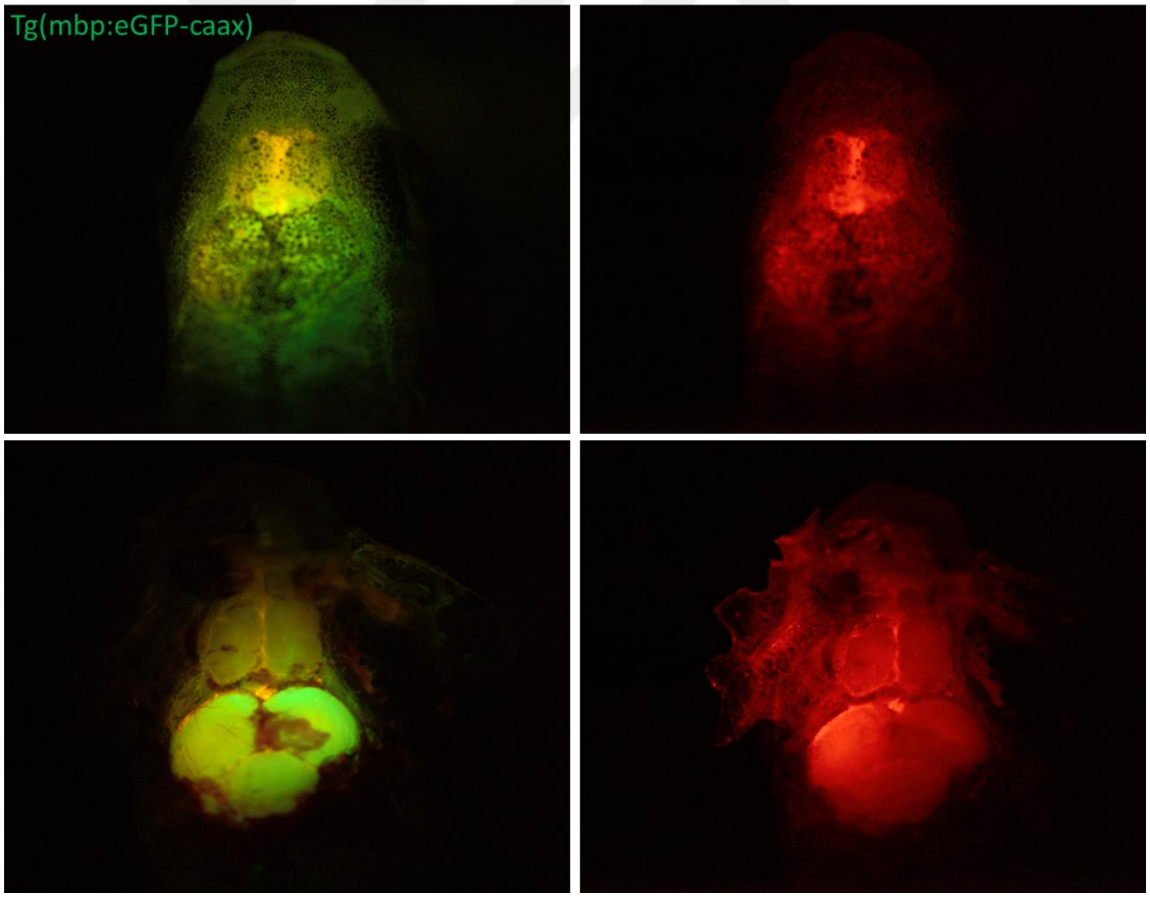

Figure 7: DiL + LPC injected fish under fluoroscent microscope to confirm succesful CVMI

To ensure the distribution of injected LPC throughout the brain, DiL labeling dye was included in the injection mixture. Following euthanasia, the fish were examined using a fluorescent croscope to confirm injection success (Figure 7). Fish that lacked fluorescent signals were excluded from the study.

4.1.3 Determination of the Demyelination and Remyelination

Myelin is a specialized cell membrane forming a multilayered sheath around the axon. Its structure is primarily composed of lipids, including cholesterol, phospholipids, and glycolipids, alongside myelin-specific proteins such as proteolipid protein (PLP), myelin basic protein (MBP), and myelin protein zero (MPZ, P0). The composition of myelin is remarkably conserved across species, such as zebrafish and mammals. However, zebrafish possess additional proteins absent in mammals, including 36K, claudin K (CLDNK), and Zwilling proteins (ZWI)(Kister & Kister, 2022; Siems et al., 2021).

To determine the stages of demyelination and remyelination, RNA was collected at 1 dpi, 3 dpi, and 7 dpi to evaluate the expression levels of myelin-related genes (Figure 8). Our findings indicate that the expression of myelin-related genes was significantly downregulated at 1 dpi and 3 dpi, while it predominantly returned to baseline levels by 7 dpi. These results suggest a temporal regulation of myelin gene expression following myelin damage, with an initial decline during early demyelination stages and a subsequent recovery during remyelination.

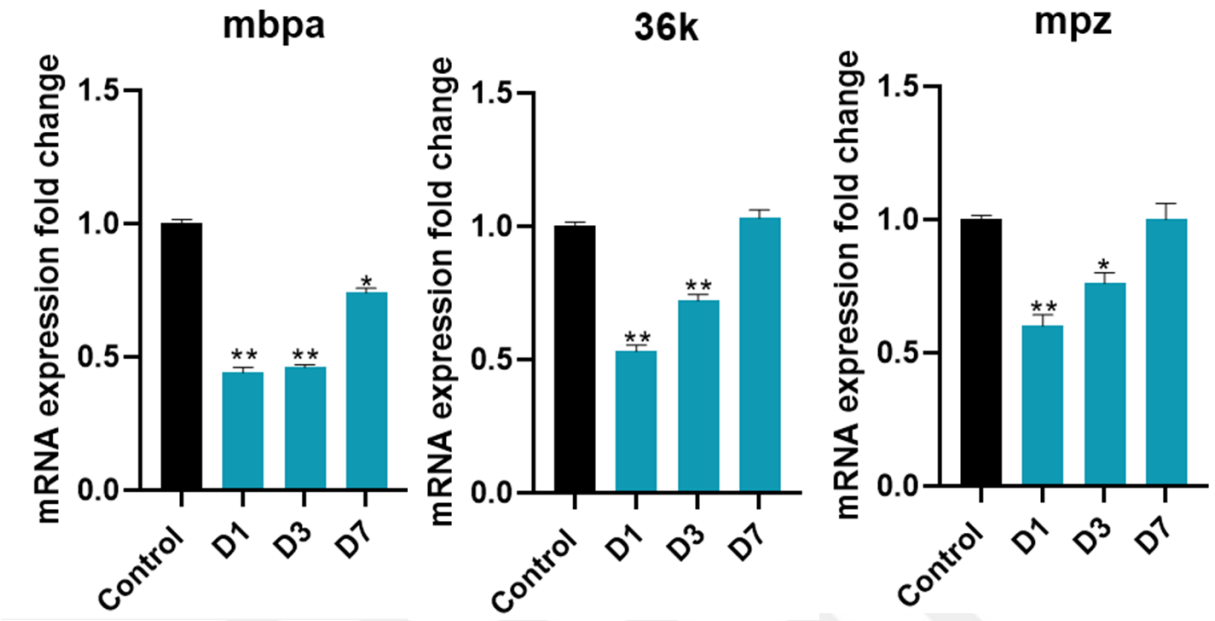

Figure 8: Determination of demyelination and remyelination stages. *Rpl13* was used as housekeeping gene. p≤0.05 (*), p≤0.01 (**), p≤0.001 (***), p≤0.0001 (****) and p>0.05 (n.s.). Error bars show standard deviation (SD).

Additionally, we assessed myelination integrity immunofluorescence microscopy. To achieve this, we utilized Tg(mbp:eGFP-caax) fish, which facilitate the labeling of myelin structures with anti-GFP staining. Results show that myelin integrity already lost starting at 1dpi, continue through 3dpi and recovered at 7dpi (Figure 9-11).

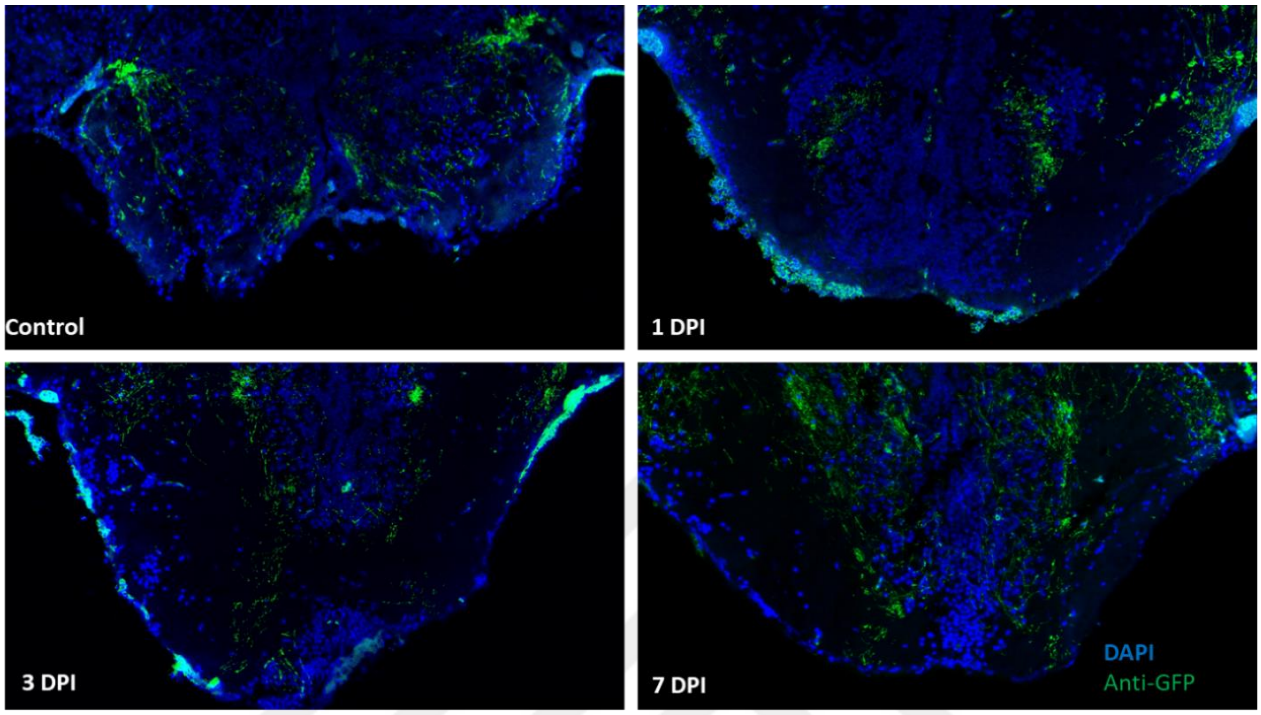

Figure 9: Anti-GFP staining of Tg(mbp:eGFP-caax) reporter line. Nucleues stained with DAPI. 40x

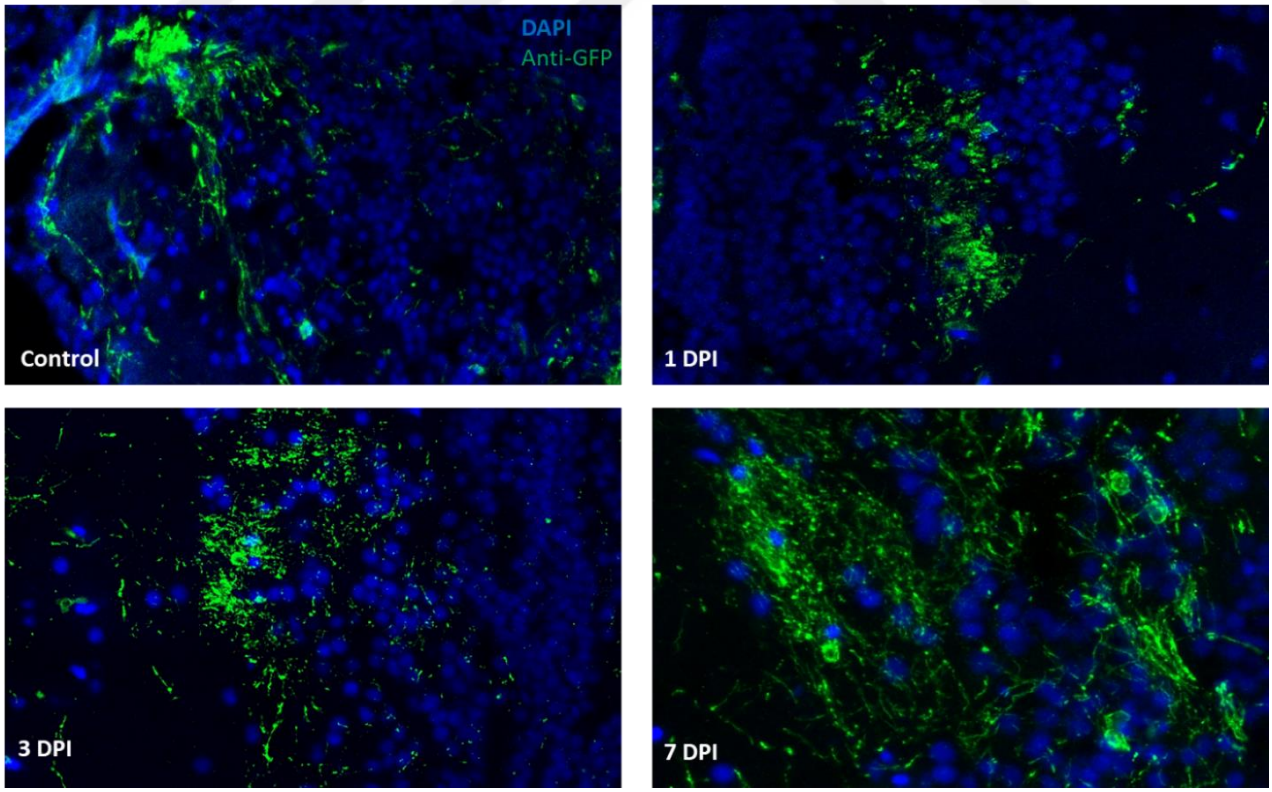

Figure 10: Anti-GFP staining of Tg(mbp:eGFP-caax) reporter line. Nucleues stained with DAPI. 40X + 2X digital zoom

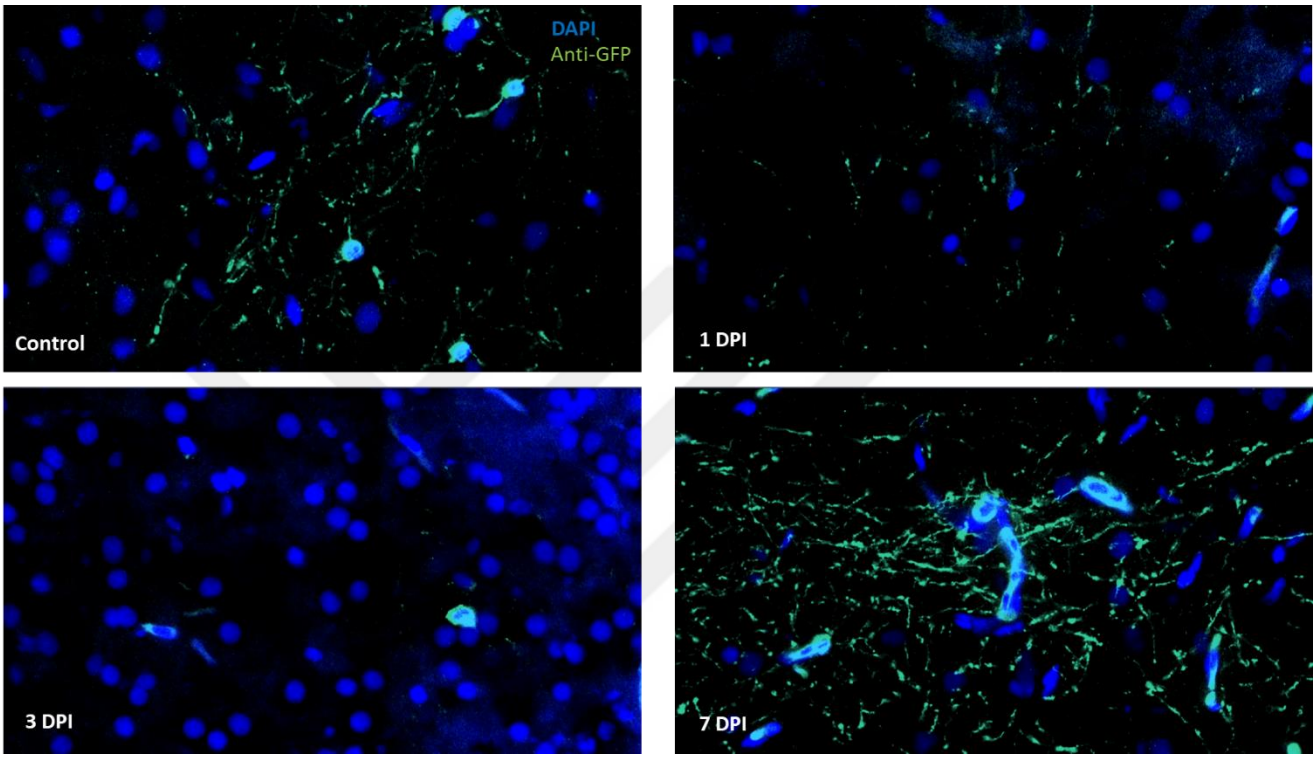

Figure 11: Anti-GFP staining of Tg(mbp:eGFP-caax) reporter line. Nucleues stained with DAPI. 40X + 4X digital zoom

Further we investigated how early demyelination occurred. To test this, we terminated the experiments at 6-hour post injection (hpi) and 12-hour post injection. Our results show that demyelination start as early as 6hpi and peaks at 12 hpi (Figure 12).

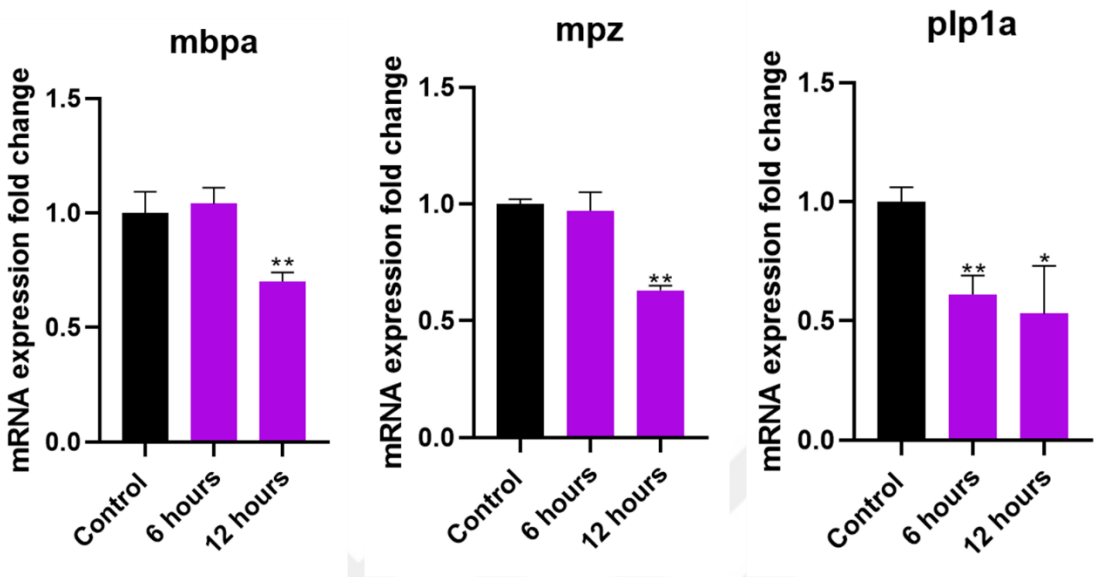

Figure 12: Relative expression changes in myelin related genes in early degeneration. *Rpl13* was used as housekeeping gene. p≤0.05 (*), p≤0.01 (**), p≤0.001 (***), p≤0.0001 (****) and p>0.05 (n.s.). Error bars show standard deviation (SD).

Remyelination is elongated process, early phases of the remyelination hypermyelination occurs by newly formed myelin sheaths, dendrites increased to find axonal cues. Later stages myelin pruning activates and eliminates excess myelin structure. To confirm this, we checked elongated periods. We found that myelin related genes overexpressed at the 10dpi (Figure 13).

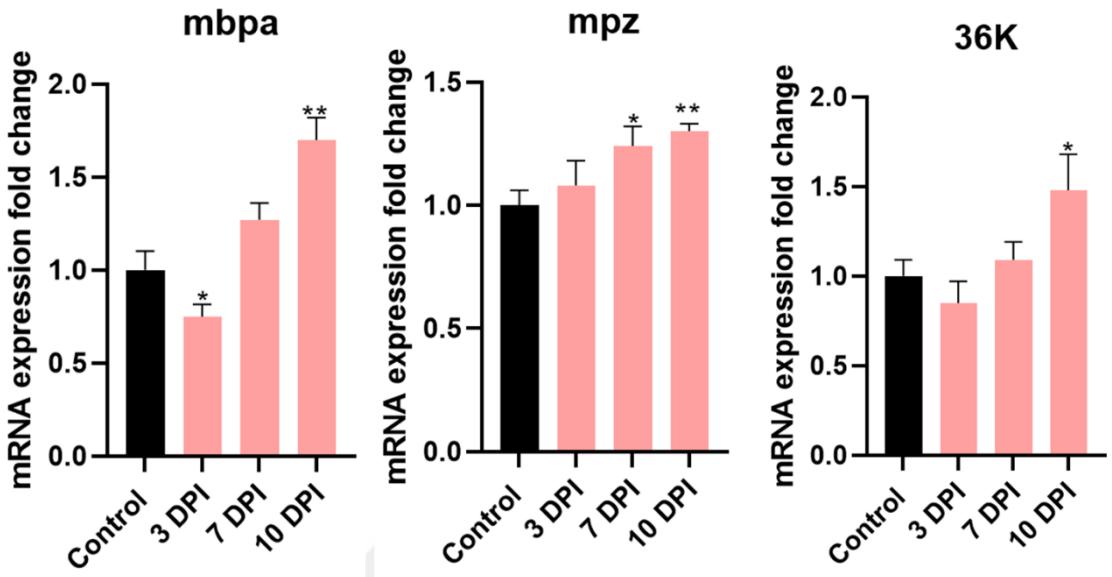

Figure 13: Relative expression changes in myelin related genes in early late remyelination. *Rpl13* was used as housekeeping gene. p≤0.05 (*), p≤0.01 (**), p≤0.001 (***), p≤0.0001 (****) and p>0.05 (n.s.). Error bars show standard deviation (SD).

4.1.4 Determination of Oligodendrocyte Lineage Related Gene Expression Changes

Oligodendrocyte regeneration encompasses multiple stages, beginning with the activation and proliferation of oligodendrocyte precursor cells (OPCs), followed by their migration, maturation, and eventual differentiation into myelinating oligodendrocytes. The transcription factor SRY-box 10 (SOX10) plays a pivotal role in orchestrating the transcriptional regulation necessary for the differentiation of oligodendrocyte lineage cells. Early research identified SOX10 as essential for oligodendrocyte maturation, functioning as a direct activator of several key genes integral to the myelination process. The transcription factors OLIG2, SOX10, NKX2.2, ZFP24, and MYRF are critical determinants in oligodendrocyte differentiation and myelination, collectively forming the core regulatory network that governs these processes. This network ensures the precise coordination required for the proper development and function of oligodendrocytes, highlighting the intricate molecular mechanisms underlying central nervous system myelination.

OLIG2 is one of the major transcription factors that expressed oligodendrocyte lineage cells. Olig2 expression significantly increased at the 1dpi and return to base levels at 3dpi and 7dpi. Nkx2.2a by OPCs and premyelinating oligodendrocytes however not by myelinating oligodendrocyte. Our results show that although, there was no significant change but trending to increase (Figure 14).

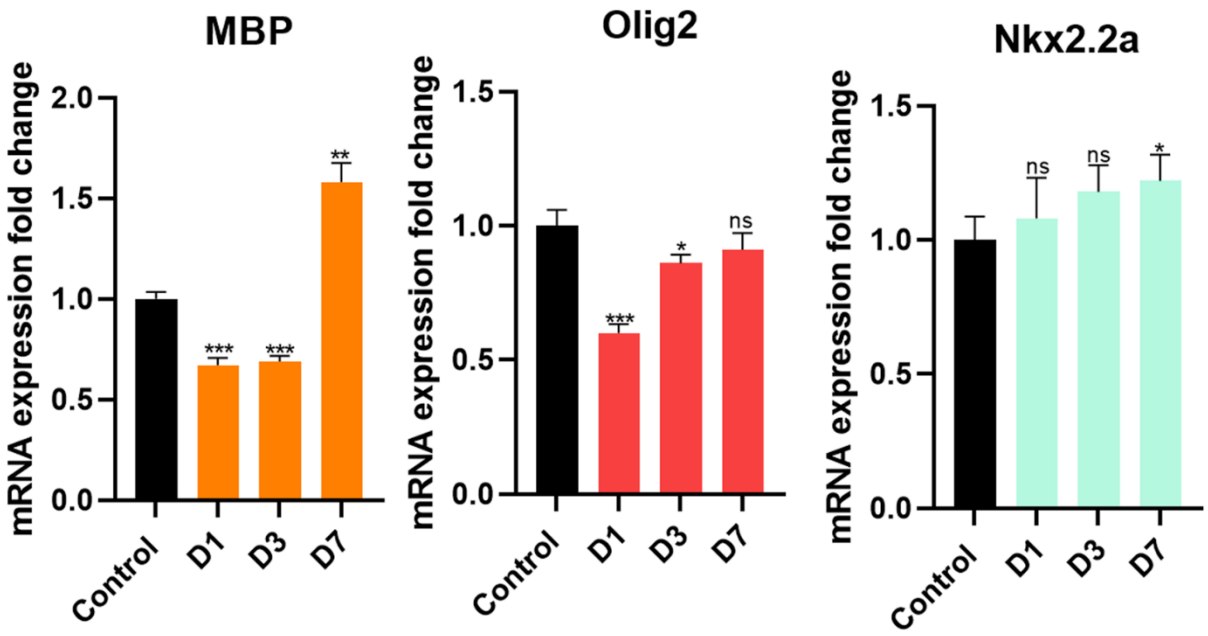

Figure 14: Relative expression changes in oligodendrocyte lineage markers. *Rpl13* was used as housekeeping gene. p≤0.05 (*), p≤0.01 (**), p≤0.001 (***), p≤0.0001 (****) and p>0.05 (n.s.). Error bars show standard deviation (SD).

4.1.5 Determination of the Neuroglial, Immun and Apoptotic Response

Demyelination and remyelination is multistep event occur with characteristic changes in each step. For example, upon demyelination, immune response, macrophage infiltration, microglia activation observed as well as -depending on the severity- axonal damage, cellular death of neurons and glia, apoptotic presence (Cunha et al., 2020; Münzel et al., 2014; T. et al., 2009).

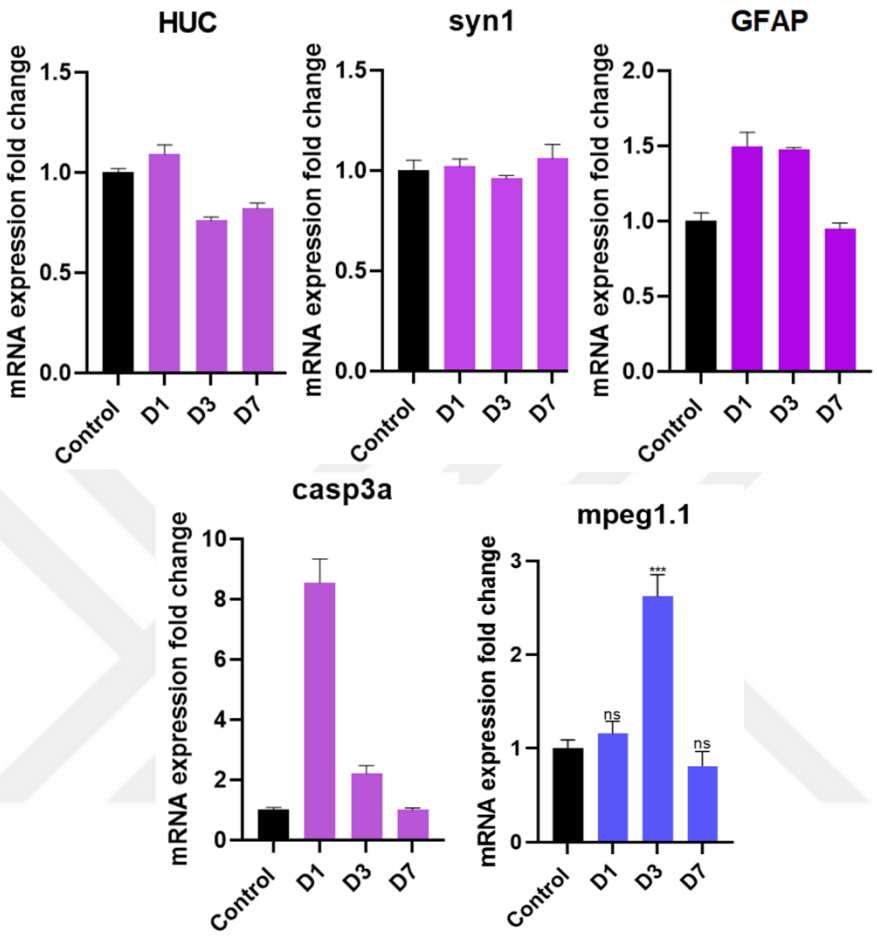

Figure 15: Relative expression changes in *huc*, neuronal marker, *syn1*, synaptic marker, *gfap*, glial marker, *casp3a*, apoptotic marker, *mpeg1.1*, microglial marker. Rpl13 was used as housekeeping gene. p≤0.05 (*), p≤0.01 (**), p≤0.001 (***), p≤0.0001 (****) and p>0.05 (n.s.). Error bars show standard deviation (SD).

Our results show that there were no significant neuronal and synaptic expression changes. Glial response was present in demyelinating stages, however, dismissed at the remyelination stage. Apoptotic responses were present in the demyelinating stages, especially at 1dpi and it is reduced to the control levels in remyelination. Finally, microglia marker, mpeg1.1, were significantly increased at the 3dpi. Overall, these data suggest that myelin damage did not affect neuronal homeostasis. Glia, apoptosis and microglia related gene expression were increased at the demyelination and return the control levels in remyelination (Figure 15).

4.1.6 Determination of the Changes of Wnt Signalling Pathway in Demyelination and Remyelination

The Wnt/β-catenin signaling pathway is crucial for regulating stem cell activation and differentiation, playing a significant role in the response to injury. Wnt pathway's function is essential for the processes of tissue repair and regeneration, highlighting its importance in maintaining cellular homeostasis and promoting regeneration. (Demirci et al., 2020; Ozhan & Weidinger, 2015; Rodriguez et al., 2014). Tcf/Lef transcription factors are evolutionarily conserved, facilitate gene expression controlled by Wnt/β-catenin signaling. To investigate how Wnt/β-Catenin signaling affected, we exploited Tg(7XTCF:mCherry) transgenic reporter line which express mCherry fluorescent protein under tcf promoter. Therefore, allow us to precisely explore changes in Wnt activity. Our results showed that early stages in demyelination have decreased Wnt activity. However, Wnt activity increased at the peak demyelination (3dpi) and decreased in the remyelination stages (Figure 16).

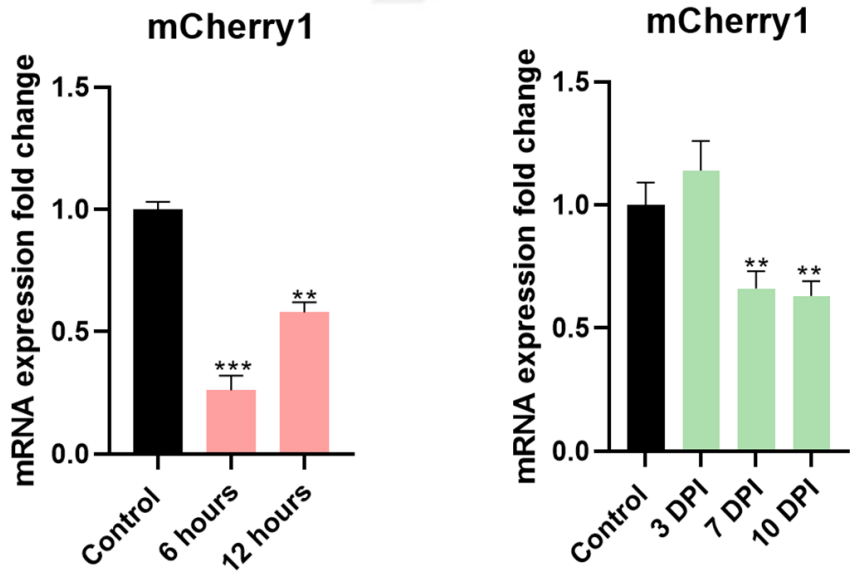

Figure 16: Relative expression changes in Wnt activity. *Rpl13* was used as housekeeping gene. p≤0.05 (*), p≤0.01 (**), p≤0.001 (***), p≤0.0001 (****) and p>0.05 (n.s.). Error bars show standard deviation (SD).

Next, we asked how would demyelination/remyelination would be affected by absence of the Wnt/β-catenin signaling. To achieve this, we administered Wnt signaling inhibitor IWR-1, which inhibits WNT-induced accumulation of β-catenin, through stabilization axin2 member of the destruction complex. First, we evaluated efficiency of IWR-1. To test this, we used Tg(7XTCF:mCherry) reporter line to verify changes of the Wnt signaling activity. Our results indicated that 10 μM IWR-1 administration for 24 hours resulted with decreased reporter activity (Figure 17).

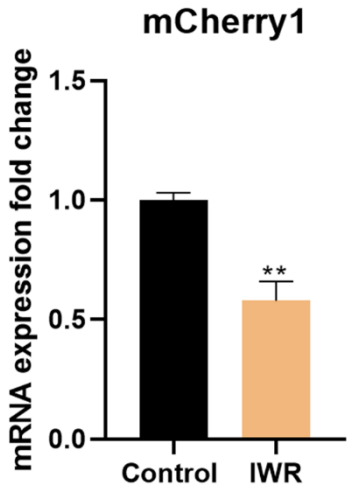

Figure 17: Relative expression changes in Wnt activity after IWR application. *Rpl13* was used as housekeeping gene. p≤0.05 (*), p≤0.01 (**), p≤0.001 (***), p≤0.0001 (****) and p>0.05 (n.s.). Error bars show standard deviation (SD).

4.1.7 Inhibition of the Wnt Signaling Alters Remyelination

Despite extensive research on how Wnt signaling regulates oligodendrocyte lineage cells, its role in remyelination remains controversial (Fancy et al., 2009; Guo et al., 2015; Xie et al., 2014). Next, we investigated how absence of the Wnt signaling affects the demyelination in remyelination. For this purpose, we compared myelin related gene expression changes with or with IWR-1. Results indicated that while there was significant decrease in myelin related gene expression at 1 dpi and 3 dpi in both groups, in remyelination stage, 7dpi, IWR administered group continue to express decreased levels of mbpa and 36K, two major myelin components in zebrafish (Figure 18-19).

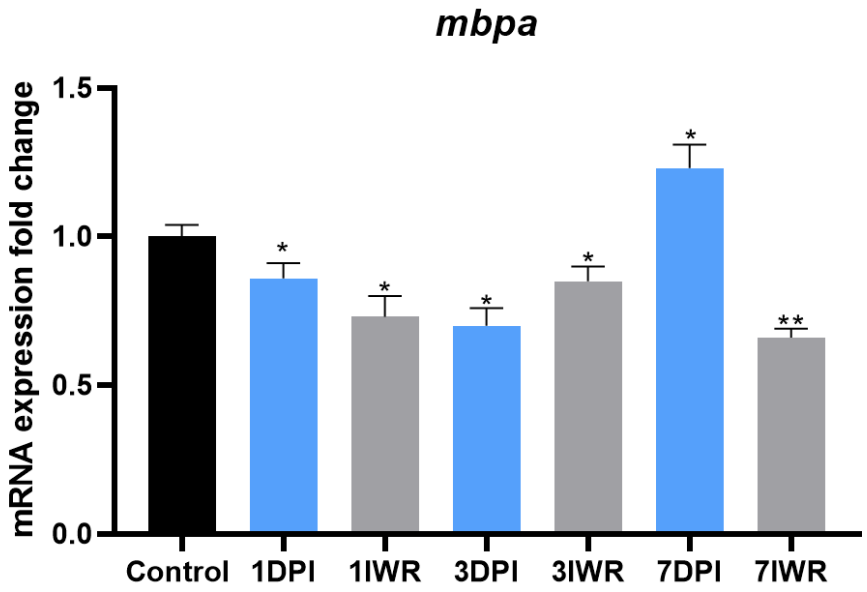

Figure 18: Relative expression changes in *mbpa* after IWR1 application. *Rpl13* was used as housekeeping gene. p≤0.05 (*), p≤0.01 (**), p≤0.001 (***), p≤0.0001 (****) and p>0.05 (n.s.). Error bars show standard deviation (SD).

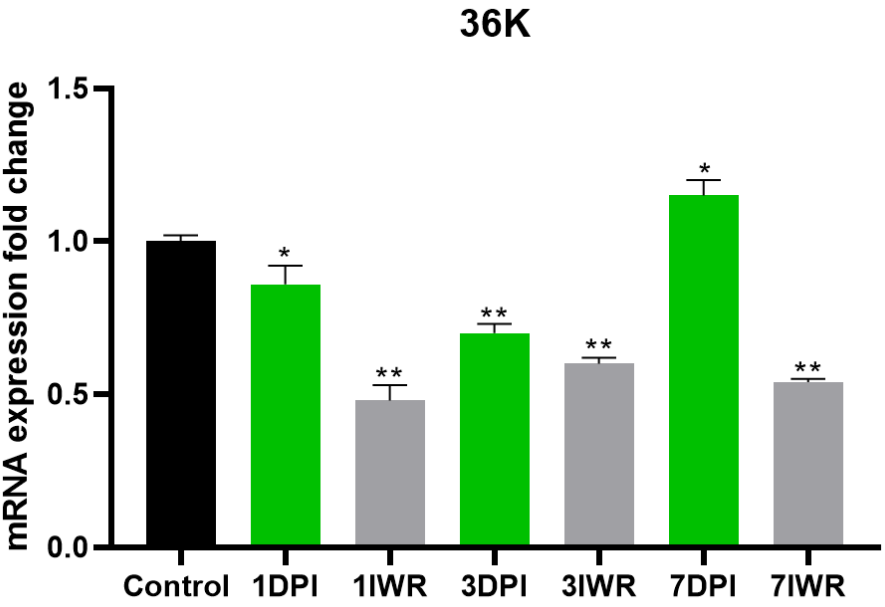

Figure 19: Relative expression changes in *36K* after IWR1 application. *Rpl13* was used as housekeeping gene. p≤0.05 (*), p≤0.01 (**), p≤0.001 (***), p≤0.0001 (****) and p>0.05 (n.s.). Error bars show standard deviation (SD).

Microglial response in demyelination plays pivotal role in the concept of debris clearence, disposal of the dead cells, clearing axonal cues. Therefore, we considered changes in the microglial marker *mpeg1.1* comparing presence of the IWR-1. Results showed that, 1dpi, *mpeg1.1* expression increased 2 folds and 3 folds in LPC injected and LPC injected/IWR administered groups, respectively. At 3 dpi, expression of *mpeg1.1* increased similarly. In the 7th day after injection, IWR treated group showed higher expression (Figure 20).

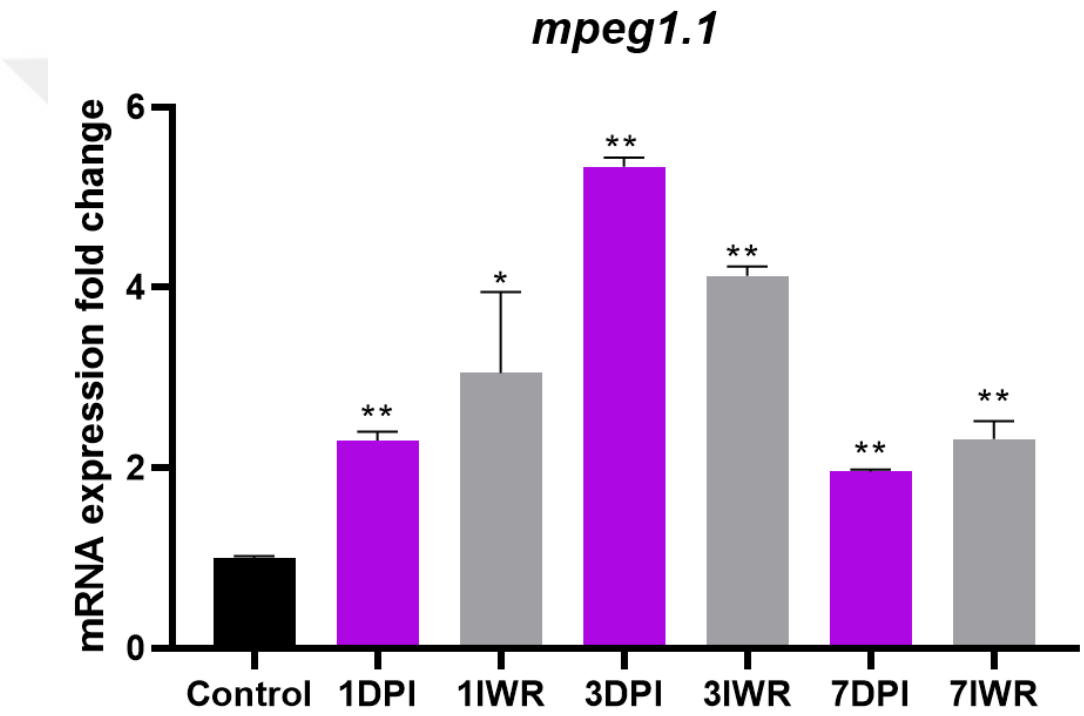

Figure 20: Relative expression changes in *mpeg1.1* after IWR1 application. *Rpl13* was used as housekeeping gene. p≤0.05 (*), p≤0.01 (**), p≤0.001 (***), p≤0.0001 (****) and p>0.05 (n.s.). Error bars show standard deviation (SD).

Finally, we investigated how oligodendrocyte lineage cell markers affected from IWR-1 presence. *Olig2* expression significantly increased, two-fold and 1.5-fold, respectively in the first day of injection. However, in the following stages inhibition of the Wnt pathway resulted with increased *olig2* expression (Figure 21).

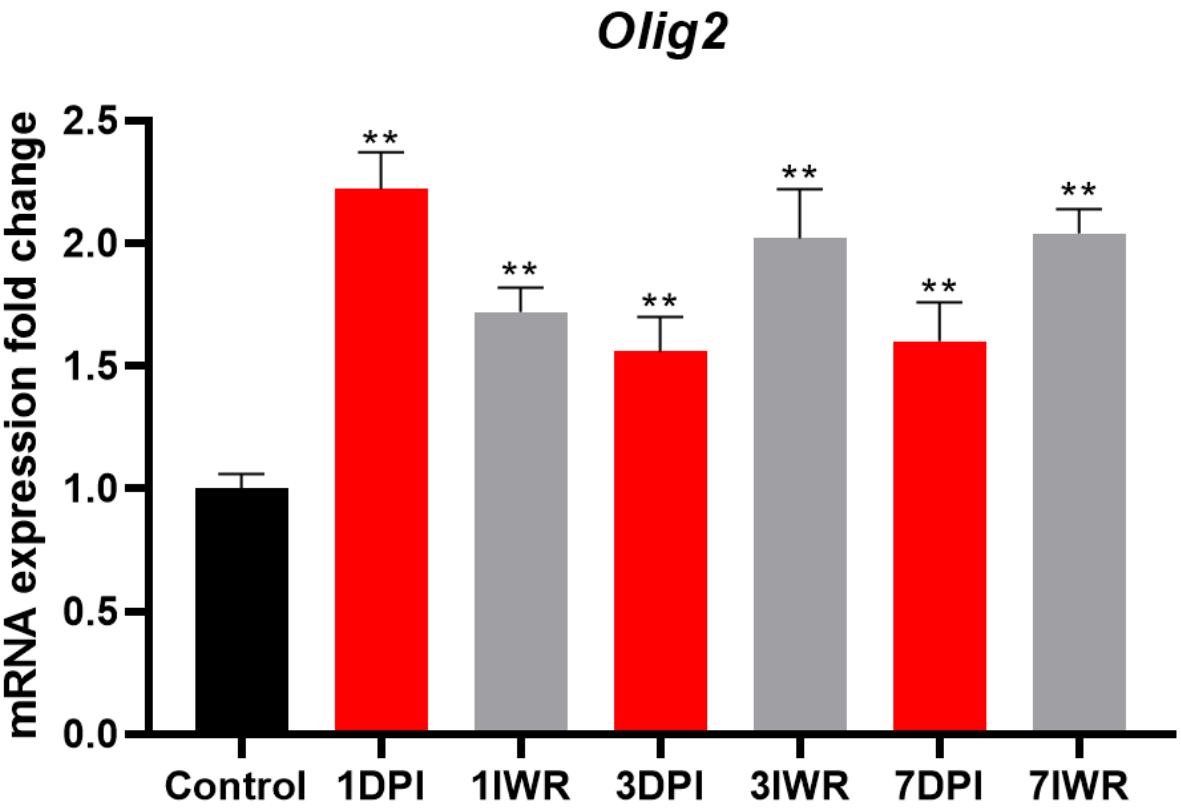

Figure 21: Relative expression changes in *olig2* after IWR1 application. *Rpl13* was used as housekeeping gene. p≤0.05 (*), p≤0.01 (**), p≤0.001 (***), p≤0.0001 (****) and p>0.05 (n.s.). Error bars show standard deviation (SD).

Furthermore, *sox10* expression were elevated 1.5-fold in the first day, however, showed no significant change in IWR-1 treated group. Interestingly, in the time course through the remyelination, *sox10* returned to control levels in the LPC injected groups, however, showed increased expression in IWR treated groups. Therefore, this data suggests that Wnt signaling promotes OPC to myelinating oligodendrocytes in zebrafish brain. Inhibition of the Wnt signaling results increased OPC related gene expression and failed remyelination.

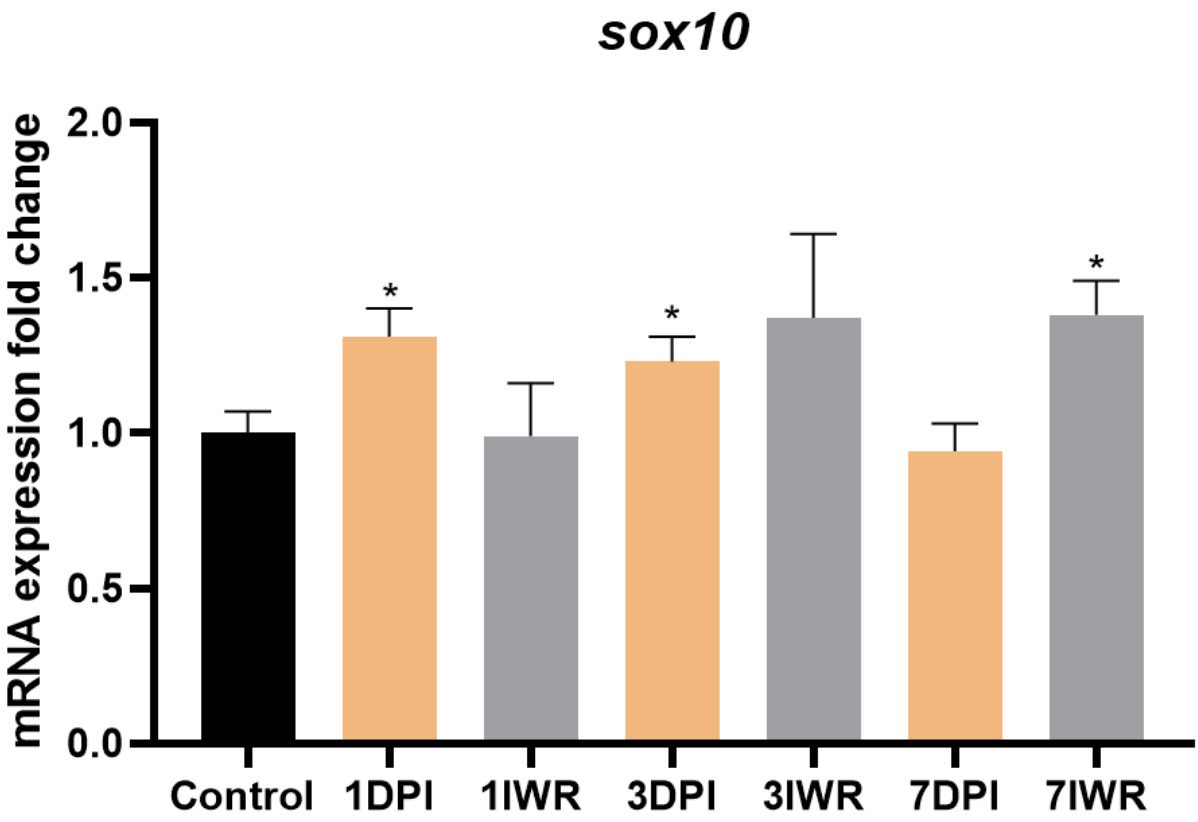

Figure 22: Relative expression changes in *sox10* after IWR1 application. *Rpl13* was used as housekeeping gene. p≤0.05 (*), p≤0.01 (**), p≤0.001 (***), p≤0.0001 (****) and p>0.05 (n.s.). Error bars show standard deviation (SD).

4.1.8 Comparative Proteomic Analysis

Next, to compare the molecular and cellular events that demyelinating and remyelinating stages, we compared proteome profiles of damage and regeneration timepoints in detail. Comparison analysis revealed 625 differentially expressed proteins in demyelination (3 DPI) and 725 differentially expressed proteins in remyelination (7dpi) (Figure 23).

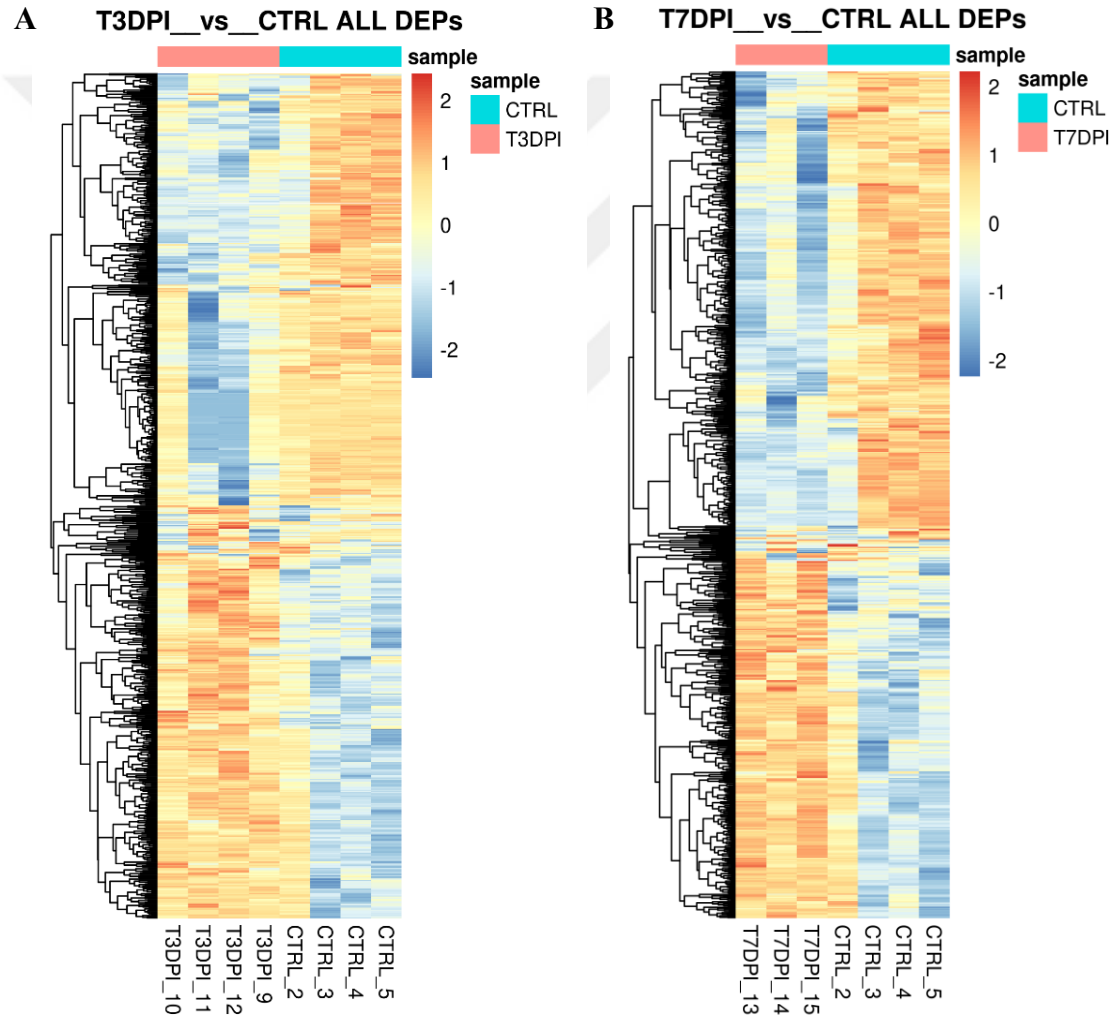

Figure 23: Differentially expressed proteins in demyelinating remyelinating stages.

(A) Differentially expressed proteins in demyelination. (B) Differentially expressed proteins in remyelination.

Next, we investigated enriched KEGG pathways to decipher cellular events in demyelination and remyelination. Our analysis revealed, neurodegenerative disease related responses were enriched in both groups (Figure 24). Oligodendrocyte lineage cells including OPCs and mature oligodendrocytes and myelination have been associated with context of neurodegenerative diseases such as Alzheimer's Disease, Parkinson's disease and Huntington's Disease (Bardile et al., 2019; Ettle et al., 2016; Papuc & Rejdak, 2020).

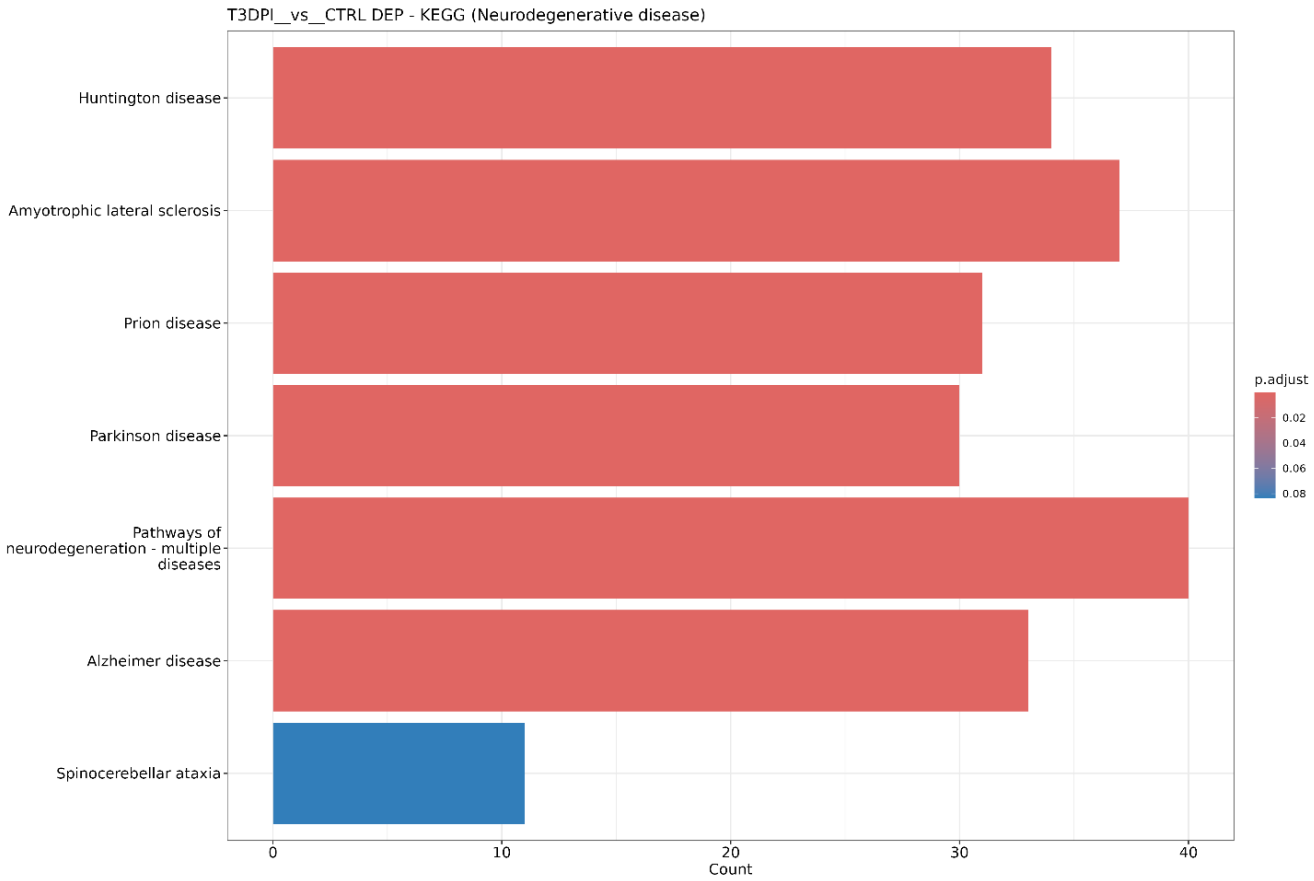

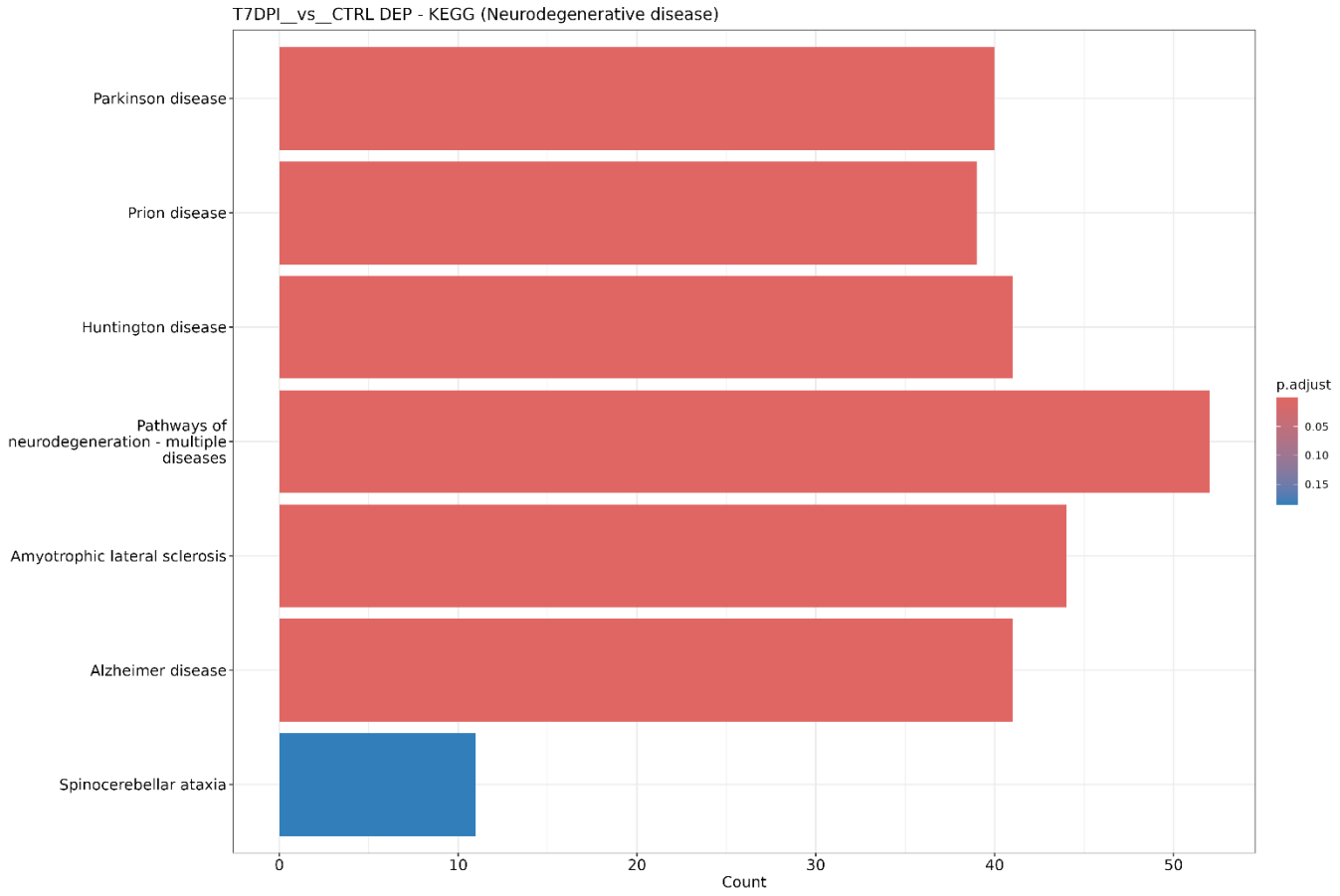

Figure 24: KEGG pathway analysis shows enriched neurodegenerative disease response in both degeneration and regeneration groups.

Myelin structure consist of several proteins, lipids and proteolipids such as myelin protein zero (mpz), myelin basic protein (mbp), sphingomyelin, cholesterol (Madeira et al., 2022; Verplank et al., 2022). KEGG pathway analysis revealed enriched proteosome and endoplasmic reticulum activity in demyelination (Figure 25).

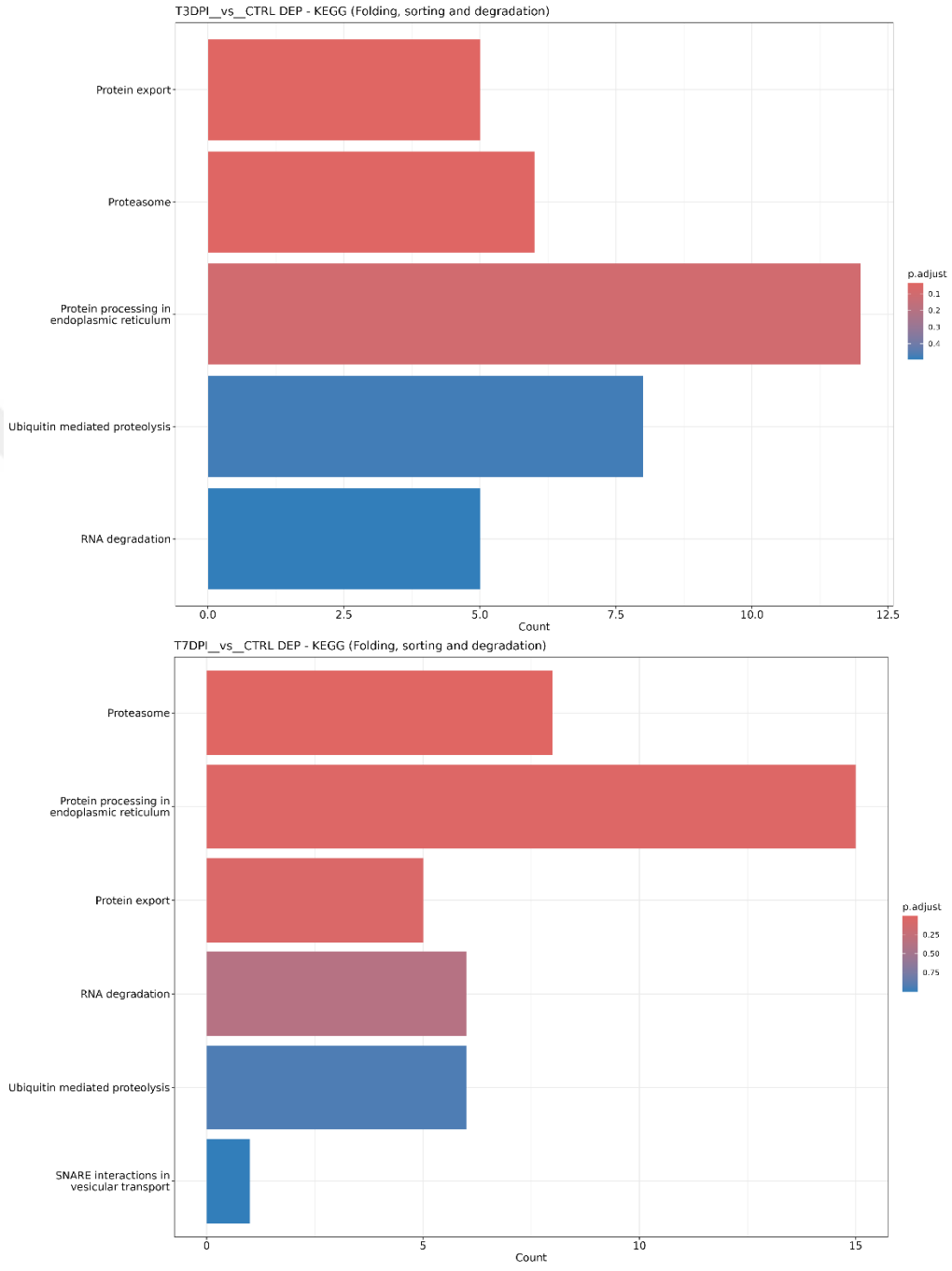

Figure 25: KEGG pathway enrichment revealed increased proteosome and endoplasmic reticulum activity in remyelination

Furthermore, fatty acid degradation was significantly enriched in demyelination stage, however, declines throughout the remyelination process and fatty acid biosynthesis were enriched in remyelination. Overall, our data suggest that demyelination and remyelination successfully occurred in our new model of adult zebrafish brain.

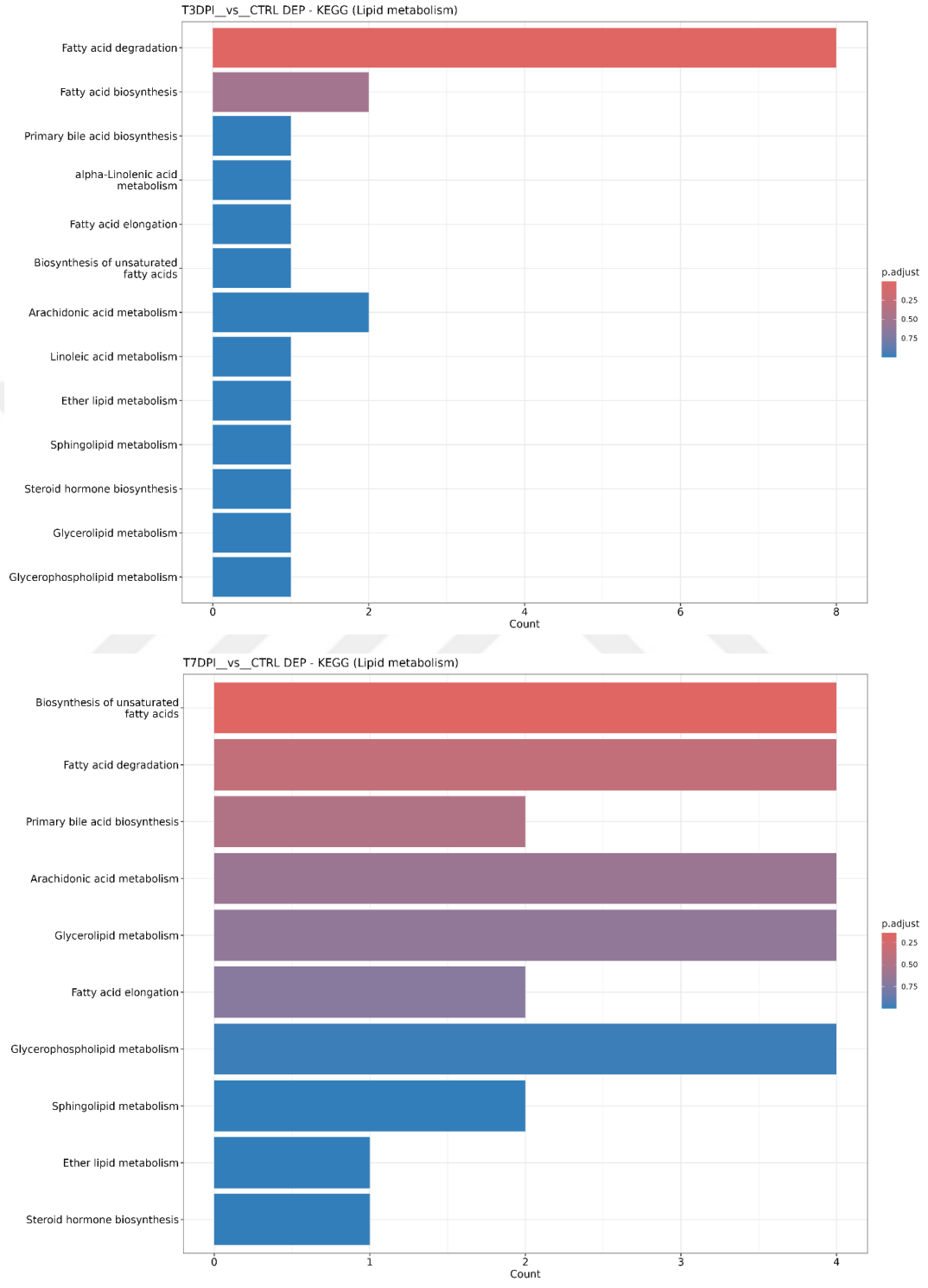

Figure 26: KEGG pathway enrichment revealed katabolic lipid process in demyelination and anabolic lipid activity in remyelination.

Next, to investigate how inhibition of Wnt signaling pathway altered remyelination we compared the proteome profiles of the demyelination and remyelination stages with or without presence of the Wnt inhibitor, IWR-1. First, we determined differentially expressed proteins for each event (Figure 27, 28).

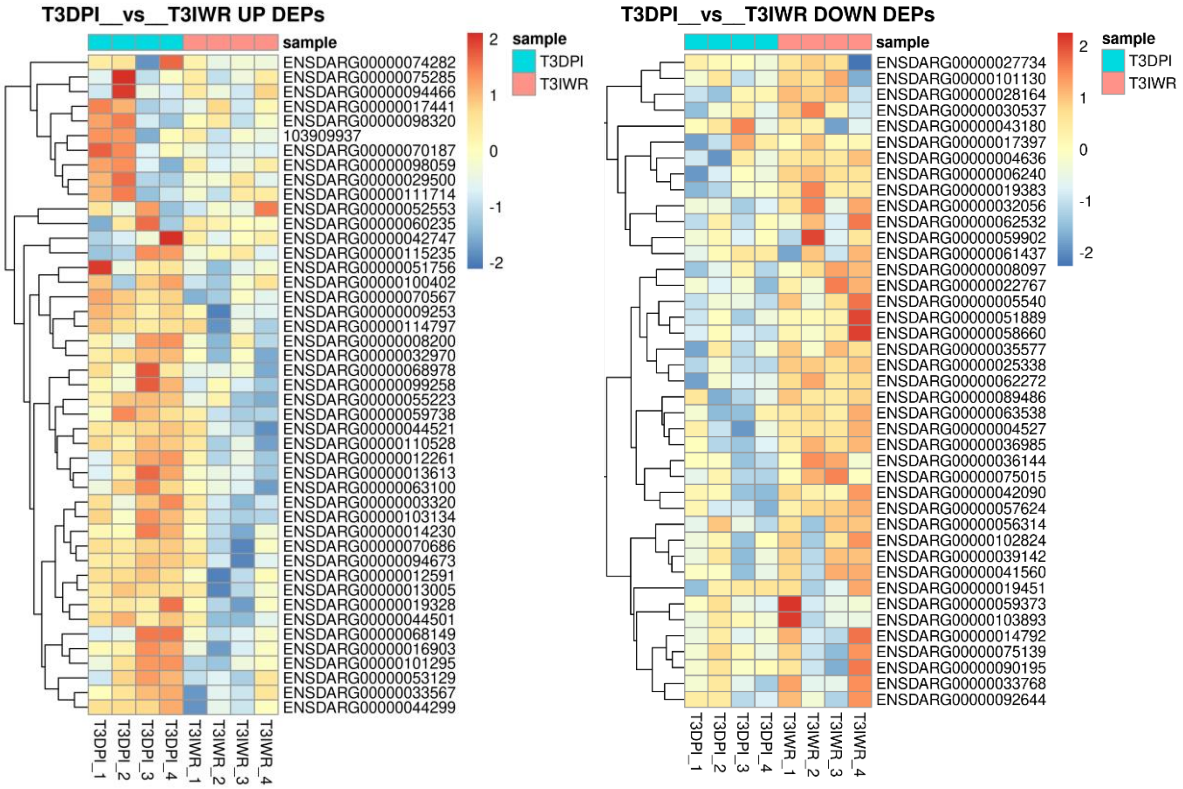

Figure 27: Differentially expressed proteins in comparison of presence of the Wnt inhibitor at demyelination.

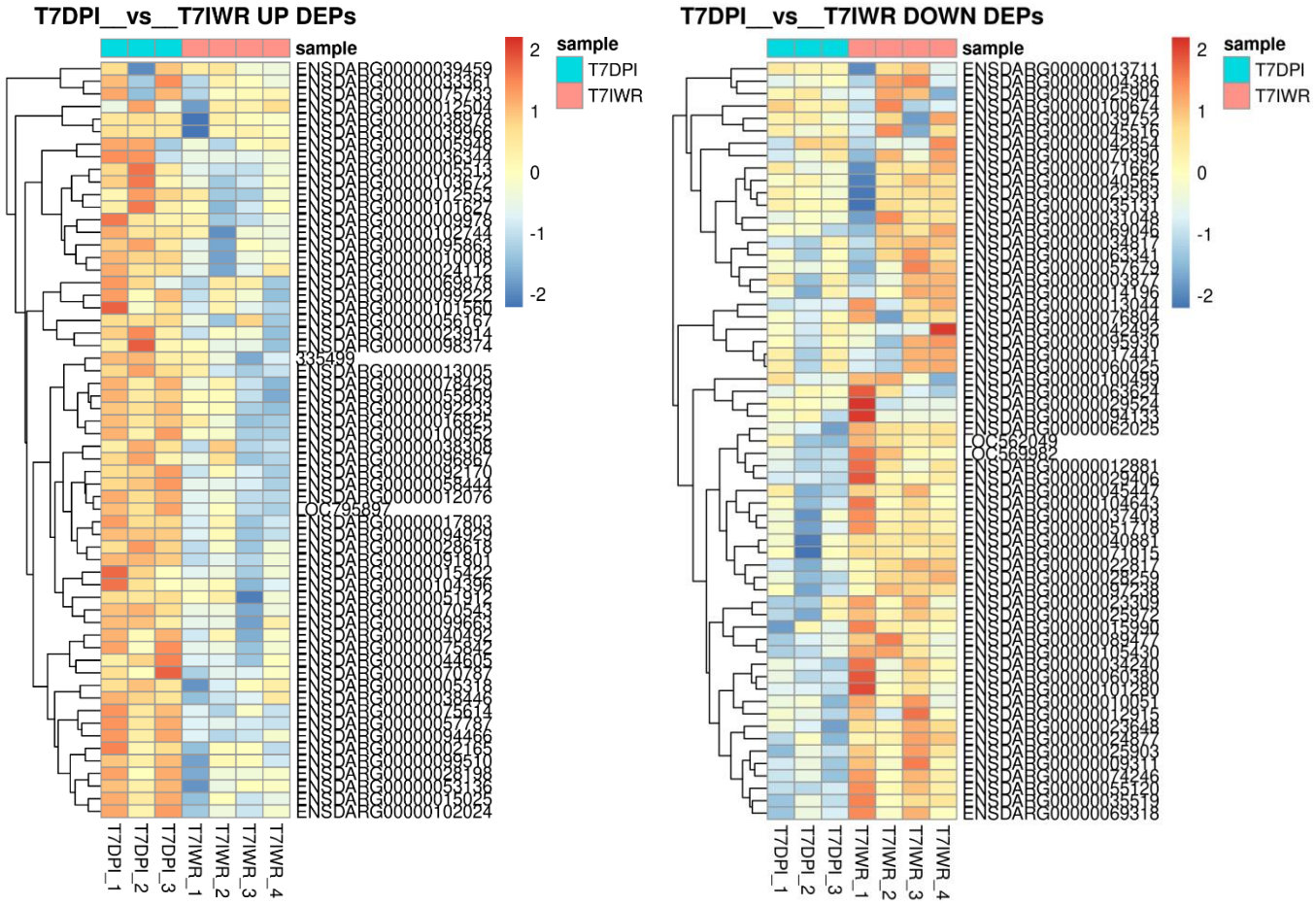

Figure 28: Differentially expressed proteins in comparison of presence of the Wnt inhibitor at remyelination.

Next, we performed GO:Term enrichment analysis to reveal which processes affected by presence of the IWR-1 and caused altered remyelination. Analysis revealed that, inhibition of the Wnt pathway caused downregulated lipid metabolism and upregulated macroautophagy (Figure 29-30)

.

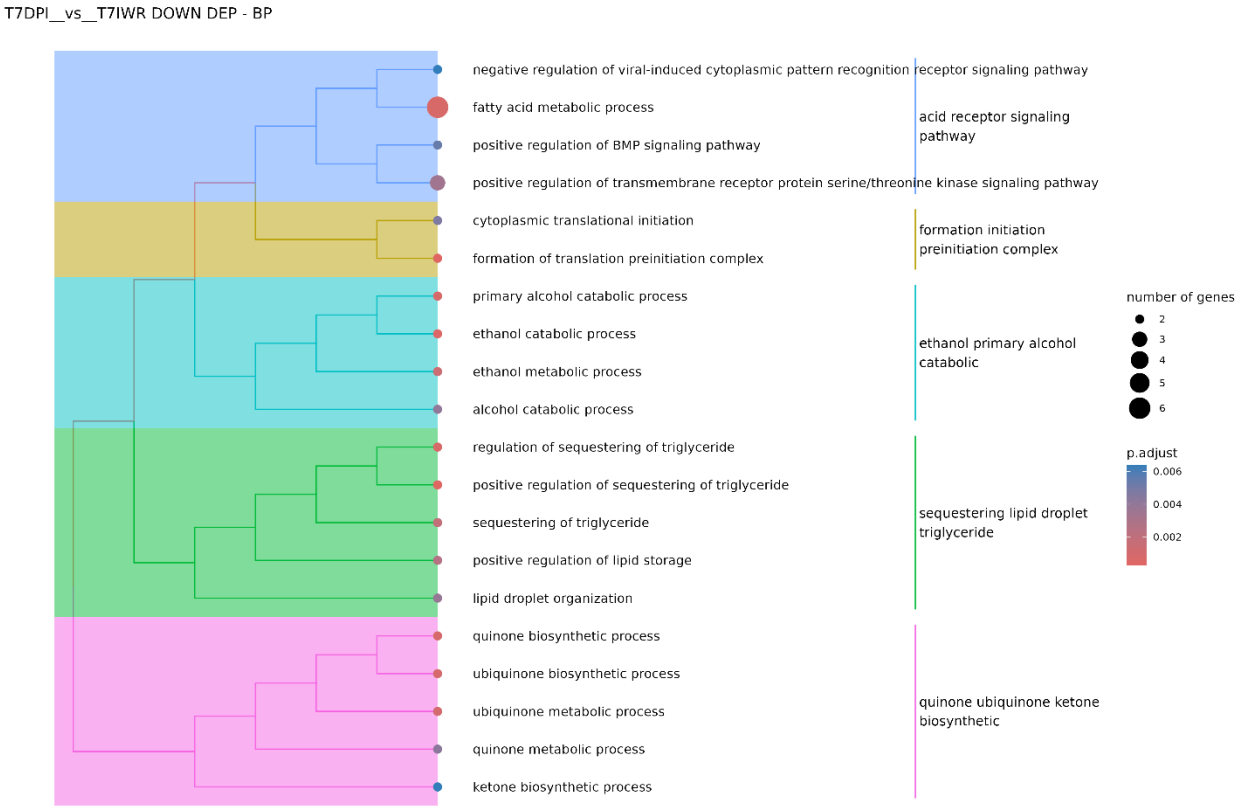

Figure 29: GO:Term enrichment analysis revealed fatty acid metabolism downregulation

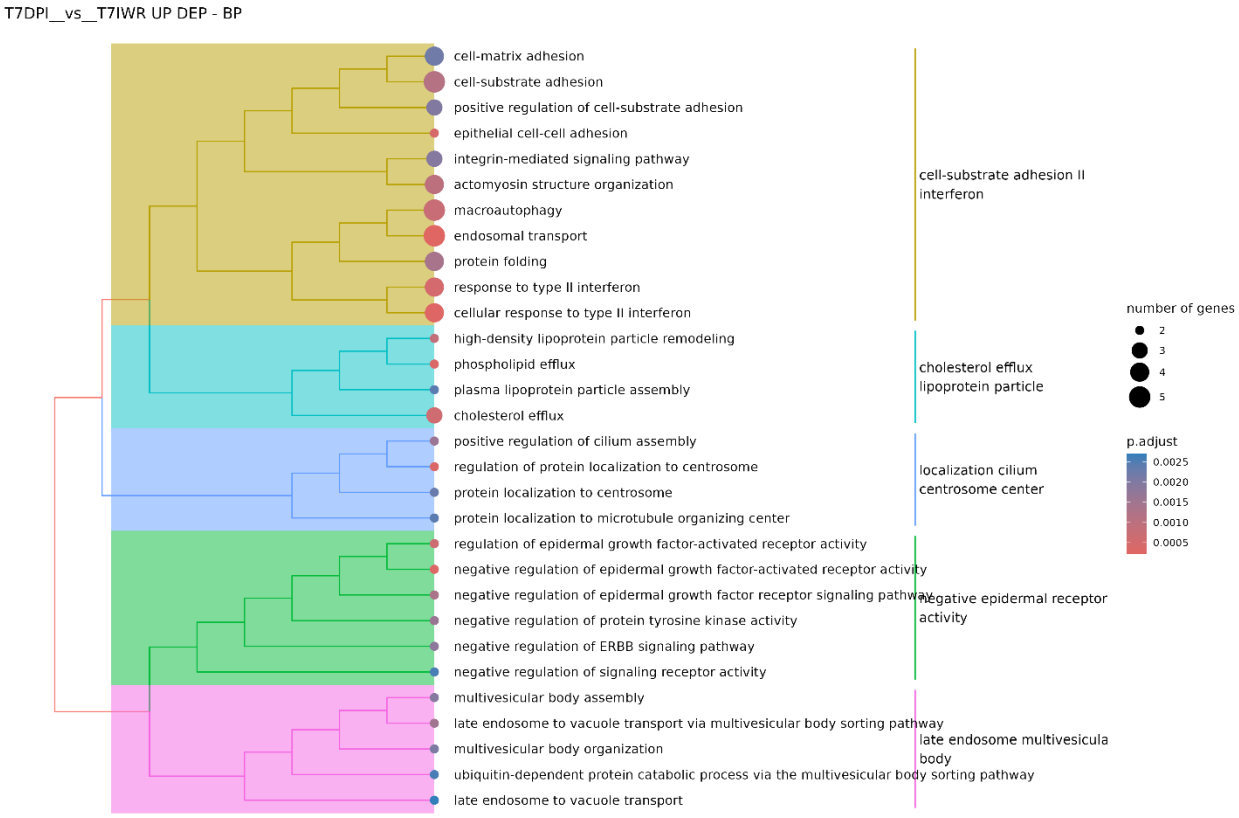

Figure 30: GO:Term enrichment analysis revealed macroautophagy upregulation

4.2 Chapter 2: Cancer and Regeneration

4.2.1 Generation of Glioma Model

The Tol2 transposase system was employed to develop a zebrafish glioma model. This involves injecting a plasmid with Tol2 enzyme cutting sites and Tol2 mRNA into single-cell embryos, leading to genomic integration. The resulting F0 line exhibits mosaic transgene expression, necessitating breeding with wild types to produce a stable F1 line (Kwan et al., 2007; Suster et al., 2009).

First, we developed a plasmid which expresses an oncogene HRasG12V along with eGFP under GFAP promoter. In this structure included Tol2 incision sites 5' and 3' of the target sequence (Figure 31). Following, single cell injection, fish were screened for mosaic expression of eGFP signal in central nervous system. Positive fish raised to adulthood. To generate stabile transgenic line, F0 (Founder Fish) were crossed with wild-type animals. Their offspring (F1) initially screened for GFP signal and positive fish were raised to adulthood.

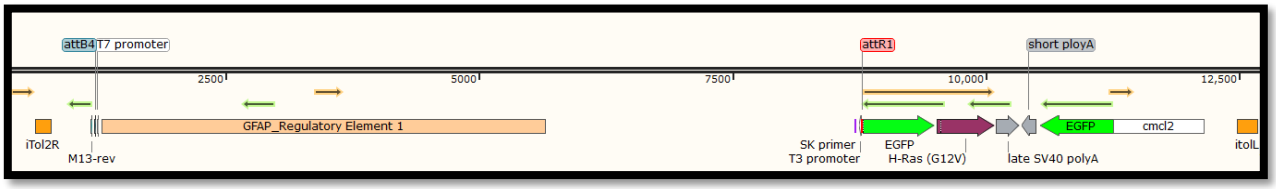

Figure 31: Plasmid design of the glioma model

However, after 6 months F1 fish show problematic eye development. Morphological examine show that fish have overgrown eye tissue, along with blindness (Figure 32).

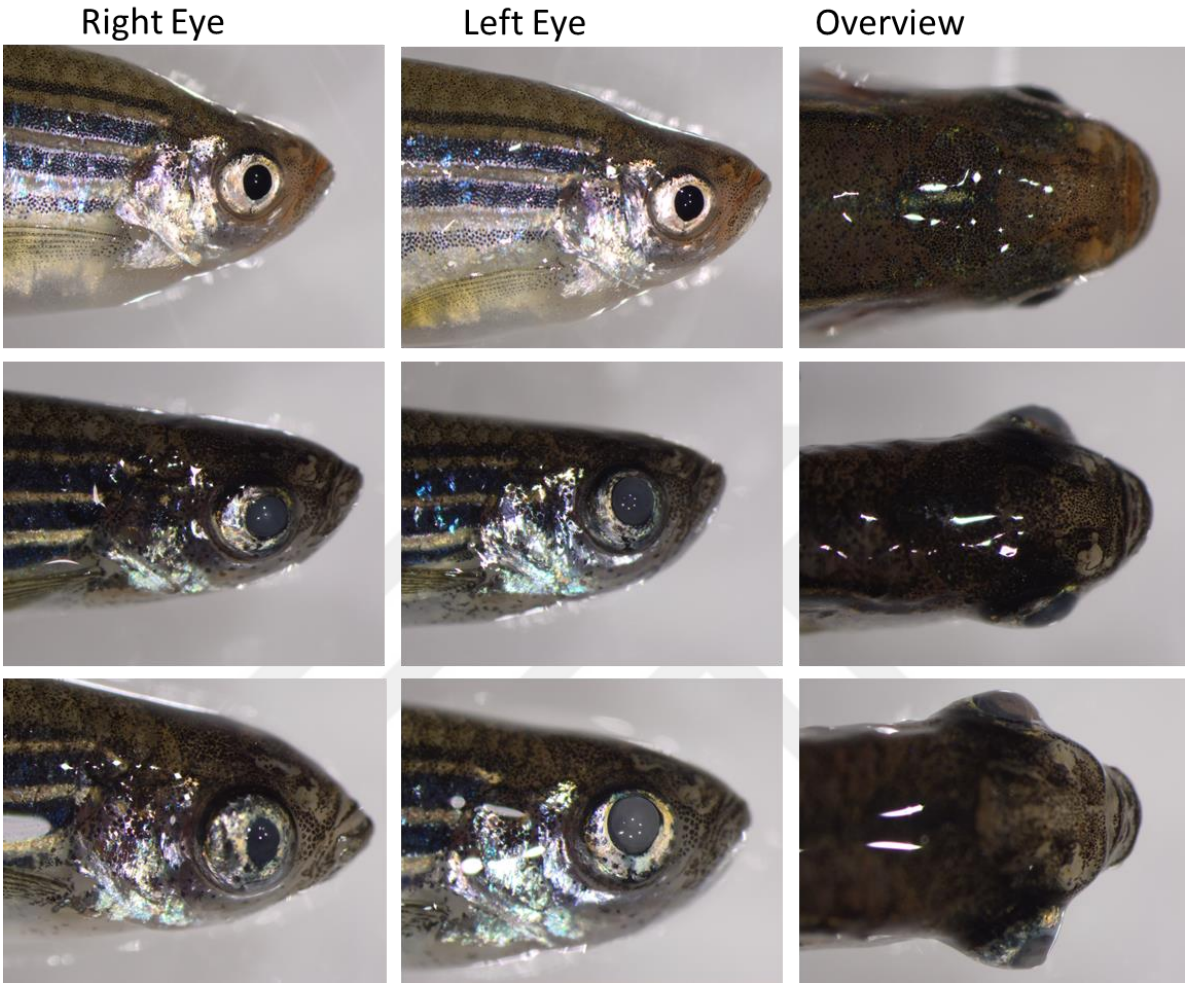

Figure 32: F1 stable line expressing HRasG12V under GFAP promoter show deficit eye development

4.2.2 Gal4:UAS System for Glioma Developing Fish

Failure of previous system, lead us to another established glioma model. This model utilizes Tol2 editing system with Gal4:UAS interaction to induce expression of target oncogenes under the UAS promoter in the driver line. In this system zic4 used as promoter due to its expression in prolific regions of the nervous system and Gal4 is under control of the zic domain. To validate with imaging, mCherry expression is present. Under UAS promoter, $HRasV^{12}$ oncogene is used to generate to tumor formation in the zebrafish brain (Mayrhofer et al., 2017).

First, single cell injection of UAS:HRasV^{12} plasmid along with Tol2 mRNA performed. Fluorescence imaging showed somatic expression of the GFP signal distributed in several regions of the brain spinal cord (Figure 33). Therefore, results suggest that potential neoplasia would develop these regions.

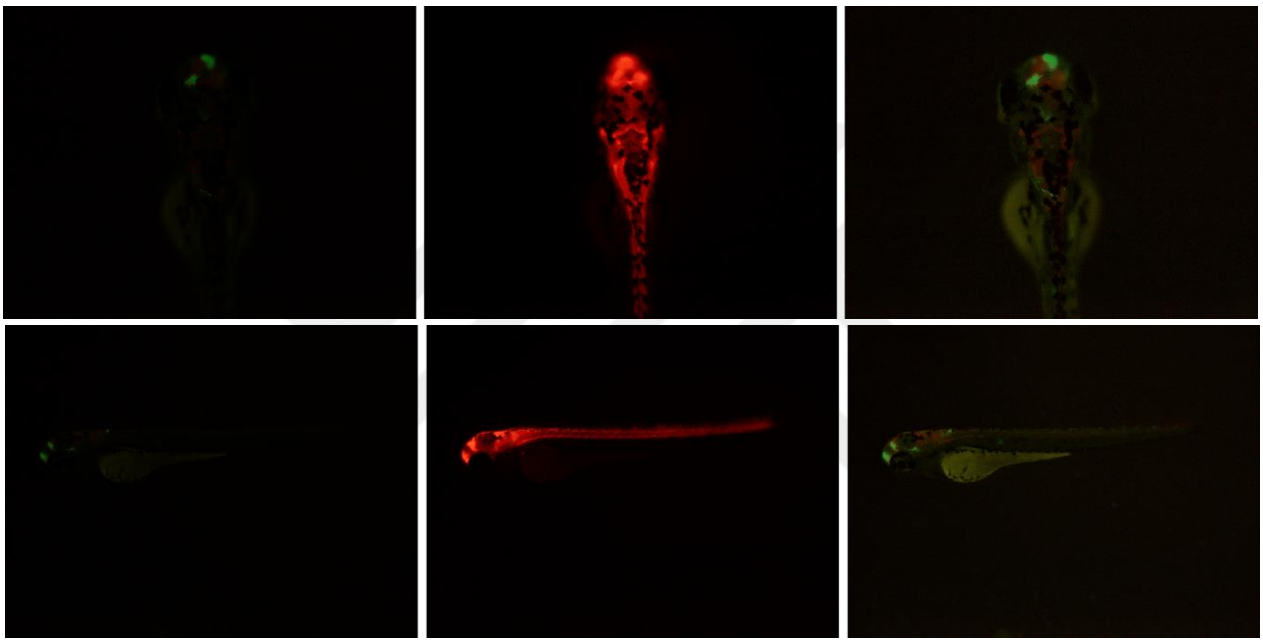

Figure 33: Somatic GFP expression of mutant HRasV12

Next, following fluorescent identification of the expression of GFP signal, positive fish were selected and raised to adulthood. Survival rate was 35-40% for the somatic expression of the HRasV12. Most of the fish developed anomalies along their brain and spinal cord area (Figure 34). These data suggest that mutant HRas expression under the zic promoter causes the development of malformations in the central nervous system

Figure 34: 3 months old mutant fish images

(A) Control fish, (B) Mutant fish 1, (C) Mutant fish 2. Mutant fish shows abnormalities around head including growth, and spinal cord malformations

Next, 3 months old fished validated once again with fluorescence microscopy before telencephalon isolation for bulk RNA sequencing. Images shows both mCherry and GFP signal were present, therefore confirms mutant fish. Furthermore, exposed telencephalons showed abnormal growth (Figure 35).

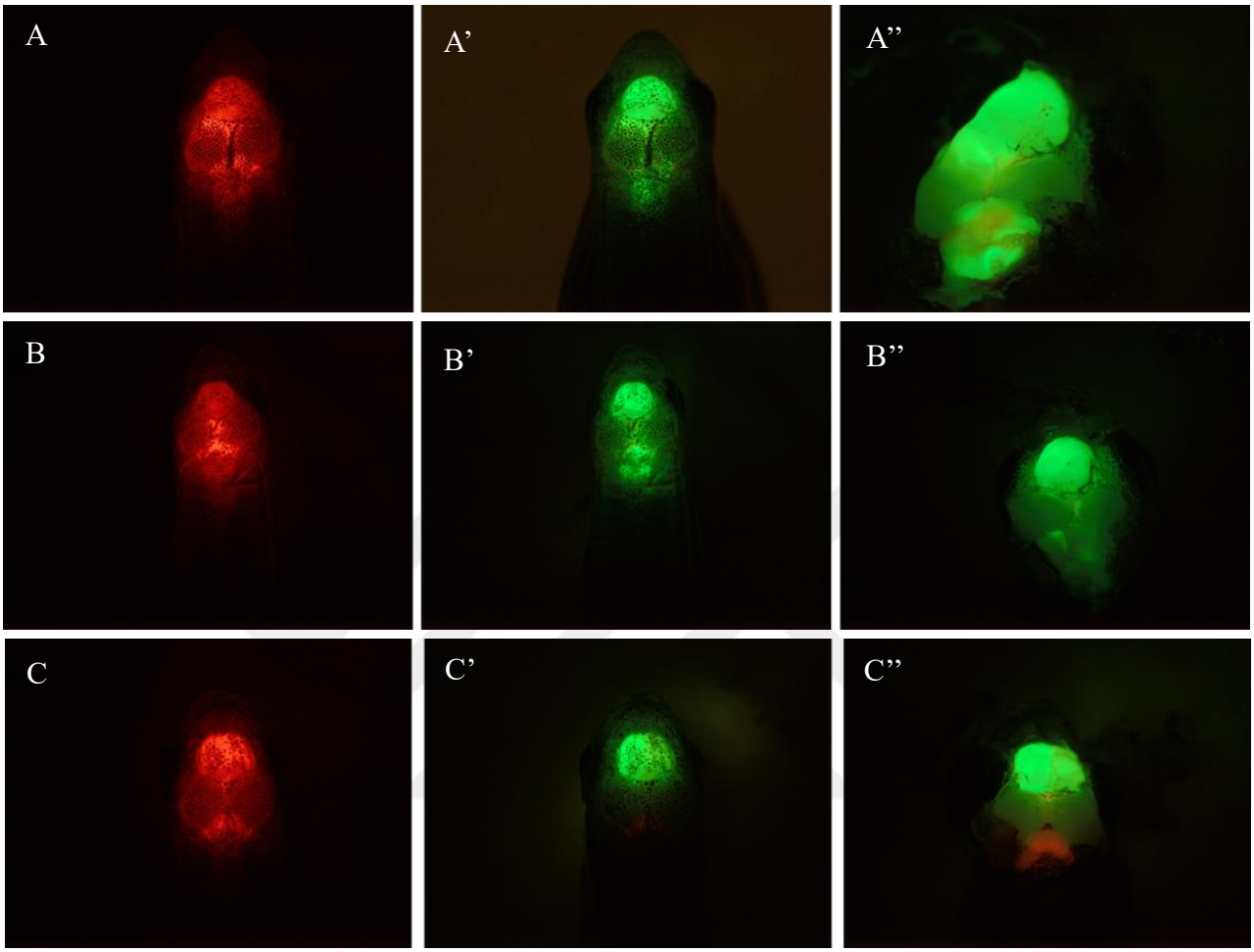

Figure 35: Verification of the samples prepared for RNA Seq analysis

A, B, C shows mCherry signal of sample 1, 2, 3 respectively. A', B', C' shows GFP signal of sample 1, 2, 3 respectively. A'', B'', C'' shows exposed telencephalon and GFP signal of sample 1, 2, 3 respectively.

Next, we isolated RNA from each sample for RNA sequence analysis. For each telencephalon 20µg/uL RNA were used. Then, forwarded to sequencing unit for library preparation (Figure 36).

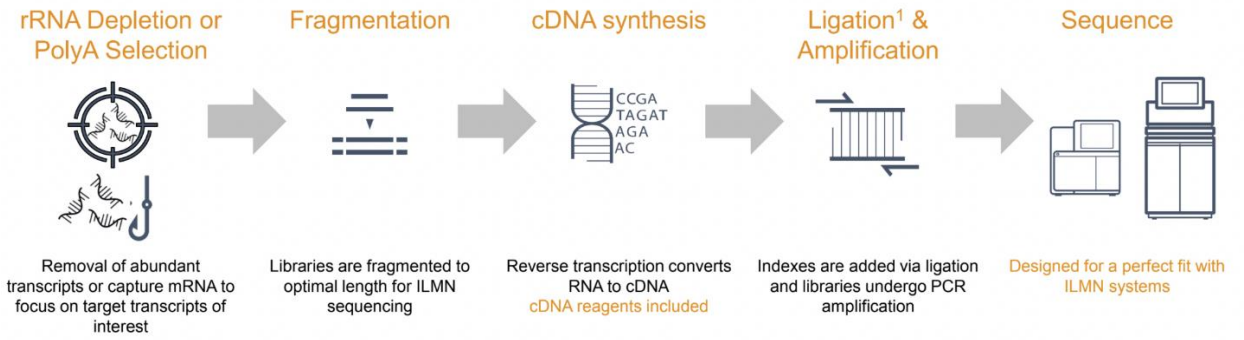

Figure 36: Representative image of library preparation steps (Adapted from Refgen).

Multidimensional scaling (MDS) or principal component analysis (PCA) plotting is one of the approaches that provides the best understanding of profile similarities for gene expression analysis between samples. These visualization approaches enable the visualization of similarities and differences between samples without prior knowledge (unsupervised analysis). Thus, one can have an idea of the extent to which differential expression can be detected before further analysis is performed (Figure 37).

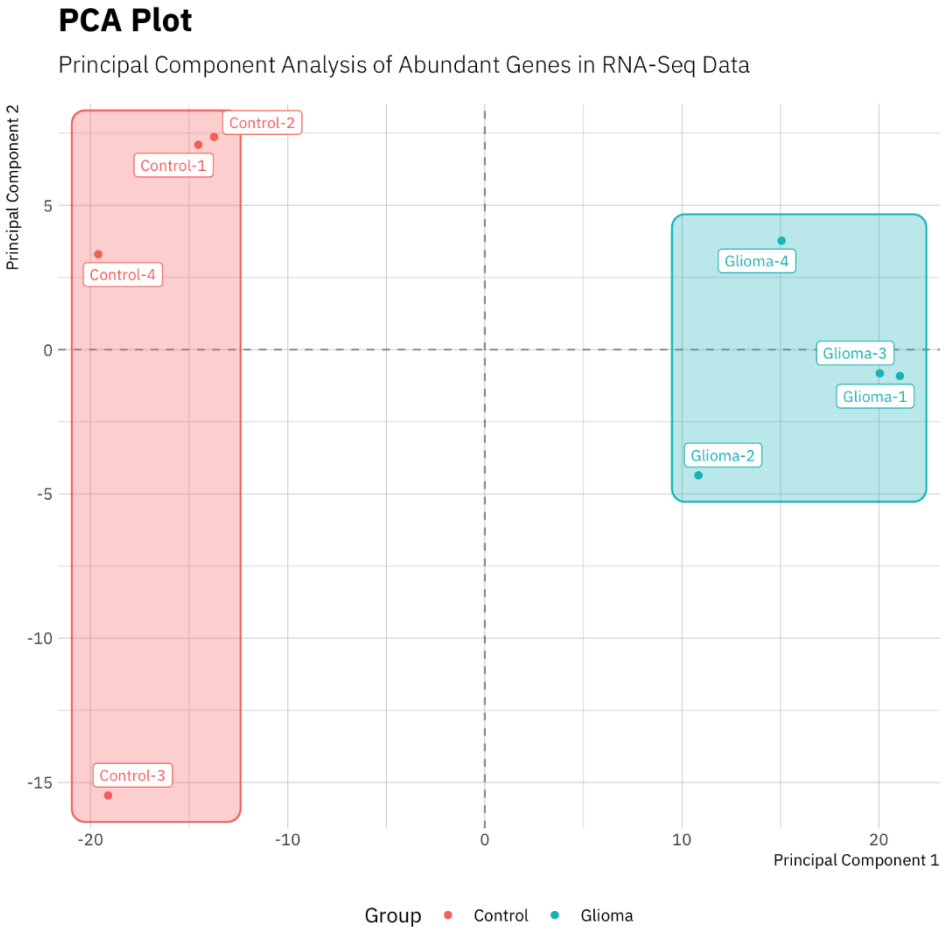

Figure 37: Distribution of samples in PC1 and PC2 planes after PCA

The heatmap shows the expression profiles of the top 50 genes that show the most variation between samples. The samples and genes in the heat graph were clustered on both axes according to their profile similarities, and the similarities were visualized with dendrograms. In the heat plot, only protein-coding genes are included (Figure 38).

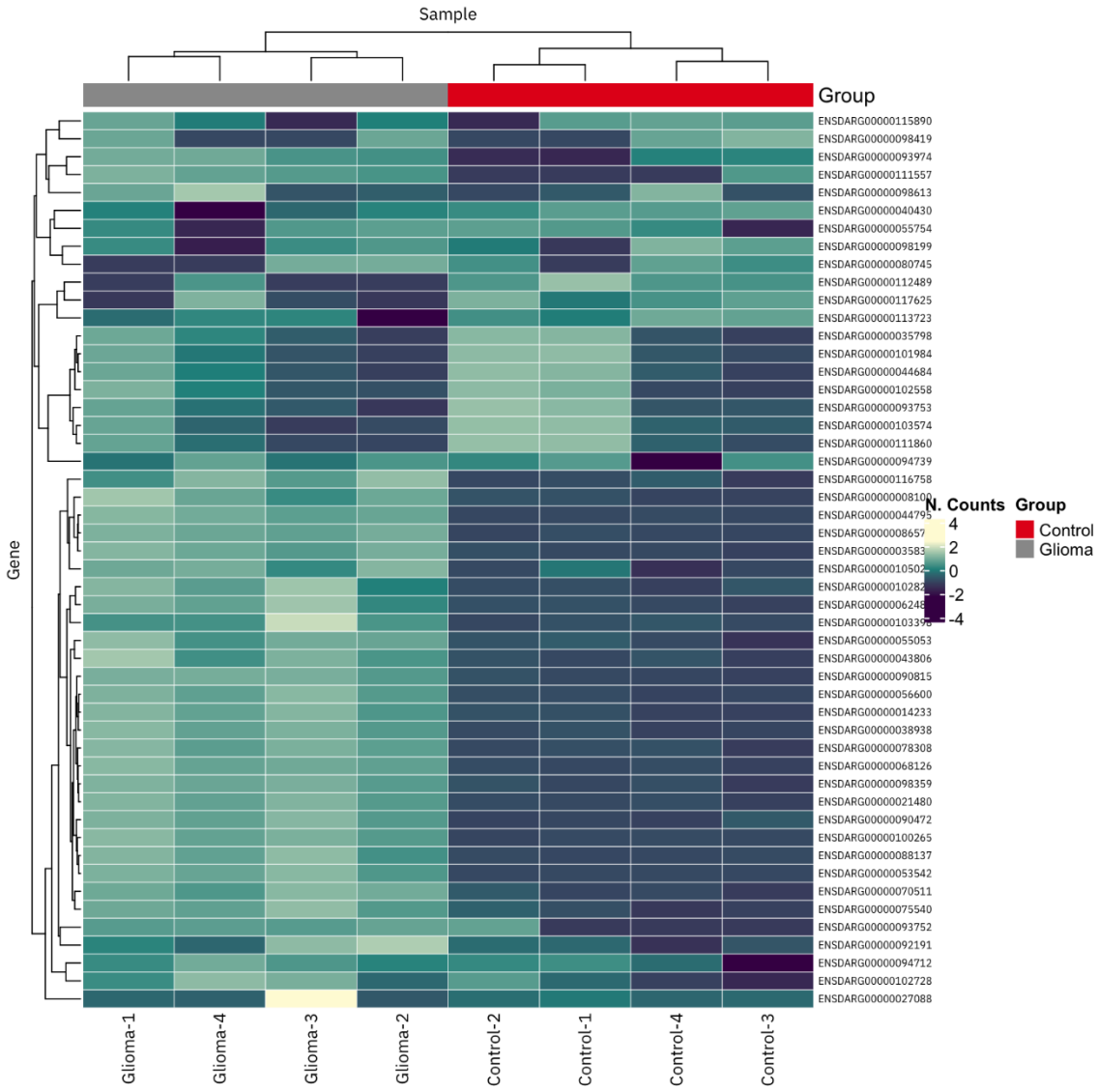

Figure 38: Expression profile of the top 50 genes showing the most variation between samples

The distributions of all genes according to logFC and FDR values are visualized with volcano representation. Each dot on the graph represents a gene. If present, dots in red indicate genes with statistically significant (FDR<0.05) differences between the two groups (Figure 39).

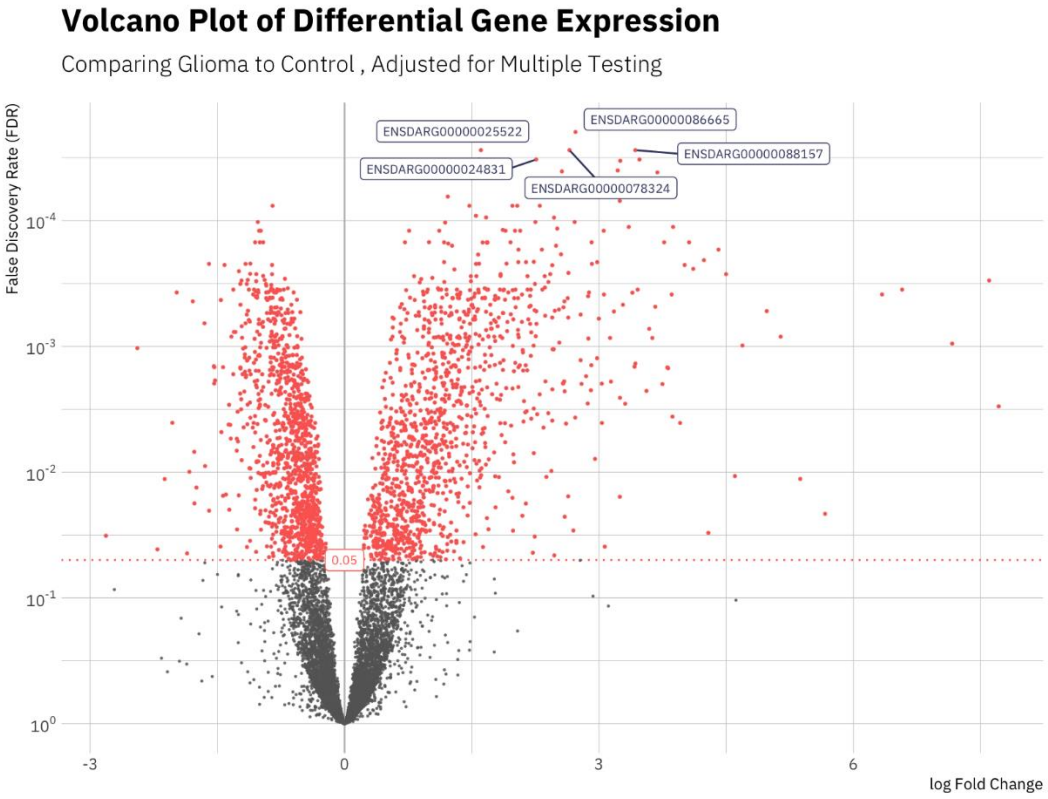

Figure 39: Volcano plot representation of genes showing the most significant variation

4.3 Chapter 3: Human Disease Modelling of Identified Novel Variants

4.3.1 Determination of the Novel Missense Variant Mutation

This study focused on an Iranian family exhibiting an autosomal dominant inheritance pattern. The affected members experienced late-onset symptoms of left ventricular noncompaction (LVNC) typically manifesting in their third decade of life. Notably, one offspring presented with the LVNC phenotype and passed away at the age of 12 (Figure 40).

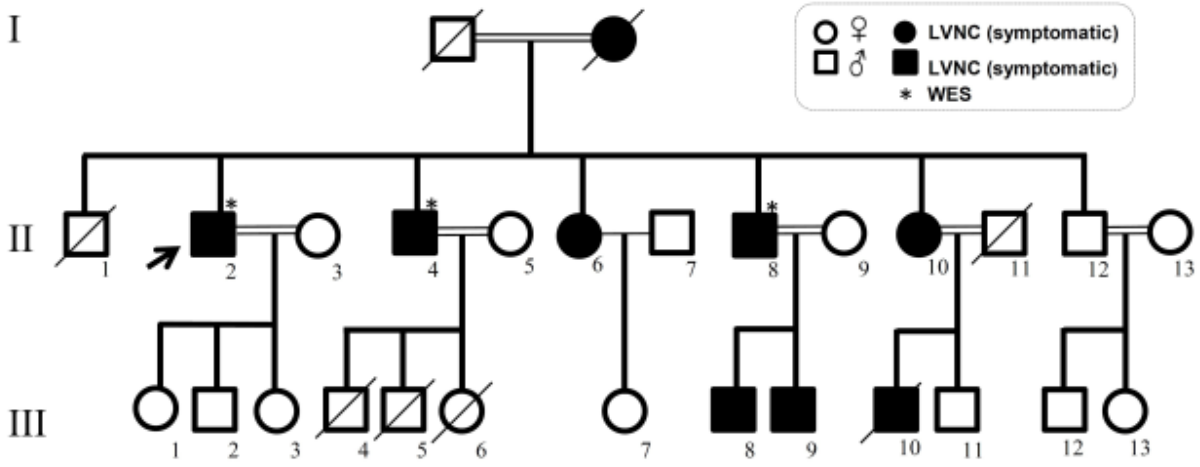

Figure 40: Pedigree analysis and clinical presentation of left ventricular non-compaction (LVNC) in the study's affected participants.

Whole genome sequencing (WGS) is a comprehensive technique for examining the entire DNA sequence of an organism's genome simultaneously. This method sequences both chromosomal DNA and mitochondrial DNA, providing an in-depth, base-level perspective of the genome. WGS facilitates the identification of genetic variations such as single nucleotide polymorphisms (SNPs), insertions, deletions, and large structural variants. This granularity is essential for elucidating the genetic underpinnings of diseases, evolutionary processes, and population genetics. Advances in next-generation sequencing (NGS) technologies have markedly reduced the cost and time for WGS, enhancing its availability for clinical and research use, thus enabling precise diagnostics and personalized medicine (Goodwin et al., 2008; Mardis, 2008)

Whole-exome sequencing (WES) was conducted on the Illumina NovaSeq platform, yielding paired-end reads of 150 base pairs with an average coverage of 100X in the three affected individuals. A novel non-synonymous MYH7 variant (c.1963C>A:p.Leu655Met, GenBank: NM_000257) was identified (Figure 41 A,B).

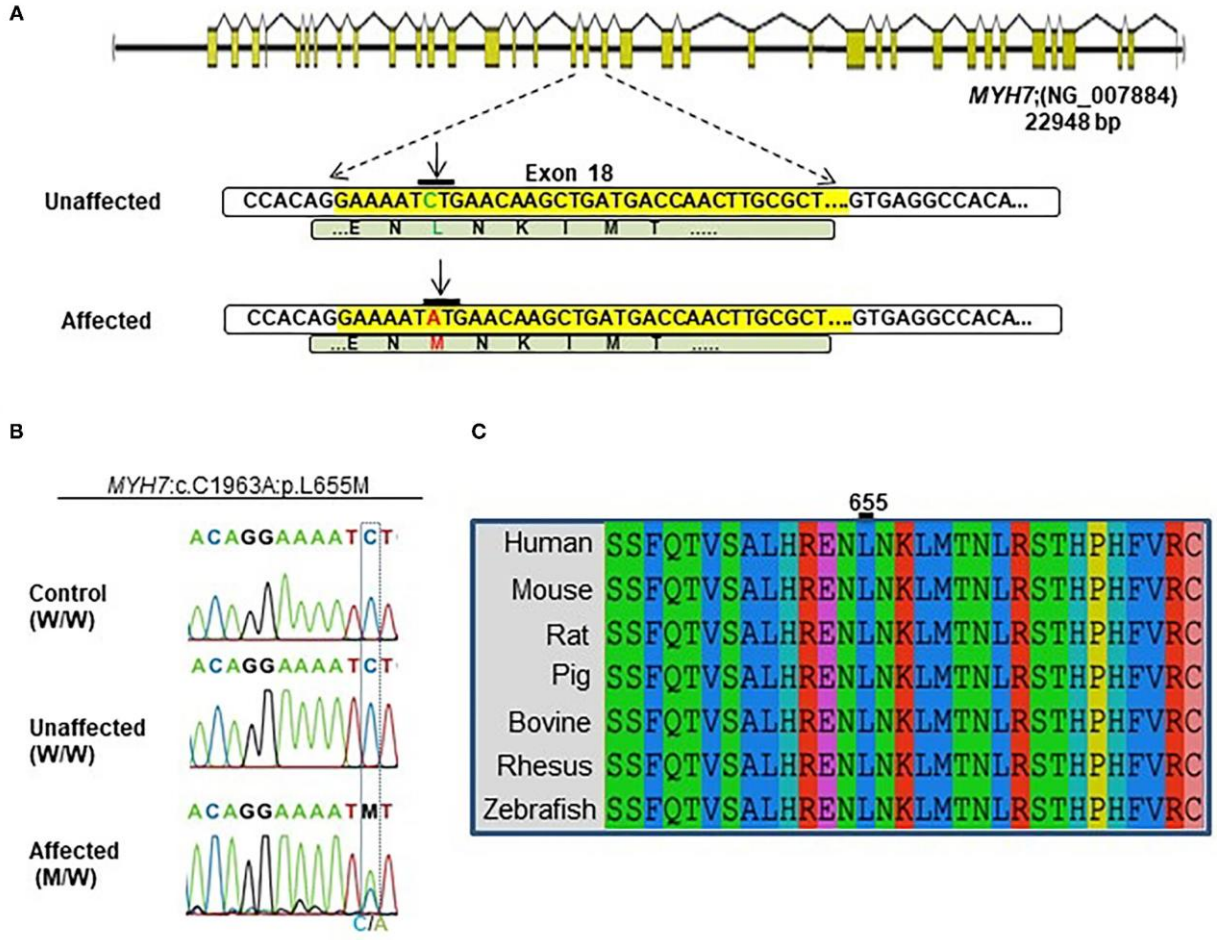

Figure 41: Detection of the MYH7 heterozygous variant was accomplished in a specific Iranian familial cohort. (A) Presentation of the variant in the human genome. (B) Identification of the variant in the from affected, unaffected, and control. (C) The evolutionary conservation of the MYH7 actin-binding domain indicates its high degree of preservation across species.

The MYH7 gene is highly conserved among species, known as the myosin heavy chain beta (MHC-β) which is classified as a type I fiber and also known as slow-twitch fiber. This protein is a critical component of sarcomeric structure and has several interactions with other key proteins such as actin TNN, MYBPC3 (Figure 41C).

4.3.2 Generating *myh7* Knockout Zebrafish

To investigate the how (c.1963C>A:p.Leu655Met, GenBank: NM_000257) mutation affect the zebrafish heart development, we take advantage of clustered regularly interspaced short palindromic repeats/CRISPR associated protein 9 (CRISPR/Cas9) gene editing system. We designed a specific single-guide RNA (sgRNA) to target exon 18, mirroring the locus of the missense mutation identified in patients. Post-microinjection of the ribonucleoprotein (RNP) complex, we conducted daily observations of the embryos using a stereomicroscope. Notably, from 3 days post-fertilization (dpf), the majority of embryos exhibited a pronounced phenotype. This methodology allowed us to precisely model the mutation's effects and facilitated a detailed analysis of the resulting developmental anomalies in zebrafish. Through this approach, we elucidated the molecular mechanisms underpinning the observed cardiac defects, thereby contributing to a deeper understanding of the mutation's role in heart development (Figure 42). This study highlights the utility of CRISPR/Cas9 technology in generating accurate genetic models for developmental research.

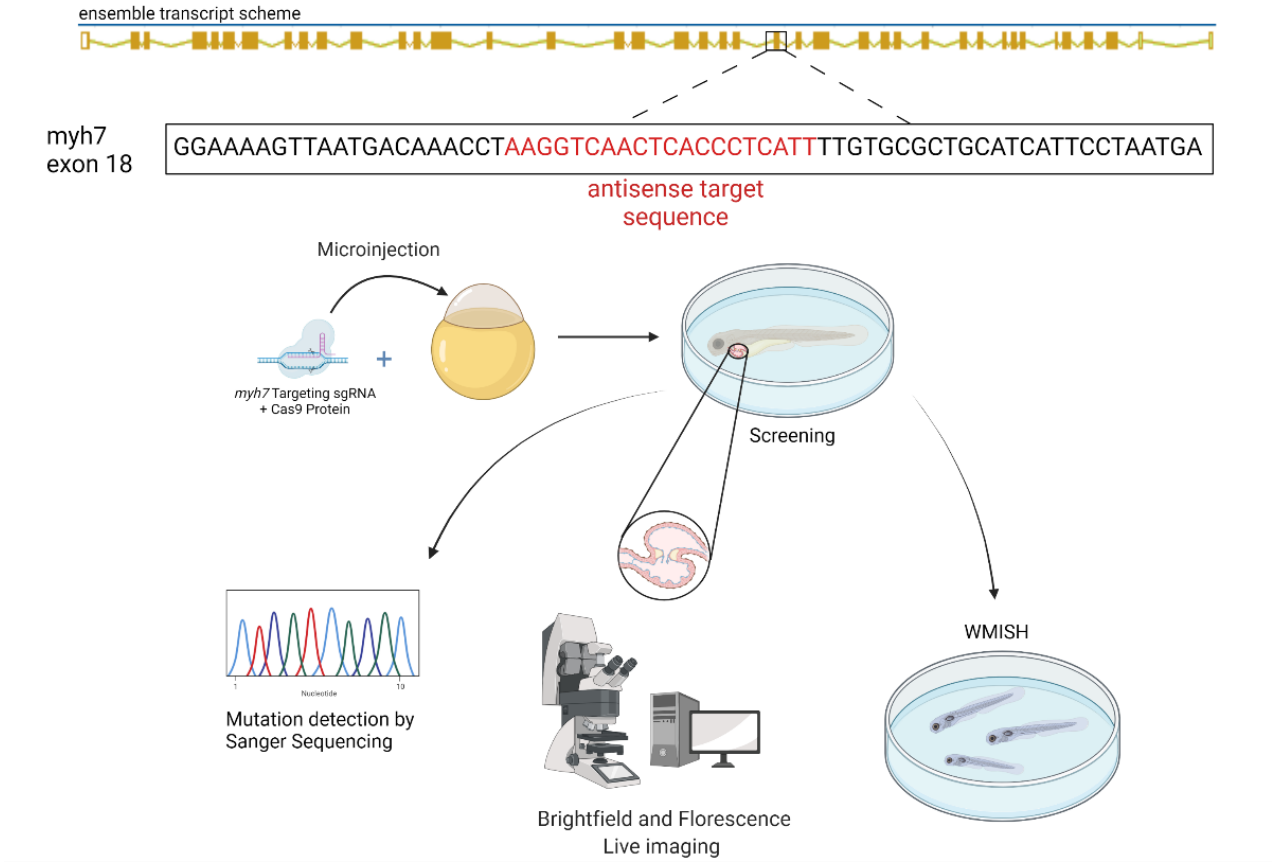

Figure 42: Schematic representation of workflow for generation and characterization of *myh7* knockout model by using CRISPR/Cas9 system

Next, we subsequently isolated genomic DNA from individual larvae at 5 days post-fertilization (dpf) and performed Sanger sequencing to identify insertions and deletions (indels). The sequencing data confirmed the successful editing target sequence and presence of indels in the MYH7 gene, demonstrating an efficiency rate of approximately 90% (Figure 43).

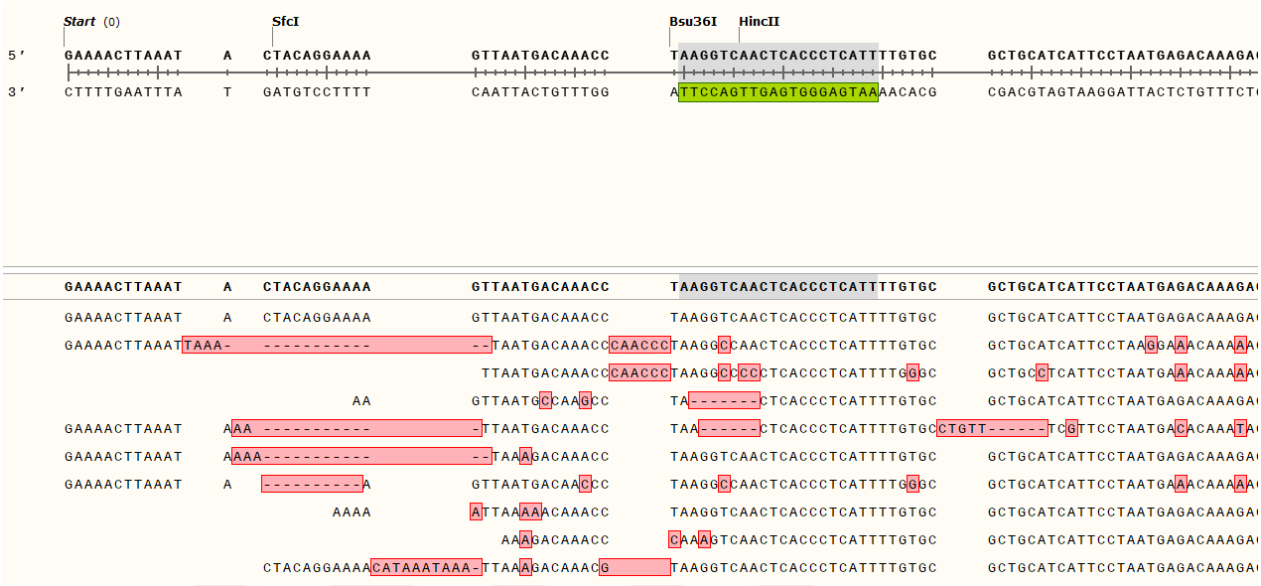

Figure 43: Sanger sequencing results from RNP complex injected 5 dpf fish

Daily observation of MYH7 knockout (KO) zebrafish larvae revealed significant cardiovascular defects, including pericardial edema, anomalous chamber formation within the pericardial sac, and misshapen hearts. These abnormalities became evident starting at 3 days post-fertilization (dpf) in comparison to control larvae injected with sgRNA. Additionally, hemorrhages were noted in various regions of the body near the heart and vascular system. Both pericardial and yolk sac/abdominal edema continued to progress until 5 dpf.

By the fifth day post-fertilization, MYH7 KO fish exhibited thickened hearts with atypical development of atrial and ventricular chambers, alongside disrupted S-looping processes. These KO zebrafish larvae demonstrated impaired heart contraction and blood flow, which likely contributed to the observed hemorrhages. Furthermore, mutant fish displayed reduced swimming ability and mobility. The severity of cardiac malformations increased over time, resulting in the mortality of most larvae by 7 dpf due to the failure of proper cardiovascular system development (Figure 44)

These findings emphasize the critical role of the MYH7 gene in cardiovascular development. The observed phenotypes, including chamber malformation, disrupted heart morphology, hemorrhage, and reduced mobility, highlight the essential nature of MYH7 for maintaining cardiovascular integrity and function during early developmental stages in zebrafish.

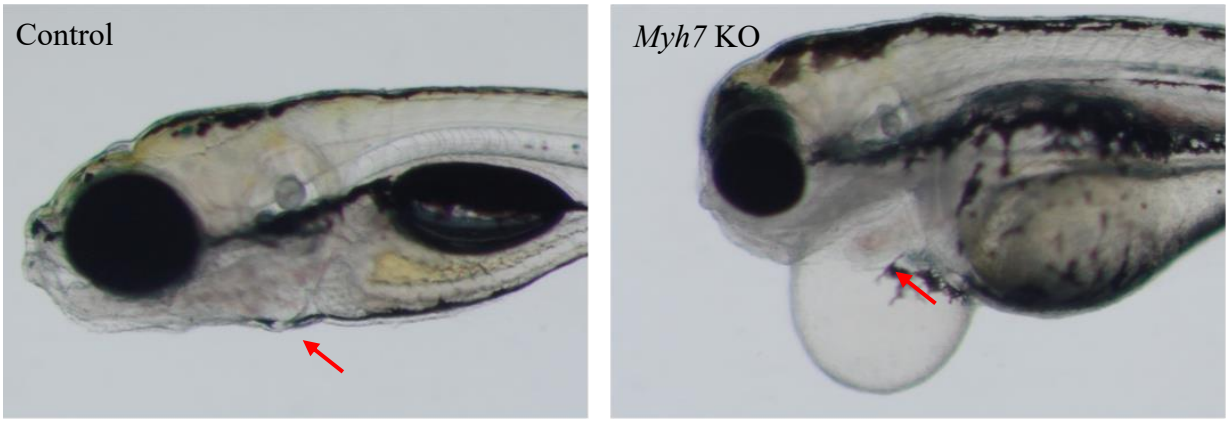

Figure 44: Morphological changes of the myh7 knockout fish at 5 dpf

Next, we investigated how heart formation is affected by *myh7* mutation exploiting Tg(actb2:hyper3) transgenic reporter line, a transgenic zebrafish reporter that contains the GFP driven by the cmlc2 promoter (cmlc2:egfp) transgenesis marker within HyPer3. *Myh7* mutant fish exhibited disorganized S-loop formation, in some cases no looping was present and fish showed tubular heart formation. Moreover, thickened ventricle and bloated cardiovascular tissue were present, causing reduced ventricular contraction and flowrate (Figure 45).

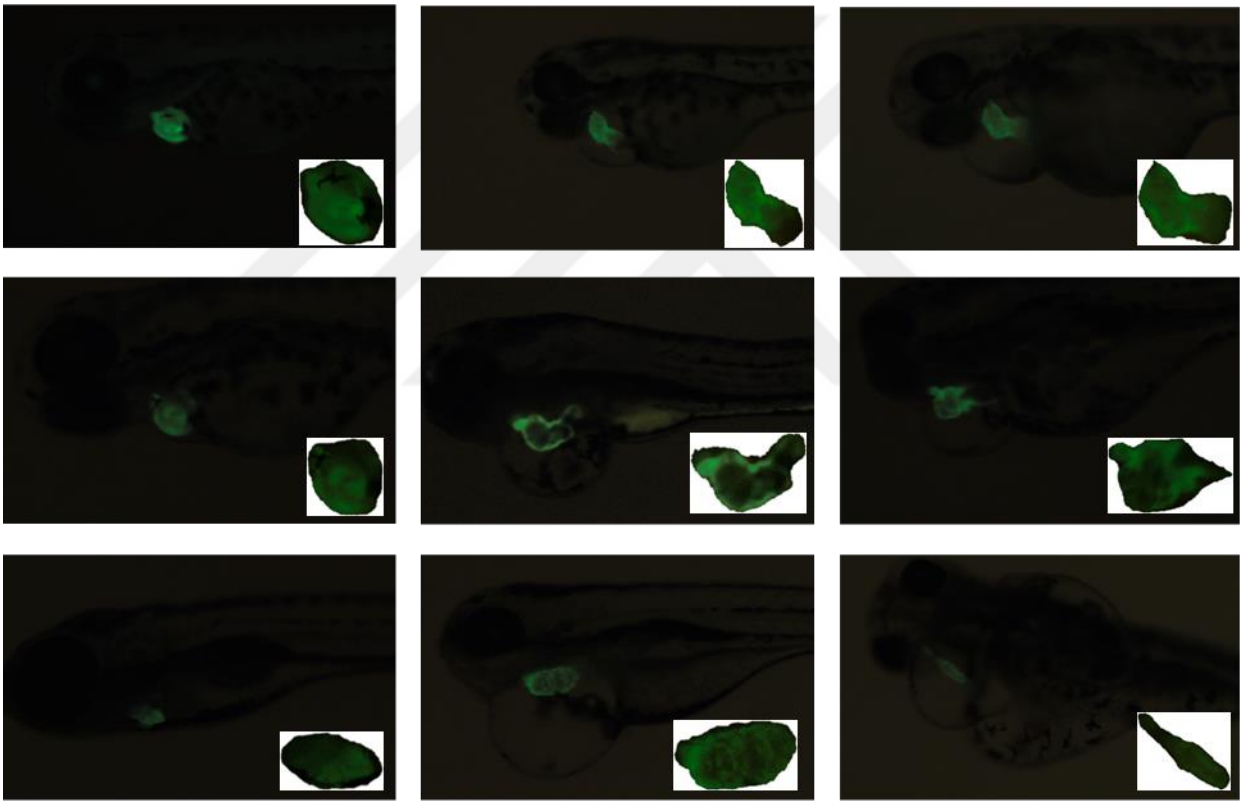

Figure 45: Investigation of the heart formation of myh7 mutant fish

Finally, we investigated how cardiovascular system related gene expression affected by *myh7* mutation. For this purpose, we take advantage of whole-mount *in-situ* hybridization (WMISH) method to using *myh7, myh7l and mylk3* anti-sense RNA probes. While control groups properly expressed all three target probes, *myh7* knockout fish showed significantly reduced expression

(Figure 46). Overall, our data suggest that MYH7 expression plays a significant role in heart development.

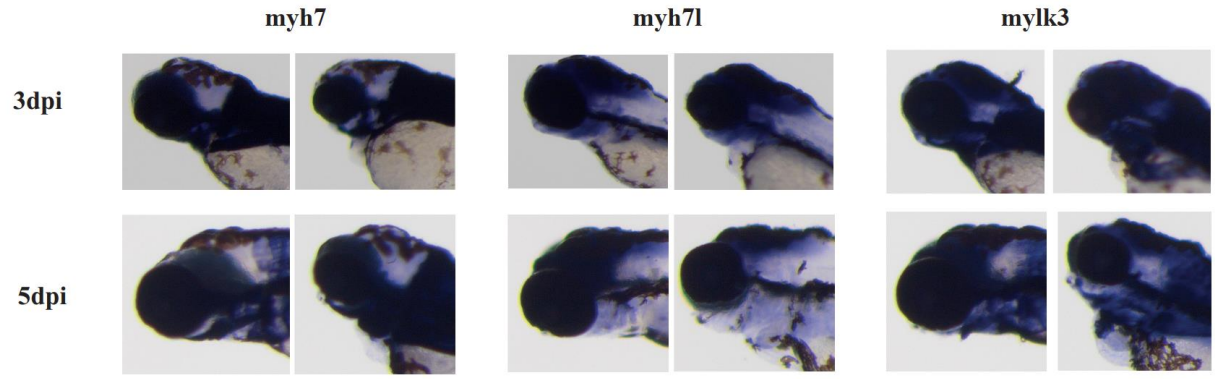

Figure 46: Effect of *myh7* knockout fish in cardiac development related genes.

5 DISCUSSION

The objective of this study was to develop models of human diseases using various methodologies to create an in vivo platform for examining the molecular mechanisms of specific cells, tissues, or genes. The zebrafish genome shares approximately 70% similarity with that of mammals, a resemblance that is even more pronounced in the nervous system. Additionally, zebrafish are capable of producing numerous offspring simultaneously and require relatively low housing costs. Advanced genetic manipulation techniques, such as CRISPR/Cas9 and the Tol2 transposon system, can be readily applied to generate mutant or transgenic lines in zebrafish. These attributes, combined with their high genetic similarity to mammals, significant regenerative capacity, and experimental versatility, position zebrafish as an exceptional vertebrate model for human disease research. Their utility is further enhanced by the ability to implement both forward and reverse genetic approaches, making them a cost-effective and powerful tool for studying human disease mechanisms.

5.1 Chapter 1: Remyelination Model of Adult Zebrafish Brain

Myelination involves the formation of a specialized axoglial structure by oligodendrocytes within the central nervous system (CNS) and Schwann cells in the peripheral nervous system (PNS). This process entails wrapping neuronal axons with lipid-rich membranes, which serves to insulate the axons, facilitate efficient conduction of action potentials, and provide essential trophic support for axonal integrity. Beyond these fundamental roles, myelination is also recognized for its significant contributions to cognitive functions such as learning and memory (Nave & Werner, 2014). Furthermore, myelination plays a critical organizational role in the nervous system by facilitating the connectivity and temporal coordination of cellular networks (Fields, 2015).

Demyelinating diseases encompass a spectrum of CNS and PNS disorders characterized by damage to the myelin sheath surrounding axons. These conditions include various CNS injuries such as stroke and trauma, neurodegenerative diseases like multiple sclerosis (MS) and leukodystrophy, as well as neuropsychiatric disorders including autism and schizophrenia (Graciarena et al., 2019; Mahoney et al., 2022; Thompson et al., 2018; Wolf et al., 2021; Yu et al., 2022). Damage to myelination disrupts nerve conduction and contributes to axonal degeneration, ultimately

culminating in neural cell death. In summary, myelination is a fundamental process crucial for the structural and functional integrity of the nervous system. Its impairment through demyelinating diseases underlies a diverse array of neurological and psychiatric conditions, highlighting its pivotal role in maintaining neural health and function.

In this study, we developed and analyzed a model of adult zebrafish brain demyelination, examining the involvement of the Wnt signaling pathway in remyelination. Zebrafish offers diverse methodologies for studying demyelination and remyelination, including laser and chemical ablation techniques, as well as genetic models. Each approach affords unique insights into various aspects of myelin pathology, encompassing demyelination, remyelination dynamics, immune responses, and cellular outcomes (Karttunen et al., 2017; Kirby et al., 2006; Morris et al., 2020; Münzel et al., 2014).

Lysolecithin (LPC) is well established chemical demyelination model for investigating remyelination (Fancy et al., 2009; Nyamoya et al., 2019; Ou et al., 2016). LPC-induced demyelination/remyelination model has been applied zebrafish in three notable studies. However, two of the studies focused larval stages and spinal cord as region of interest while one utilized adult zebrafish optic nerve (Cunha et al., 2020; Morris et al., 2020; Münzel et al., 2014). In the adult optic nerve model, the investigation centered on the effects of aging on remyelination capacity. In the present study we developed LPC-induced remyelination model in the adult zebrafish brain for the first time. Moreover, we established methodologies for assessing demyelination and remyelination, enabling the exploration of further approaches. Our results indicated that significant reduction of myelin related genes expression levels in the first 3 days and back to control levels around 7^{th} day of injection, similarly to LPC-induced rodent demyelination models. Moreover, we also discerned immune response related gene expression levels significantly increased at 3 dpi. Our results recapitulate 2 most important indication of demyelination, myelin damage and immune response. This advancement provides a novel platform for investigating the underlying mechanisms of remyelination in the adult zebrafish brain.

Wnt/β-catenin signaling plays central role in stem cell biology and regeneration including oligodendrocytes progenitors, thus myelination. However, conflicted results have been reported and its role in remyelination still remains uncertain (Xie et al., 2014). Studies involving

remyelination often focuses oligodendrocyte lineage specific role of the Wnt signaling, despite Wnt pathway also plays significant role in tissue regeneration in an intercellular communication (Chavali et al., 2020; Choi et al., 2020; Marchetti & Pluchino, 2013). Our results revealed that complete inhibition Wnt signalling by IWR-1 causes halted remyelination and increased immune response. Glycerophosphodiester phosphodiesterase 2 (GDE2 or GDPD5) is a six-transmembrane protein expressed from cortical neurons and regulates canonical Wnt signaling. Wnt activation leads to phosphacan release. GDE2 lacking animals showed that altered Wnt signaling in neurons causes impairment of phosphacan release and inhibited oligodendrocyte maturation (Choi et al., 2020). In another study revealed that Wnt signalling regulates microglial response. To start remyelination artefacts from broken down myelin structure, myelin debris, should be cleared and then, OPC differentiation and remyelination occurs. M2c microglia secretes Wnt7a which promotes multipotent cells to differentiate to oligodendrocyte lineage cells. Therefore, lack of Wnt cascades alters both demyelination events and consequently causes failure of remyelination. Our proteomic analysis revealed lipid degradation mechanisms upregulated in demyelination and decreseas overtime, in the same context lipid synthesis metabolism enriched in remyelination. Similar data previously reported in a proteomics and lipidomics applied demyelination model (Penkert et al., 2021). Moreover, we revealed, inhibition of Wnt signaling causes elevated immune response and altered lipid synthesis metabolism. Overall, our study provides a new platform for investigating demyelination and remyelination of zebrafish brain, a model organism with high regenerative capacity of nervous system. Furthermore, our results reveal that complete lacking Wnt signaling causes failure of remyelination.

5.2 Chapter 2: Cancer and Tissue Regeneration

The aim of Tol2 editing is to establish a system that enhances the streamlined construction of expression constructs and the production of stable transgenic organisms. Tol2 offers accessible methods for generating transgenic fish of interest. The cloning vector must incorporate Tol2 cut sites; between these sites, genes of interest such as oncogenes, fluorescent sequences, or other relevant sequences can be inserted. This system facilitates precise manipulation and efficient integration of desired genetic elements into the genome, enabling detailed studies on gene function and expression in transgenic models (Kwan et al., 2007; Liao et al., 2012; Suster et al., 2009).

Despite numerous studies exploring the shared and unique molecular mechanisms of regeneration and cancer, a comprehensive comparison of brain regeneration and brain cancer at the gene expression level remains understudied (Demirci et al., 2022). Our laboratory investigated early and late responses to brain injury and role of the Wnt signaling pathway. Results revealed expression profiles of 3 different phases of regeneration including, early and late response and injured and uninjured hemispheres (Demirci et al., 2020). To investigate similarities and differences of regeneration and brain cancer, we utilized GFAP promoter, expressing oncogene HRasV12. However, our results showed that aberrant proliferation and neoplasia occurred in eyes rather than telencephalic regions. Therefore, we switch another well established model, using Gal4:UAS system, under zic promoter, mutant HRasV12 is expressed through central nervous system (Mayrhofer et al., 2017). Furthermore, utilizing somatic expression, we acquired unique tumor formation in telencephalic area for individual fish. Following, bulk RNA sequencing, PCA analysis shows clear grouping between cancer groups and controls. Initial analysis revealed, differentially expressed gene profiles. Our study continues with further analysis for comparing regenerative phases with cancer profile. Overall, we aim to determine the differentially expressed genes between regenerative phases and cancer to further, reprogram neuronal and cancer cells to investigate candidate genes for therapeutic approaches.

OPCs are abundant neural progenitors of the adult brains. OPCs have ability to differentiate into mature oligodendrocytes, however, interestingly they can also differentiate into astrocytes through signaling mechanisms in context of tissue regeneration. Furthermore, in the presence of oncogenes they can promote gliomagenesis. Huang et al., presented that OPCs not only initiates vascularization and orchestrates glioma invasion. One of the possible reason that OPCs and angiogenic endothelial cells share high degree of molecular mechanisms, therefore, they may initiate crosstalk in different occasions (Ilkanizadeh et al., 2014). GBM has the highest mortality rate in brain cancers and approximately 35% of proneural subtype of the glioma lesions have increased focal PDGFRA expression. Other OPC marker genes also expressed in proneural GBMs and OPCs can form glioma lesions in manipulation of the PDGF ligands. For example, NG2+ cells in postnatal mice shows increased proliferation in presence of the PDGF ligands through altered WNT and PI3K signaling (Lindberg et al., 2009). Asymmetric cellular division of the stem cells

are defense mechanism against neoplastic transformation. Studies discovered that in proneural brain cancers SOX2, OLIG2 and NG2 expressing cells are present in the tumors, however tumor OPCs exposed to slight dedifferentiation through the ongogenic activity. NG2 activity is key factor in OPC fate switching and part of the asymmetrical division. Recent study shown that, OPCs turn into tumor initiating cells when asymmetrical division mechanism is defected (Sugiarto et al., 2011). An effective way to understanding the molecular mechanisms and effect of the different cellular populations contribution to cancer is investigating cellular specific regeneration and comparison to cancer for discover differences and similarities. For this purpose, studies in chapter 1 and chapter 2 can be combined to investigate oligodendrocyte lineage cell behavior and contribution to gliomagenesis.

5.3 Chapter 3: Human Disease Modeling for Identified Mutations

The identification of human candidate disease genes is progressing continuously and swiftly through whole exome sequencing (WES) and genome-wide association studies (GWAS). These identified candidates require thorough functional validation. Zebrafish have emerged as a valuable model organism for this purpose, offering an effective balance between rapid testing and a close approximation to human biology, relatively affordable and easily applied forward and reverse genetic techniques(Davis et al., 2014). Several approaches have been identified for genomic modification of zebrafish i.e. morpholine knockdown, CRISPR/Cas9 knockout models. However, while morpholino knockdowns shows higher off-target effects, CRISPR based knockout models provides better phenotypic and genotypic results. Furthermore, comparing zebrafish CRISPR/Cas9 mediated genome editing with *in-vitro* studies, again zebrafish models exceeds with better phenotypic results, ability to generate stable lines, low off-target effects and provides multi-organ and intercellular interaction research platform. The effectiveness of sgRNAs tailored for particular target genes displays variability, likely influenced by chromatin structure, unidentified SNPs, alternative sites of transcriptional initiation, or events of alternative splicing. Upon successful targeting, mechanisms of nonhomologous end joining can produce mutants with alleles that are either functional or show diminished functionality (Wu et al., 2018). Moreover, efficiency of the successful editing depends on the nature of the study. For example, in our study we targeted a loci around 50 bases since our aim was to duplicate a novel missense variant mutation which

significantly affected our approach (Hesaraki et al., 2022). However, in another research focused on functionality of a gene, it would be possible to select through several exons, strategize utilizing combinations of several sgRNAs. Overall, zebrafish CRISPR/Cas9 models provides rapid, precise and cost-effective platform for human genetic diseases.

In this study, we developed a zebrafish knockout model for MYH7 using CRISPR/Cas9 genome editing technology to investigate MYH7's role in cardiac morphogenesis and ventricular contraction. The predominant phenotypic indicators of cardiomyopathy in zebrafish include (i) edema in the heart and pericardial sac, (ii) disrupted S-looping morphogenesis, and (iii) anatomical heart deformities. These phenotypic traits align with those observed in other cardiomyopathy models highlighting the utility of the zebrafish model in cardiomyopathy research (Cohn et al., 2019; Kustermann et al., 2018; Lu et al., 2020).

The MYH7 protein represents a significant sarcomeric constituent prominently expressed in the zebrafish cardiac tissue. Zebrafish harbor nine homologs of the human MYH gene, seven of which exhibit over 80% protein homology with human MYH7 (Shih et al., 2015). As a constituent of the myosin complex, zebrafish MYH7 manifests in various embryonic structures such as the heart primordium, pericardial region, and musculature. Notably, high MYH7 expression levels are discernible in the cardiac ventricle of zebrafish embryos. Consequently, the observed disrupted cardiac development and subsequent mortality in MYH7 knockout larvae proved its pivotal involvement in cardiovascular system ontogenesis.

A mouse model of left ventricular non-compaction (LVNC), induced by a missense mutation in the dystrobrevin-α gene within cardiac muscle, exhibits multiple trabeculations, left ventricular dilation, and impaired cardiac contractility(Cao et al., 2017). In parallel, our MYH7 knockout zebrafish model manifests a malformed heart phenotype characterized by pericardial edema, extensive hemorrhage, chamber distortion, and contractile dysfunction. The concurrence of these phenotypic traits across both models substantiates the utility of our zebrafish model as a platform for investigating the molecular underpinnings of MYH7-related disorders, particularly non-compaction cardiomyopathies. This comparative approach underscores the potential of zebrafish as a valuable tool in elucidating pathogenic mechanisms in cardiac diseases associated with MYH7 mutations.

6 CONCLUSION

In this study, three different disease modelling developed using different approaches, chemical, genetic and genome editing, respectively. In sense of zebrafish as a model organism, our results ensuring that very capable for understanding human diseases and developing therapeutic approaches. First chapter brings a new concept to study adult brain remyelination in zebrafish. Furthermore, our results revealed that blocking Wnt pathway altered remyelination. Inhibition of the Wnt pathway completely rather than cell of interest contributed to conflicted topic since Wnt signaling has promoting or inhibiting effects on remyelination depending on the context and timing, as well as intercellular interactions. Second chapter describes a glioma inducing genetic model suitable for investigate numerous aspects of brain cancer. Taken together first and second chapter provides two important platform to both study OPC regeneration and its role in the brain tumors. Finally, third chapter describes CRISPR/Cas9 based disease modelling for novel variants. Overall, this thesis provides tools for designing different aspects of human diseases. Combinatorial use of these tools will enable researchers to evaluate different levels of human diseases.

7 REFERENCES

Bardile, C. F., Garcia-Miralles, M., Caron, N. S., Rayan, N. A., Langley, S. R., Harmston, N., Rondelli, A. M., Yi Teo, R. T., Waltl, S., Anderson, L. M., Bae, H. G., Jung, S., Williams, A., Prabhakar, S., Petretto, E., Hayden, M. R., & Pouladi, M. A. (2019). Intrinsic mutant HTT-mediated defects in oligodendroglia cause myelination deficits and behavioral abnormalities in Huntington disease. *Proceedings of the National Academy of Sciences of the United States of America*, *116*(19), 9622–9627. https://doi.org/10.1073/pnas.1818042116

Beachy, P. A., Karhadkar, S. S., & Berman, D. M. (2004). Tissue repair and stem cell renewal in carcinogenesis. *Nature*, *432*(7015), 324–331. https://doi.org/10.1038/nature03100

Bergles, D. E., & Richardson, W. D. (2016). Oligodendrocyte development and plasticity. *Cold Spring Harbor Perspectives in Biology*, *8*(2), 1–27. https://doi.org/10.1101/cshperspect.a020453

Cao, Q., Shen, Y., Liu, X., Yu, X., Yuan, P., Wan, R., Liu, X., Peng, X., He, W., Pu, J., & Hong, K. (2017). Phenotype and functional analyses in a transgenic mouse model of left ventricular noncompaction caused by a DTNA mutation. *International Heart Journal*, *58*(6), 939–947. https://doi.org/10.1536/ihj.16-019

Chavali, M., Ulloa-Navas, M. J., Pérez-Borredá, P., Garcia-Verdugo, J. M., McQuillen, P. S., Huang, E. J., & Rowitch, D. H. (2020). Wnt-Dependent Oligodendroglial-Endothelial Interactions Regulate White Matter Vascularization and Attenuate Injury. *Neuron*, *108*(6), 1130-1145.e5. https://doi.org/10.1016/j.neuron.2020.09.033

Chia, K., Klingseisen, A., Sieger, D., & Priller, J. (2022). Zebrafish as a model organism for neurodegenerative disease. *Frontiers in Molecular Neuroscience*, *15*(October), 1–27. https://doi.org/10.3389/fnmol.2022.940484

Choi, B. R., Cave, C., Na, C. H., & Sockanathan, S. (2020). GDE2-Dependent Activation of Canonical Wnt Signaling in Neurons Regulates Oligodendrocyte Maturation. *Cell Reports*, *31*(5), 107540. https://doi.org/10.1016/j.celrep.2020.107540

Cohn, R., Thakar, K., Lowe, A., Ladha, F. A., Pettinato, A. M., Romano, R., Meredith, E., Chen, Y. S., Atamanuk, K., Huey, B. D., & Hinson, J. T. (2019). A Contraction Stress Model of Hypertrophic Cardiomyopathy due to Sarcomere Mutations. *Stem Cell Reports*, *12*(1), 71–83. https://doi.org/10.1016/j.stemcr.2018.11.015

Cristobal, C. D., & Lee, H. K. (2022). Development of myelinating glia: An overview. *Glia*, *70*(12), 2237–2259. https://doi.org/10.1002/glia.24238

Cunha, M. I., Su, M., Cantuti-Castelvetri, L., Müller, S. A., Schifferer, M., Djannatian, M., Alexopoulos, I., van der Meer, F., Winkler, A., van Ham, T. J., Schmid, B., Lichtenthaler, S. F., Stadelmann, C., & Simons, M. (2020). Pro-inflammatory activation following demyelination is required for myelin clearance and oligodendrogenesis. *Journal of Experimental Medicine*, *217*(5). https://doi.org/10.1084/jem.20191390

Davis, E. E., Frangakis, S., & Katsanis, N. (2014). Interpreting human genetic variation with in vivo zebrafish assays. *Biochimica et Biophysica Acta - Molecular Basis of Disease*, *1842*(10), 1960–1970. https://doi.org/10.1016/j.bbadis.2014.05.024

Demirci, Y., Cucun, G., Poyraz, Y. K., Mohammed, S., Heger, G., Papatheodorou, I., & Ozhan, G. (2020). Comparative Transcriptome Analysis of the Regenerating Zebrafish Telencephalon Unravels a Resource With Key Pathways During Two Early Stages and Activation of Wnt/β-Catenin Signaling at the Early Wound Healing Stage. *Frontiers in Cell and Developmental Biology*, *8*(October). https://doi.org/10.3389/fcell.2020.584604

Demirci, Y., Heger, G., Katkat, E., Papatheodorou, I., Brazma, A., & Ozhan, G. (2022). Brain Regeneration Resembles Brain Cancer at Its Early Wound Healing Stage and Diverges From Cancer Later at Its Proliferation and Differentiation Stages. *Frontiers in Cell and Developmental Biology*, *10*(February), 1–21. https://doi.org/10.3389/fcell.2022.813314

Duncan, R. N., Panahi, S., Piotrowski, T., & Dorsky, R. I. (2015). Identification of wnt genes expressed in neural progenitor zones during zebrafish brain development. *PLoS ONE*, *10*(12). https://doi.org/10.1371/journal.pone.0145810

Elbaz, B., & Popko, B. (2019). Molecular Control of Oligodendrocyte Development. *Trends in*

Neurosciences, *42*(4), 263–277. https://doi.org/10.1016/j.tins.2019.01.002

Emery, B. (2010). Regulation of oligodendrocyte differentiation and myelination. *Science*, *330*(6005), 779–782. https://doi.org/10.1126/science.1190927

Ettle, B., Schlachetzki, J. C. M., & Winkler, J. (2016). Oligodendroglia and Myelin in Neurodegenerative Diseases: More Than Just Bystanders? *Molecular Neurobiology*, *53*(5), 3046–3062. https://doi.org/10.1007/s12035-015-9205-3

Fancy, S. P. J., Baranzini, S. E., Zhao, C., Yuk, D. I., Irvine, K. A., Kaing, S., Sanai, N., Franklin, R. J. M., & Rowitch, D. H. (2009). Dysregulation of the Wnt pathway inhibits timely myelination and remyelination in the mammalian CNS. *Genes and Development*, *23*(13), 1571–1585. https://doi.org/10.1101/gad.1806309

Fields, R. D. (2015). A new mechanism of nervous system plasticity: Activity-dependent myelination. *Nature Reviews Neuroscience*, *16*(12), 756–767. https://doi.org/10.1038/nrn4023

Franklin, R. J. M., Frisén, J., & Lyons, D. A. (2021). Revisiting remyelination: Towards a consensus on the regeneration of CNS myelin. *Seminars in Cell and Developmental Biology*, *116*(October 2020), 3–9. https://doi.org/10.1016/j.semcdb.2020.09.009

Goldschmidt, T., Antel, J., König, F. B., Brück, W., & Kuhlmann, T. (2009). Remyelination capacity of the MS brain decreases with disease chronicity. *Neurology*, *72*(22), 1914–1921. https://doi.org/10.1212/WNL.0b013e3181a8260a

Goodwin, S., McPherson, J. D., McCombie, W. R., & Mardis, E. R. (2008). Coming of age: Ten years of next-generation sequencing technologies. *Annual Review of Genomics and Human Genetics*, *9*(6), 333–351. https://doi.org/10.1146/annurev.genom.9.081307.164359

Gorter, R. P., & Baron, W. (2022). Recent insights into astrocytes as therapeutic targets for demyelinating diseases. *Current Opinion in Pharmacology*, *65*, 102261. https://doi.org/10.1016/j.coph.2022.102261

Graciarena, M., Seiffe, A., Nait-Oumesmar, B., & Depino, A. M. (2019). Hypomyelination and

oligodendroglial alterations in a mouse model of autism spectrum disorder. *Frontiers in Cellular Neuroscience*, *12*(January), 1–11. https://doi.org/10.3389/fncel.2018.00517

Greten, F. R., & Grivennikov, S. I. (2019). Inflammation and Cancer: Triggers, Mechanisms, and Consequences. *Immunity*, *51*(1), 27–41. https://doi.org/10.1016/j.immuni.2019.06.025

Guo, F., Lang, J., Sohn, J., Hammond, E., Chang, M., & Pleasure, D. (2015). Canonical Wnt signaling in the oligodendroglial lineage-puzzles remain. *Glia*, *63*(10), 1671–1693. https://doi.org/10.1002/glia.22813

Hesaraki, M., Bora, U., Pahlavan, S., & Salehi, N. (2022). *A Novel Missense Variant in Actin Binding Domain of MYH7 Is Associated With Left Ventricular Noncompaction*. *9*(April). https://doi.org/10.3389/fcvm.2022.839862

Hussain, R., Zubair, H., Pursell, S., & Shahab, M. (2018). Neurodegenerative diseases: Regenerative mechanisms and novel therapeutic approaches. *Brain Sciences*, *8*(9). https://doi.org/10.3390/brainsci8090177

Ilkanizadeh, S., Lau, J., Huang, M., Foster, D. J., Wong, R., Frantz, A., Wang, S., Weiss, W. A., & Persson, A. I. (2014). Glial progenitors as targets for transformation in Glioma. In *Advances in Cancer Research* (1st ed., Vol. 121). Elsevier Inc. https://doi.org/10.1016/B978-0-12-800249-0.00001-9

Karttunen, M. J., Czopka, T., Goedhart, M., Early, J. J., & Lyons, D. A. (2017). Regeneration of myelin sheaths of normal length and thickness in the zebrafish CNS correlates with growth of axons in caliber. *PloS One*, *12*(5), e0178058. https://doi.org/10.1371/journal.pone.0178058

Kirby, B. B., Takada, N., Latimer, A. J., Shin, J., Carney, T. J., Kelsh, R. N., & Appel, B. (2006). In vivo time-lapse imaging shows dynamic oligodendrocyte progenitor behavior during zebrafish development. *Nature Neuroscience*, *9*(12), 1506–1511. https://doi.org/10.1038/nn1803

Kister, A., & Kister, I. (2022). Overview of myelin, major myelin lipids, and myelin-associated proteins. *Frontiers in Chemistry*, *10*(February), 1–9. https://doi.org/10.3389/fchem.2022.1041961

Kroehne, V., Freudenreich, D., Hans, S., Kaslin, J., & Brand, M. (2011). Regeneration of the adult zebrafish brain from neurogenic radial glia-type progenitors. *Development*, *138*(22), 4831–4841. https://doi.org/10.1242/dev.072587

Kustermann, M., Manta, L., Paone, C., Kustermann, J., Lausser, L., Wiesner, C., Eichinger, L., Clemen, C. S., Schröder, R., Kestler, H. A., Sandri, M., Rottbauer, W., & Just, S. (2018). Loss of the novel Vcp (valosin containing protein) interactor Washc4 interferes with autophagy-mediated proteostasis in striated muscle and leads to myopathy in vivo. *Autophagy*, *14*(11), 1911–1927. https://doi.org/10.1080/15548627.2018.1491491

Kwan, K. M., Fujimoto, E., Grabher, C., Mangum, B. D., Hardy, M. E., Campbell, D. S., Parant, J. M., Yost, H. J., Kanki, J. P., & Chien, C.-B. (2007). The Tol2kit: a multisite gateway-based construction kit for Tol2 transposon transgenesis constructs. *Developmental Dynamics : An Official Publication of the American Association of Anatomists*, *236*(11), 3088–3099. https://doi.org/10.1002/dvdy.21343

Liao, H. K., Wang, Y., Noack Watt, K. E., Wen, Q., Breitbach, J., Kemmet, C. K., Clark, K. J., Ekker, S. C., Essner, J. J., & McGrail, M. (2012). Tol2 gene trap integrations in the zebrafish amyloid precursor protein genes appa and aplp2 reveal accumulation of secreted APP at the embryonic veins. *Developmental Dynamics*, *241*(2), 415–425. https://doi.org/10.1002/dvdy.23725

Lindberg, N., Kastemar, M., Olofsson, T., Smits, A., & Uhrbom, L. (2009). Oligodendrocyte progenitor cells can act as cell of origin for experimental glioma. *Oncogene*, *28*(23), 2266–2275. https://doi.org/10.1038/onc.2009.76

Lu, S., Hu, M., Wang, Z., Liu, H., Kou, Y., Lyu, Z., & Tian, J. (2020). Generation and application of the zebrafish heg1 mutant as a cardiovascular disease model. *Biomolecules*, *10*(11), 1–15. https://doi.org/10.3390/biom10111542

Madeira, M. M., Hage, Z., & Tsirka, S. E. (2022). Beyond Myelination: Possible Roles of the Immune Proteasome in Oligodendroglial Homeostasis and Dysfunction. *Frontiers in Neuroscience*, *16*(May), 1–10. https://doi.org/10.3389/fnins.2022.867357

Mahoney, S. O., Chowdhury, N. F., Ngo, V., Imms, P., & Irimia, A. (2022). Mild Traumatic Brain Injury Results in Significant and Lasting Cortical Demyelination. *Frontiers in Neurology*, *13*(June), 1–16. https://doi.org/10.3389/fneur.2022.854396

Marchetti, B., & Pluchino, S. (2013). Wnt your brain be inflamed? Yes, it Wnt! *Trends in Molecular Medicine*, *19*(3), 144–156. https://doi.org/10.1016/j.molmed.2012.12.001

Mardis, E. R. (2008). Next-generation DNA sequencing methods. *Annual Review of Genomics and Human Genetics*, *9*, 387–402. https://doi.org/10.1146/annurev.genom.9.081307.164359

Marisca, R., Hoche, T., Agirre, E., Hoodless, L. J., Barkey, W., Auer, F., Castelo-Branco, G., & Czopka, T. (2020). Functionally distinct subgroups of oligodendrocyte precursor cells integrate neural activity and execute myelin formation. *Nature Neuroscience*, *23*(3), 363–374. https://doi.org/10.1038/s41593-019-0581-2

Martin, J. B. (1999). Molecular basis of the neurodegenerative disorders. *The New England Journal of Medicine*, *340*(25), 1970–1980. https://doi.org/10.1056/NEJM199906243402507

Masson, M. A., & Nait-Oumesmar, B. (2023). Emerging concepts in oligodendrocyte and myelin formation, inputs from the zebrafish model. *Glia*, *71*(5), 1147–1163. https://doi.org/10.1002/glia.24336

Matilla-Dueñas, A., Corral-Juan, M., Rodríguez-Palmero Seuma, A., Vilas, D., Ispierto, L., Morais, S., Sequeiros, J., Alonso, I., Volpini, V., Serrano-Munuera, C., Pintos-Morell, G., Álvarez, R., & Sánchez, I. (2017). Rare neurodegenerative diseases: Clinical and genetic update. In *Advances in Experimental Medicine and Biology* (Vol. 1031). https://doi.org/10.1007/978-3-319-67144-4_25

Mayrhofer, M., Gourain, V., Reischl, M., Affaticati, P., Jenett, A., Joly, J. S., Benelli, M., Demichelis, F., Poliani, P. L., Sieger, D., & Mione, M. (2017). A novel brain tumour model in zebrafish reveals the role of YAP activation in MAPK- and PI3K-induced malignant growth. *DMM Disease Models and Mechanisms*, *10*(1), 15–28. https://doi.org/10.1242/dmm.026500

Mirahmadi, M., Rezanejadbardaji, H., Irfan-Maqsood, M., Mokhtari, M. J., & Naderi-Meshkin, H.

(2016). Stem Cell Therapy for Neurodegenerative Diseases: Strategies for Regeneration against Degeneration. *Cell Therapy and Regenerative Medicine Journal*, *1*(1), 3. https://doi.org/10.15562/ctrm.11

Morris, A. D., & Kucenas, S. (2021). A Novel Lysolecithin Model for Visualizing Damage in vivo in the Larval Zebrafish Spinal Cord. *Frontiers in Cell and Developmental Biology*, *9*(May). https://doi.org/10.3389/fcell.2021.654583

Morris, A. D., Kucenas, S., Cunha, M. I., Su, M., Cantuti-Castelvetri, L., Müller, S. A., Schifferer, M., Djannatian, M., Alexopoulos, I., van der Meer, F., Winkler, A., van Ham, T. J., Schmid, B., Lichtenthaler, S. F., Stadelmann, C., & Simons, M. (2020). A Novel Lysolecithin Model for Visualizing Damage in vivo in the Larval Zebrafish Spinal Cord. *Frontiers in Cell and Developmental Biology*, *217*(May). https://doi.org/10.1084/jem.20191390

Mueller, T., & Wullimann, M. F. (2009). An evolutionary interpretation of teleostean forebrain anatomy. *Brain, Behavior and Evolution*, *74*(1), 30–42. https://doi.org/10.1159/000229011

Münzel, E. J., Becker, C. G., Becker, T., & Williams, A. (2014). Zebrafish regenerate full thickness optic nerve myelin after demyelination, but this fails with increasing age. *Acta Neuropathologica Communications*, *2*(1), 1–14. https://doi.org/10.1186/s40478-014-0077-y

Nave, K. A., & Werner, H. B. (2014). Myelination of the nervous system: Mechanisms and functions. *Annual Review of Cell and Developmental Biology*, *30*, 503–533. https://doi.org/10.1146/annurev-cellbio-100913-013101

Nyamoya, S., Leopold, P., Becker, B., Beyer, C., Hustadt, F., Schmitz, C., Michel, A., & Kipp, M. (2019). G-Protein-Coupled Receptor Gpr17 Expression in Two Multiple Sclerosis Remyelination Models. *Molecular Neurobiology*, *56*(2), 1109–1123. https://doi.org/10.1007/s12035-018-1146-1

Ou, Z., Sun, Y., Lin, L., You, N., Liu, X., Li, H., Ma, Y., Cao, L., Han, Y., Liu, M., Deng, Y., Yao, L., Lu, Q. R., & Chen, Y. (2016). Olig2-targeted G-protein-coupled receptor Gpr17 regulates oligodendrocyte survival in response to lysolecithin-induced demyelination. *Journal of Neuroscience*, *36*(41), 10560–10573. https://doi.org/10.1523/JNEUROSCI.0898-16.2016

Oviedo, N. J., & Beane, W. S. (2009). Regeneration: The origin of cancer or a possible cure? *Seminars in Cell & Developmental Biology*, *20*(5), 557–564. https://doi.org/10.1016/j.semcdb.2009.04.005

Ozhan, G., & Weidinger, G. (2015). Wnt/β-catenin signaling in heart regeneration. *Cell Regeneration*, *4*(1), 4:3. https://doi.org/10.1186/s13619-015-0017-8

Papuc, E., & Rejdak, K. (2020). The role of myelin damage in Alzheimer's disease pathology. *Archives of Medical Science*, *16*(2), 345–351. https://doi.org/10.5114/aoms.2018.76863

Patani, R., Balaratnam, M., Vora, A., & Reynolds, R. (2007). Remyelination can be extensive in multiple sclerosis despite a long disease course. *Neuropathology and Applied Neurobiology*, *33*(3), 277–287. https://doi.org/10.1111/j.1365-2990.2007.00805.x

Patton, E. E., Zon, L. I., & Langenau, D. M. (2021). Zebrafish disease models in drug discovery: from preclinical modelling to clinical trials. *Nature Reviews Drug Discovery*, *20*(8), 611–628. https://doi.org/10.1038/s41573-021-00210-8

Penkert, H., Bertrand, A., Tiwari, V., Breimann, S., Müller, S. A., Jordan, P. M., Gerl, M. J., Klose, C., Cantuti-Castelvetri, L., Bosch-Queralt, M., Levental, I., Lichtenthaler, S. F., Werz, O., & Simons, M. (2021). Proteomic and lipidomic profiling of demyelinating lesions identifies fatty acids as modulators in lesion recovery. *Cell Reports*, *37*(4). https://doi.org/10.1016/j.celrep.2021.109898

Polito, A., & Reynolds, R. (2005). NG2-expressing cells as oligodendrocyte progenitors in the normal and demyelinated adult central nervous system. *Journal of Anatomy*, *207*(6), 707–716. https://doi.org/10.1111/j.1469-7580.2005.00454.x

Powezka, K., Khan, T., Narlawar, R., & Antoniou, G. A. (2020). *Dyemylination in multiple sclerosis*. *January*.

Rodriguez, J. P., Coulter, M., Miotke, J., Meyer, R. L., Takemaru, K. I., & Levine, J. M. (2014). Abrogation of β-Catenin signaling in oligodendrocyte precursor cells reduces glial scarring and promotes axon regeneration after CNS injury. *Journal of Neuroscience*, *34*(31), 10285–10297. https://doi.org/10.1523/JNEUROSCI.4915-13.2014

Sanchez-Gonzalez, R., Koupourtidou, C., Lepko, T., Zambusi, A., Novoselc, K. T., Durovic, T., Aschenbroich, S., Schwarz, V., Breunig, C. T., Straka, H., Huttner, H. B., Irmler, M., Beckers, J., Wurst, W., Zwergal, A., Schauer, T., Straub, T., Czopka, T., Trümbach, D., … Ninkovic, J. (2022). Innate Immune Pathways Promote Oligodendrocyte Progenitor Cell Recruitment to the Injury Site in Adult Zebrafish Brain. *Cells*, *11*(3), 1–36. https://doi.org/10.3390/cells11030520

Shenoy, A., Banerjee, M., Upadhya, A., Bagwe-Parab, S., & Kaur, G. (2022). The Brilliance of the Zebrafish Model: Perception on Behavior and Alzheimer's Disease. *Frontiers in Behavioral Neuroscience*, *16*(June), 1–17. https://doi.org/10.3389/fnbeh.2022.861155

Shih, Y. H., Zhang, Y., Ding, Y., Ross, C. A., Li, H., Olson, T. M., & Xu, X. (2015). Cardiac Transcriptome and Dilated Cardiomyopathy Genes in Zebrafish. *Circulation: Cardiovascular Genetics*, *8*(2), 261–269. https://doi.org/10.1161/CIRCGENETICS.114.000702

Siems, S. B., Jahn, O., Hoodless, L. J., Jung, R. B., Hesse, D., Möbius, W., Czopka, T., & Werner, H. B. (2021). Proteome Profile of Myelin in the Zebrafish Brain. *Frontiers in Cell and Developmental Biology*, *9*(April), 1–17. https://doi.org/10.3389/fcell.2021.640169

Smith, C. I. E., Bergman, P., & Hagey, D. W. (2022). Estimating the number of diseases – the concept of rare, ultra-rare, and hyper-rare. *IScience*, *25*(8), 104698. https://doi.org/10.1016/j.isci.2022.104698

Steinmetz, J. D., Seeher, K. M., Schiess, N., Nichols, E., Cao, B., Servili, C., Cavallera, V., Cousin, E., Hagins, H., Moberg, M. E., Mehlman, M. L., Abate, Y. H., Abbas, J., Abbasi, M. A., Abbasian, M., Abbastabar, H., Abdelmasseh, M., Abdollahi, M., Abdollahi, M., … Dua, T. (2024). Global, regional, and national burden of disorders affecting the nervous system, 1990–2021: a systematic analysis for the Global Burden of Disease Study 2021. *The Lancet Neurology*, *23*(4), 344–381. https://doi.org/10.1016/S1474-4422(24)00038-3

Stern, C. D. (2000). Conrad H. Waddington's contributions to avian and mammalian development, 1930-1940. *The International Journal of Developmental Biology*, *44*(1), 15–22.

Sugiarto, S., Persson, A. I., Munoz, E. G., Waldhuber, M., Lamagna, C., Andor, N., Hanecker, P.,

Ayers-Ringler, J., Phillips, J., Siu, J., Lim, D. A., Vandenberg, S., Stallcup, W., Berger, M. S., Bergers, G., Weiss, W. A., & Petritsch, C. (2011). Asymmetry-defective oligodendrocyte progenitors are glioma precursors. *Cancer Cell*, *20*(3), 328–340. https://doi.org/10.1016/j.ccr.2011.08.011

Sundar, S. J., Hsieh, J. K., Manjila, S., Lathia, J. D., & Sloan, A. (2014). The role of cancer stem cells in glioblastoma. *Neurosurgical Focus*, *37*(6), E6. https://doi.org/10.3171/2014.9.FOCUS14494

Suster, M. L., Kikuta, H., Urasaki, A., Asakawa, K., & Kawakami, K. (2009). *Transgenesis in Zebrafish with the Tol2 Transposon System BT - Transgenesis Techniques: Principles and Protocols* (E. J. Cartwright (ed.); pp. 41–63). Humana Press. https://doi.org/10.1007/978-1-60327-019-9_3

T., G., J., A., F.B., K., W., B., & T., K. (2009). Remyelination capacity of the MS brain decreases with disease chronicity. *Neurology*, *72*(22), 1914–1921. http://ovidsp.ovid.com/ovidweb.cgi?T=JS&PAGE=reference&D=emed9&NEWS=N&AN=2009338457

Thompson, A. J., Banwell, B. L., Barkhof, F., Carroll, W. M., Coetzee, T., Comi, G., Correale, J., Fazekas, F., Filippi, M., Freedman, M. S., Fujihara, K., Galetta, S. L., Hartung, H. P., Kappos, L., Lublin, F. D., Marrie, R. A., Miller, A. E., Miller, D. H., Montalban, X., … Cohen, J. A. (2018). Diagnosis of multiple sclerosis: 2017 revisions of the McDonald criteria. *The Lancet. Neurology*, *17*(2), 162–173. https://doi.org/10.1016/S1474-4422(17)30470-2

Valente, A., Huang, K. H., Portugues, R., & Engert, F. (2012). Ontogeny of classical and operant learning behaviors in zebrafish. *Learning and Memory*, *19*(4), 170–177. https://doi.org/10.1101/lm.025668.112

Verkhratsky, A., & Butt, A. (2013). Glial Physiology and Pathophysiology. *Glial Physiology and Pathophysiology*. https://doi.org/10.1002/9781118402061

Verplank, J. J. S., Gawron, J., Silvestri, N. J., Feltri, M. L., Wrabetz, L., & Goldberg, A. L. (2022). Raising cGMP restores proteasome function and myelination in mice with a proteotoxic

neuropathy. *Brain*, *145*(1), 168–178. https://doi.org/10.1093/brain/awab249

Virchow, R. (1854). Ueber das ausgebreitete Vorkommen einer dem Nervenmark analogen Substanz in den thierischen Geweben. *Archiv Für Pathologische Anatomie Und Physiologie Und Für Klinische Medicin*, *6*(4), 562–572. https://doi.org/10.1007/BF02116709

Waddington, C. H. (1935). Cancer and the Theory of Organisers. *Nature*, *135*(3416), 606–608. https://doi.org/10.1038/135606a0

Wang, J., & Cao, H. (2021). Zebrafish and medaka: Important animal models for human neurodegenerative diseases. *International Journal of Molecular Sciences*, *22*(19). https://doi.org/10.3390/ijms221910766

Wilson, D. M., Cookson, M. R., Van Den Bosch, L., Zetterberg, H., Holtzman, D. M., & Dewachter, I. (2023). Hallmarks of neurodegenerative diseases. *Cell*, *186*(4), 693–714. https://doi.org/10.1016/j.cell.2022.12.032

Wolf, N. I., ffrench-Constant, C., & van der Knaap, M. S. (2021). Hypomyelinating leukodystrophies — unravelling myelin biology. *Nature Reviews Neurology*, *17*(2), 88–103. https://doi.org/10.1038/s41582-020-00432-1

Wu, R. S., Lam, I. I., Clay, H., Duong, D. N., Deo, R. C., & Coughlin, S. R. (2018). A Rapid Method for Directed Gene Knockout for Screening in G0 Zebrafish. *Developmental Cell*, *46*(1), 112-125.e4. https://doi.org/10.1016/j.devcel.2018.06.003

Xiao, Y., & Czopka, T. (2023). Myelination-independent functions of oligodendrocyte precursor cells in health and disease. *Nature Neuroscience*, *26*(October), 1663–1669. https://doi.org/10.1038/s41593-023-01423-3

Xiao, Y., Petrucco, L., Hoodless, L. J., Portugues, R., & Czopka, T. (2022). Oligodendrocyte precursor cells sculpt the visual system by regulating axonal remodeling. *Nature Neuroscience*, *25*(3), 280–284. https://doi.org/10.1038/s41593-022-01023-7

Xie, C., Li, Z., Zhang, G. X., & Guan, Y. (2014). Wnt signaling in remyelination in multiple sclerosis: Friend or foe? *Molecular Neurobiology*, *49*(3), 1117–1125.

https://doi.org/10.1007/s12035-013-8584-6

Yu, G., Su, Y., Guo, C., Yi, C., Yu, B., Chen, H., Cui, Y., Wang, X., Wang, Y., Chen, X., Wang, S., Wang, Q., Chen, X., Hu, X., Mei, F., Verkhratsky, A., Xiao, L., & Niu, J. (2022). Pathological oligodendrocyte precursor cells revealed in human schizophrenic brains and trigger schizophrenia-like behaviors and synaptic defects in genetic animal model. *Molecular Psychiatry*, *27*(12), 5154–5166. https://doi.org/10.1038/s41380-022-01777-3

Zalc, B. (2016). The acquisition of myelin: An evolutionary perspective. *Brain Research*, *1641*, 4–10. https://doi.org/10.1016/j.brainres.2015.09.005

8 APPENDIX

8.1 Ethical Approval

İZMİR BİYOTIP VE GENOM MERKEZİ
Hayvan Deneyleri Yerel Etik Kurulu

Doç Dr. H. Güneş ÖZHAN

"CRISPR/Cas9 tabanlı hastalık modellerinin üretilmesi ve zebra balıklarında rejenerasyonun moleküler mekanizmalarının araştırılması" başlıklı tez çalışması kapsamında yapılan çalışmalar kurulumuz 2020-039 protokol no'lu ve 2022-007 protokol no'lu izinler kapsamında etik açıdan uygun bulunmuştur.

Dr. Gülçin ÇAKAN AKDOĞAN
İBG-HADYEK Kurul Başkanı

14.09.2022

Adres: Dokuz Eylül Üniversitesi Sağlık Yerleşkesi Mithatpaşa Cad. No:58/5 35340 Balçova-İZMİR
Telefon: +90 (232) 299 41 00

8.2 Curriculum Vitae

RAMAZAN UĞUR BORA

Kişisel Bilgiler

İletişim Bilgileri

İletişim Adresi

Telefon

E-posta

İnternet Sayfası

Öğrenim Bilgileri

26 Şubat 2019 - Şu Anda (5 yıl 6 ay)
Doktora, Doktora, DOKUZ EYLÜL ÜNİVERSİTESİ, TÜRKİYE
İZMİR ULUSLARARASI BİYOTIP VE GENOM ENSTİTÜSÜ, MOLEKÜLER BİYOLOJİ VE GENETİK (DR) (İNGİLİZCE)
Ağırlıklı Genel Not Ortalaması: 3.71 / 4.0

01 Eylül 2015 - 31 Ocak 2019 (3 yıl 5 ay)
Yüksek Lisans, Tezli Program, DOKUZ EYLÜL ÜNİVERSİTESİ, TÜRKİYE
SAĞLIK BİLİMLERİ ENSTİTÜSÜ, TEMEL SİNİR BİLİMLER (YL) (TEZLİ)
Diploma Numarası: 201900537
Ağırlıklı Genel Not Ortalaması: 3.33 / 4.0

01 Eylül 2009 - 16 Ocak 2015 (5 yıl 5 ay)
Lisans, Anadal/Normal Öğretim, EGE ÜNİVERSİTESİ, TÜRKİYE
FEN FAKÜLTESİ, BİYOLOJİ PR.
Diploma Numarası: 2014/04/0101
Ağırlıklı Genel Not Ortalaması: 2.3 / 4.0

Deneyim / İşyeri Bilgileri

Kasım 2022 - Aralık 2022 (2 ay) (Tam Zamanlı)
MİSAFİR ARAŞTIRMACI, DOKTORA ÖĞRENCİSİ, BONN UNİVERSİTAT

Şubat 2019 - Şu Anda (5 yıl 6 ay) (Tam Zamanlı)
ARAŞTIRMACI, DOKTORA ÖĞRENCİSİ, İZMİR BİYOTIP VE GENOM MERKEZİ

Ekim 2016 - Ocak 2017 (4 ay) (Tam Zamanlı)
MİSAFİR ARAŞTIRMACI, YÜKSEK LİSANS ÖĞRENCİSİ, KUMAMOTO UNIVERSITY

Haziran 2012 - Eylül 2012 (4 ay) (Tam Zamanlı)
STAJYER, EGE ÜNİVERSİTESİ

Yabancı Dil Bilgileri

İNGİLİZCE (Okuma: İyi, Yazma: İyi, Konuşma: İyi)

Ar-Ge Yetkinlik

Makaleler

R. U. BORA, A Novel Missense Variant in Actin Binding Domain of MYH7 Is Associated With Left Ventricular Noncompaction, Frontiers in Cardiovascular Medicine, 2022, 2297-055X, 9, 0, 0.

R. U. BORA, Increased plasma levels of 8-oxoguanine DNA glycosylase-1 in bipolar disorder, Psychiatry and Clinical Neurosciences, 2019, 1440-1819, 73, 11, 719-720.

Bildiriler

R. U. BORA, E. S. DEMİRBAŞOĞLU, E. TURHANLAR ŞAHİN, H. GÜNER & H. G. ÖZHAN, Adult Zebrafish Brain as a Demyelination Model and Role of Wnt Signaling in Remyelination, Poster Sunumu, The 48th FEBS Congress, 29 Haziran 2024, 03 Temmuz 2024.

R. U. BORA, İ. AYDOĞDU & H. G. ÖZHAN, A Novel Method to Explore Demyelination and Reactive Remyelination in the Adult Zebrafish Brain, Poster Sunumu, The 47th FEBS Congress, 08 Temmuz 2023, 12 Temmuz 2023.

R. U. BORA, P. AKAN, Ö. TEZCAN, T. ŞAN ERKOÇ & K. BAYSAL, Conditioned Medium From Wharton?s Jelly Mesenchymal Stem Cells Increased The Viability Shsy 5y Cells, Poster Sunumu, 11th Fens Forum Of Neuroscience, 07 Temmuz 2018, 11 Ekim 2018.

Ö. TEZCAN, R. U. BORA, P. AKAN, D. ÖZTEKİN & K. BAYSAL, Characterization Of Wharton Jelly Mesenchymal Stem Cells From The Human Umbilical Cord And Investigation Of The Role Of Cellular Metabolism On Their In Vitro Differentiation, Poster Sunumu, The 41nd Febs Congress, 03 Eylül 2016, 08 Eylül 2016, 283, S1, 1 - 441.

P. AKAN, Ö. GÜRSOY DORUK, R. U. BORA & A. S. KOÇTÜRK, The Effects Of Nmda Receptor Subunits And Cholesterol On Amyloid Beta Toxicity In Shsy-5y Cells, Poster Sunumu, 1st International Cell Death Research Congress, 04 Mayıs 2016, 07 Mayıs 2016.

TÜBİTAK Burs ve Destekleri

Proje Bilgileri

121Z900, Alzheimer Hastalığında Nöronal Dejenerasyon ve Rejenerasyon Yanıtlarının Oluşumunda Wnt/ß-Katenin Sinyal İletiminin ve P75NTR Homoloğu Nradd'ın Rollerinin Zebrabalığı Amiloid ß42 Toksisite Modelinde Araştırılması, BİDEB Burslusu, Yürürlükte, SBAG - Sağlık Bilimleri Araştırma Destek Grubu, 1001 - Araştırma, ARDEB, Projeye Katılma/Ayrılma Tarihleri: 11.03.2022 - 10.07.2024, Proje Başlangıç/Bitiş Tarihleri: 01.03.2022 - 01.03.2025.

219Z040, Melanosit Rejenerasyonunun ve Melanomun Moleküler Mekanizmalarının Zebrabalığı Modelinde Karşılaştırmalı Analizi ve Melanom Hücrelerinde Gen İfadesi Profillerinin CRISPR/Cas9 Yöntemi ile Düzenlenerek Rejenerasyon Benzeri Bir İlerleyişin İndüklenmesi, Burslu, Sonuçlandı, SBAG - Sağlık Bilimleri Araştırma Destek Grubu, 1001 - Araştırma, ARDEB, Projeye Katılma/Ayrılma Tarihleri: 01.06.2021 - 01.09.2021, Proje Başlangıç/Bitiş Tarihleri: 15.07.2020 - 15.07.2023.

217Z141, Sağlıkta ve Hastalıkta Plazma Membranında Wnt/ß-Katenin Sinyal İletiminin Araştırılması, Burslu, Sonuçlandı, KBAG - Kimya Biyoloji Araştırma Destek Grubu, Uluslararası / 2551-İngiltere-BritishCouncil, ARDEB, Projeye Katılma/Ayrılma Tarihleri: 31.08.2019 - 30.09.2019, Proje Başlangıç/Bitiş Tarihleri: 15.06.2018 - 15.09.2020.

217Z123, Nörotrofin Reseptörü ile İlişkili Ölüm Bölgesi Proteininin Wnt/ß-Katenin Sinyal Iletiminin Düzenlenmesindeki Rolünün Zebrabalığı Modelinde Araştırılması, Burslu, Sonuçlandı, KBAG - Kimya Biyoloji Araştırma Destek Grubu, 1001 - Araştırma, ARDEB, Projeye Katılma/Ayrılma Tarihleri: 01.10.2019 - 01.06.2021, Proje Başlangıç/Bitiş Tarihleri: 01.06.2018 - 01.06.2021.

115S355, EMA (Expert Meeting On Neonatal And Pediatric Sepsis Consensus 2010) Kriterleri Yenidoğan Sepsisini Öngörmede Geçerli Midir? Yeni Kriterlere Gereksinim Var Mıdır?, Burslu, Sonuçlandı, SBAG - Sağlık Bilimleri Araştırma Destek Grubu, 1001 - Araştırma, ARDEB, Projeye Katılma/Ayrılma Tarihleri: 29.05.2017 - Devam ediyor, Proje Başlangıç/Bitiş Tarihleri: 01.10.2015 - 01.10.2018.

BİDEB Destekleri

RAMAZAN UĞUR BORA, Etkinlik Destekleri ve Eğitim Bursları Müdürlüğü, 2250-Lisansüstü Bursları Performans Programı, Destek Sona Erdi, 2022 - 1.

RAMAZAN UĞUR BORA, Etkinlik Destekleri ve Eğitim Bursları Müdürlüğü, 2250-Lisansüstü Bursları Performans Programı, Destek Sona Erdi, 2023 - 1.

RAMAZAN UĞUR BORA, Etkinlik Destekleri ve Eğitim Bursları Müdürlüğü, 2250-Lisansüstü Bursları Performans Programı, Destek Sona Erdi, 2023 - 2.

RAMAZAN UĞUR BORA, Etkinlik Destekleri ve Eğitim Bursları Müdürlüğü, 2250-Lisansüstü Bursları Performans Programı, Destek Sona Erdi, 2024 - 1.

RAMAZAN UĞUR BORA, Etkinlik Destekleri ve Eğitim Bursları Müdürlüğü, 2211-C Öncelikli Alanlara Yönelik Yurt İçi Doktora Burs Programı, Destekleniyor, 2021 - 2, 01.10.2021 - 30.09.2024.

Panelistlik/İzleyicilik/Raportörlük Sayısı

Görev	ARDEB	BİDEB	BİLİM TOPLUM	UİDB	TEYDEB	Toplam
Hakemlik/Panelistlik/Dış Danışmanlık Sayısı	0	0	0	0	0	0
Moderatorlük Sayısı	0	0	0	0	0	0
İzleyicilik/Danışmanlık Sayısı	0	0	0	0	0	0
Raportörlük Sayısı	0	0	0	0	0	0
Katılmadığı Panelistlik/Dış Danışmanlık Sayısı	0	0	0	0	0	0

8.3 Publication

frontiers | Frontiers in Cardiovascular Medicine

ORIGINAL RESEARCH
published: 08 April 2022
doi: 10.3389/fcvm.2022.839862

A Novel Missense Variant in Actin Binding Domain of *MYH7* Is Associated With Left Ventricular Noncompaction

Mahdi Hesaraki[1,2†], Ugur Bora[3,4†], Sara Pahlavan[2], Najmeh Salehi[5,6], Seyed Ahmad Mousavi[2], Maryam Barekat[7], Seyed Javad Rasouli[8], Hossein Baharvand[1,2], Gunes Ozhan[3,4] and Mehdi Totonchi[2,5,6*]*

[1] Department of Developmental Biology, School of Basic Sciences and Advanced Technologies in Biology, University of Science and Culture, Tehran, Iran, [2] Department of Stem Cells and Developmental Biology, Cell Science Research Center, Royan Institute for Stem Cell Biology and Technology, ACECR, Tehran, Iran, [3] Izmir Biomedicine and Genome Center (IBG), Dokuz Eylul University Health, Izmir, Turkey, [4] Izmir International Biomedicine and Genome Institute (IBG-Izmir), Dokuz Eylul University, Izmir, Turkey, [5] Department of Genetics, Reproductive Biomedicine Research Center, Royan Institute for Reproductive Biomedicine, ACECR, Tehran, Iran, [6] School of Biological Science, Institute for Research in Fundamental Sciences (IPM), Tehran, Iran, [7] Department of Regenerative Medicine, Cell Science Research Center, Royan Institute for Stem Cell Biology and Technology, ACECR, Tehran, Iran, [8] Department of Tissue Morphogenesis, Max Planck Institute for Molecular Biomedicine, Münster, Germany

OPEN ACCESS

Edited by:
Mads Kjolby,
Aarhus University, Denmark

Reviewed by:
Keiichi Hirono,
University of Toyama, Japan
Anna Meyfour,
Shahid Beheshti University of Medical Sciences, Iran

***Correspondence:**
Gunes Ozhan
gunes.ozhan@ibg.edu.tr
Mehdi Totonchi
m.totonchi@royaninstitute.org

† These authors have contributed equally to this work

Specialty section:
This article was submitted to Cardiovascular Genetics and Systems Medicine, a section of the journal Frontiers in Cardiovascular Medicine

Received: *20 December 2021*
Accepted: *22 February 2022*
Published: *08 April 2022*

Citation:
Hesaraki M, Bora U, Pahlavan S, Salehi N, Mousavi SA, Barekat M, Rasouli SJ, Baharvand H, Ozhan G and Totonchi M (2022) A Novel Missense Variant in Actin Binding Domain of MYH7 Is Associated With Left Ventricular Noncompaction. Front. Cardiovasc. Med. 9:839862. doi: 10.3389/fcvm.2022.839862

Cardiomyopathies are a group of common heart disorders that affect numerous people worldwide. Left ventricular non-compaction (LVNC) is a structural disorder of the ventricular wall, categorized as a type of cardiomyopathy that mostly caused by genetic disorders. Genetic variations are underlying causes of developmental deformation of the heart wall and the resultant contractile insufficiency. Here, we investigated a family with several affected members exhibiting LVNC phenotype. By whole-exome sequencing (WES) of three affected members, we identified a novel heterozygous missense variant (c.1963C>A:p.Leu655Met) in the gene encoding myosin heavy chain 7 (*MYH7*). This gene is evolutionary conserved among different organisms. We identified *MYH7* as a highly enriched myosin, compared to other types of myosin heavy chains, in skeletal and cardiac muscles. Furthermore, *MYH7* was among a few classes of *MYH* in mouse heart that highly expresses from early embryonic to adult stages. *In silico* predictions showed an altered actin-myosin binding, resulting in weaker binding energy that can cause LVNC. Moreover, CRISPR/Cas9 mediated *MYH7* knockout in zebrafish caused impaired cardiovascular development. Altogether, these findings provide the first evidence for involvement of p.Leu655Met missense variant in the incidence of LVNC, most probably through actin-myosin binding defects during ventricular wall morphogenesis.

Keywords: cardiomyopathy, LVNC, WES, myosin heavy chain 7, zebrafish

INTRODUCTION

Left ventricular non-compaction (LVNC) is a structural abnormality of the cardiac muscle that presents in the ventricular wall, especially in the left ventricle, leading to extended trabeculation (1), and ultimately resulting in cardiomyopathies. LVNC follows an autosomal dominant inheritance pattern (2, 3), and could develop into both hypertrophic cardiomyopathy (HCM) and dilated

cardiomyopathy (DCM) (4). Often, a genetic cause leads to LVNC that can be traced in a family which affects only the heart. The age of diagnosis varies between individuals, and ranges from birth to late adulthood. The precise cellular and molecular mechanisms of some LVNC subtypes are presently unknown. However, the time of onset and severity of the disease might be influenced by genetic conditions or developmental events such as tension heterogeneity-induced cardiac trabeculation (5, 6). Previously, mutations in various sarcomeric genes such as *MYH7* (OMIM# 160760), *MYBPC3* (OMIM# 600958), or *TNNT2* (OMIM# 1910450) were associated to LVNC and introduced as major causes for this phenotype (4, 7). However, the myocardial wall morphogenesis should be also taken into account which has been shown to be tightly regulated by several signaling pathways, including TGFβ signaling (5, 8), NOTCH signaling (5, 9), Neuregulin/Erbb signaling (5, 8), and FGF signaling (8). Given the importance of sarcomeric structure and its function in cardiac contractility, any defects in sarcomeric components could result in cardiomyopathy leading to abnormalities in cardiovascular system (10). However, pathogenic variations in sarcomeric genes specifically actin and myosin, might also influence cardiac wall development (5) and cause cardiomyopathy.

The *MYH7* gene known as the myosin heavy chain beta (MHC-β) which is classified as a type I fiber and also known as slow-twitch fiber (11). This protein is a critical component of sarcomeric structure and has several interactions with other key proteins such as actin TNN, MYBPC3 (12, 13).

Here, we report a novel heterozygous missense variant in the *MYH7* gene in an Iranian family with a high prevalence of LVNC. *In silico* analysis was performed to check the availability and developmental presence of cardiac *MYH7* transcripts. Moreover, the effect of this missense variation in *MYH7*-actin binding was modeled which suggests its potential impact on the development of LVNC in this family. Using CRISPR/Cas9 genome editing system, a zebrafish model of *MYH7* was generated which showed developmental defects in early stages of heart formation. To our knowledge, this is the first *MYH7* knockout model of zebrafish that also has an apparent cardiovascular malformation.

MATERIALS AND METHODS

Ethical Statement

The Institutional Review Board of the Royan Institute Research Center and the Royan Ethics Committee (Tehran, Iran) approved this study. Written informed consent was obtained from all members of this family or their guardians. Zebrafish are maintained in accordance with the guidelines of the Izmir Biomedicine and Genome Center's Animal Care and Use Committee. All animal experiments were performed with the approval of the Animal Experiments Local Ethics Committee of Izmir Biomedicine and Genome Center (IBG-AELEC). All methods were performed in accordance with the declaration of Helsinki 1975.

Subjects

This study was performed between 2018 and 2019 in Iran and comprised 20 genetically dependent members diagnosed with LVNC, who were between 12 and 53 years of age. The patients were diagnosed at the Royan Institute Cardiac Clinic (Tehran-Iran) by physical examination, electrocardiogram (ECG), and echocardiogram (Echo) assessments. All affected members had severe deep recesses and extended trabeculations in their left ventricular myocardia, and had normal heart valve function without additional symptoms related to other disorders (**Table 1**).

Genomic Characterization

Peripheral blood samples were obtained for molecular analysis from all members of the family ($n = 20$). All genomic DNA was isolated by the salting out DNA extraction method and quantified with a NanoDrop 1000 Spectrophotometer (Thermo Fisher). The inheritance of LVNC in this pedigree follows an autosomal dominant pattern. Thus, we included 3 brothers of second generation in the WES study and skipped others. WES was performed using the Illumina NovaSeq platform and generated paired-end reads of 150 base pairs with an average coverage of 100X. Reads were aligned to genome reference consortium human 19 (GrCh37) with the Burrows-Wheeler Aligner (BWA, V.0.7.17) (14). The duplicated reads were removed by the Sequencing Picard tool. The Genome Analysis Toolkit (GATK, V4), followed by the best practice pipeline (15), was used for preprocessing the alignment results, detection and removal of duplicate reads, base recalibration, and variant calling. The VCF Filter toolkit was used for post-processing the variant calling results and variants that had a minimum depth of 12, mapping quality of 40, and quality of 30 were retained. The wANNOVAR website (http://wannovar.wglab.org/) was used for annotations (16). After the annotation process, all synonymous variations and those with ExAC frequency >0.01 were filtered by PolyPhen-2 (http://genetics.bwh.harvard.edu/pph2/), the prediction algorithms. The sorting intolerant from tolerant (SIFT) (http://sift.bii.a-star.edu.sg/) and MutationTaster (http://www.mutationtaster.org) were used to evaluate candidate variations.

Segregation Analysis and Sanger Sequencing

DNA samples from 20 members of the family were screened for the *MYH7* candidate variant via the semi-nested PCR and Sanger sequencing methods. The primers used in this study were: F1: 5-ACTGTCGTGGGCTTGTATCA-3; F2: 5-CTGTCTCCTTGGTGCATTCG-3; and R1: 5-TGGTGGTAGGTAGGGAGATG-3. All PCRs were carried out in 25 μl volumes that consisted of a 12.5 μl PCR master mix, ∼100 ng DNA, 1 μL of each primer (10 μM), and ∼15 μL double distilled water (DDW). Cycling conditions involved denaturation (94 °C, 10 min) followed by 30 cycles of 94°C for 40 s, 54/57°C for 35 s, 72°C for 45/35 s, and a final extension at 72°C for 5 min. Finally, the sequencing results were aligned to the reference sequence in the CLC Main Workbench 5.5 software.

MYH7 Expression Patterns

The expressions of the MYH protein classes in different tissues were compared using public databases. The BioGPS (http://

TABLE 1 | Overview of clinical features of LVNC in the affected family members.

Individual identifier	1	2	3	4	5	6	7	8
Affected individual	II-2	II-4	II-8	II-6	II-10	III-8	III-9	III-10
Gender	M	M	M	F	F	M	M	M
Age at last examination (years)	54	50	43	53	56	17	12	Died at 12
Gene	*MYH7*	*MYH7*	*MYH7*	*MYH7*	*MYH7*	*MYH7*	*MYH7*	unknown
Chromosome change (Hg19)	c.C1963A	c.C1963A	c.C1963A	c.C1963A	c.C1963A	c.C1963A	c.C1963A	unknown
Protein change	p.L655M	p.L655M	p.L655M	p.L655M	p.L655M	p.L655M	p.L655M	unknown
Mutation type	Missense	Missense	Missense	Missense	Missense	Missense	Missense	-
Allele type	Hetero	Hetero	Hetero	Hetero	Hetero	Hetero	Hetero	unknown
Confirmation method	WES and S.S	WES and S.S	WES and S.S	S.S	S.S	S.S	S.S	-
ECG	Abnormal	Abnormal	Abnormal	Abnormal	Abnormal	Abnormal	Abnormal	Abnormal
Echo	LVNC	LVNC	LVNC	LVNC	LVNC	LVNC	LVNC	LVNC
MRI	LVNC	LVNC	LVNC	-	-	LVNC	LVNC	-
Other	Diabetes, hypertension		Dizziness, hypertension, peripheral edema, dyspnea					

M, Male; F: Female; LVNC, Left ventricular non-compaction cardiomyopathy; Hetero, Heterozygous; ECG, Electrocardiography; Echo, Echocardiography; MRI, Magnetic resonance imaging; WES, Whole-exome sequencing; SS, Sanger sequencing.

biogps.org/) expression database was the best to evaluate all *MYHs* expression patterns in the human tissues. In the next step, the expression pattern of *MYH7* during developmental stages of the mouse heart (E10.5-Old) was checked in a high-throughput expression data set (GEO: GSE93271, expression profiling by array,) and a $p < 0.05$ was considered as significantly different in the signal intensity (17). Then, the expression level of *MYH7* (also known as ventricle myosin heavy chain like (*vmhcl*) as a zebrafish homolog of *MYH7* in human) was checked in zebrafish heart at different developmental stages using a high throughput expression dataset (GEO: GSE120236, RNA-sequencing) (18) and a $p < 0.05$ on normalized counts was considered as significantly different. All expression analyses were performed using pheatmap package in RStudio.

Structural Analysis of *MYH7*

The 3D structure of *MYH7* was retrieved from the RCSB database (PDB ID:5TBY) for structural analysis. The p.Leu655Met mutation of the protein structure was induced by the psfgen plugin of VMD 1.9.3 (19). Both the wild type and mutant structures were minimized for 20 000 steps by the conjugate gradient method. Minimizations were done in NAMD 2.12 package (20) with CHARMM27 force field (21). The HADDOCK2.2 web server, which is an information-driven flexible docking approach (22, 23), was used to evaluate the effect of the p.Leu655Met mutation on the interaction between *MYH7* and actin. The actin binding regions in *MYH7* (655 to 677 and 757 to 771 residues) were set as the "active residues." The surface neighbors of the active residues were selected as the "passive residues" that were automatically determined by HADDOCK2.2. The actin 3D structure and binding residues in interaction with *MYH7* (residues of 3, 23, 24, 28, 30, 146–148, 333–345, 348, 350 from PDB ID of 4A7F) and the common binding site for actin-binding proteins on the actin surface (residues of 143, 144, 146, 148, 168, 341, 345, 346, 349, 351, 355) (24) were set as the "active residues" in interaction with *MYH7*. All other HADDOCK settings were kept at the default values. The docking results were ranked based on the HADDOCK score, which is a weighted sum of intermolecular electrostatic (Elec), van der Waals (vdW), desolvation (Dsolv), and buried surface area (BSA) (22, 23). All complex conformations were shown and analyzed by VMD 1.9.32.

Targeting Zebrafish

Target sequence of *MYH7* gene was selected by using the cloud-based informatics platform "Benchling" (https://www.benchling.com/crispr/). GRCz11 genome dataset was selected for determination of the target and guanine nucleotide was added to the 5′ of the target sequence to increase the efficiency of *in vitro* transcription. Template was generated by PCR using Phusion High-Fidelity DNA Polymerase (ThermoFisher Scientific) with the forward primer containing T7 promoter and targeted sgRNA sequence and the reverse primer encoding for the standard chimeric sgRNA scaffold (**Supplementary Table 1**). Scrambled

(scr) gRNA was used as control. DNA template was purified with NucleoSpin Gel and PCR Clean up Kit (Macherey-Nagel GmbH & Co KG). sgRNAs were transcribed *in vitro* by using HiScribe™ T7 High Yield RNA Synthesis Kit (New England Biolabs). Transcription products were purified with RNA Clean & Concentrator-25 kit (Zymo Research, CA). RNA quantity was determined by NanoDrop™ OneC (Thermo Fischer Scientific).

Ribonucleoprotein (Rnp) Complex Preparation and Microinjection

sgRNA and Guide-it™ Recombinant Cas9 (Takara Bio Inc) were mixed at 1:1 (500/500 ng/μL) and incubated at room temperature for 5 min to generate the RNP complex. 0.05% phenol red was added to the mixture for visualization of injection. 1–1.5 nL of solution was injected directly into the cytoplasm of 1-cell stage zebrafish embryos.

Zebrafish Genotyping

Embryos injected with RNPs were used for genotyping at 5 dpf. Ten larvae were transferred individually to 1.5 mL tubes in 50 μL DNA extraction buffer (10 mM Tris HCl pH:8.0, 50 mM KCl, 0.3% Tween 20, 1 mM EDTA) and incubated at 98°C for 10 min. Next, 3 μl of proteinase K solution (5 mg/mL; Sigma Aldrich) was added and incubated at 55°C overnight. Samples were incubated at 98°C for 10 min to inactivate proteinase K and centrifuged at 14.000 rpm for 4 min. Supernatants were transferred into new tubes, mixed with 50 μL ddH_2O, 10 μL 3M sodium acetate, 180 μl isopropanol, vortexed and kept on ice for 10 min. Samples were centrifuged at 14,000 rpm for 15 min at 4°C. Supernatants were discarded and pellets were washed with ice-cold 70% ethanol and air-dried for 15 min. Pellets were resuspended in 10 μL nuclease-free water. Genomic DNA quantity was determined by NanoDrop™ OneC. Targeted *MYH7* loci that were amplified with PCR, used for Sanger sequencing. Genomic DNA was used as template at 100 ng/μL concentration and mixed with CloneAmp HiFi PCR Premix (Takara Bio Inc). Primers were designed to contain the mutation area (**Supplementary Table 1**). Final volume was adjusted to 25 μL with nuclease-free water. PCR was performed in SimpliAmp Thermal Cycler (Thermo Fischer Scientific) using the following conditions: 98°C for 1 min; 35 cycles of 98°C for 30 s, 62°C for 30 s and 72°C for 20 s; 72°C for 10 min. 1 μL of each sample was loaded into 1% agarose gel and electrophoresed. PCR products were cleaned up with NucleoSpin Gel and PCR Clean-up Kit. Products were quantified by using NanoDrop™ OneC.

In vivo Imaging of Zebrafish Embryos and Larvae

Phenotypic evaluation of embryos and larvae was performed using an Olympus SZX2-ILLB stereomicroscope (Olympus Corporation, Japan). Images were captured with an Olympus SC50 microscope camera (Olympus Corporation, Japan).

Whole-Mount *in situ* Hybridization

Larvae were collected at 3 dpf and 5dpf and fixed in 4% PFA for 48 h. Larvae were washed twice with PBT, twice with methanol for 5 min each at RT and stored at −20°C for further use. Antisense RNA probes for *MYH7, MYH7l, and mylk3* were synthesized. Briefly, a forward primer and two reverse primers were designed for each gene. One of the reverse primers were with T7 promoter sequence for *in vitro* transcription. First round of PCR was performed for amplification of the template. Second round of PCR was carried out to add T7 promoter. Probes were transcribed *in vitro* by using T7 RNA Polymerase (Thermo Fischer Scientific). Larvae were rehydrated by serial washes in 75% to 25% methanol/PBT for 5 min each followed by four PBT washes. Next, larvae were treated with Proteinase K (40 μg/μL) for 30 min, re-fixed in 4% PFA for 20 min and thoroughly washed afterwards. WMISH was performed as described previously (25, 26). Following prehybridization in hybridization buffer (Hyb) for 5 h at 67°C, samples were incubated with antisense probes in Hyb o/n at 67°C. The next morning, Hyb with probes were replaced with Hyb and incubated at 67°C for 20 min. Serial washes at 67°C were performed as follows: Three times in 2X 50% SSCT/50% formamide for 20 min, twice in 2X SSCT for 20 min and four times in 0.2X SSCT for 30 min. After a brief wash in PBT at RT, larvae were blocked with 5% sheep serum (Sigma-Aldrich) and 10 mg/ml BSA in PBT for 2 h and incubated in anti-Digoxigenin-AP Fab fragments o/n at 4°C (Merck&Co). After the removal of the antibody, larvae were washed in PBT over 3 h with 7–8 changes. Larvae were washed three times with NTMT buffer for 5 min, transferred into a 24 well-plate, stained with BCIP/NBT in NTMT buffer. Larvae were washed twice with PBT, incubated in stop solution for 1 h, washed twice with PBT and kept in 80% glycerol/20% stop solution until imaging (26, 27).

RESULTS

Patients' Information

The Iranian family examined in this study, consisted of individuals with an autosomal dominant inheritance pattern. The proband was 55 years old with diabetes mellitus and hypertension since age 34 due to multivessel nonsignificant coronary artery disease and moderate left ventricular dysfunction (LVEF: 35–40%). He received anti-ischemic therapy without any LVNC diagnosis. The second brother was 44 years old and had repeated non-angina chest pain since age 36. We recruited a 46-year-old brother as the third member, who was asymptomatic until age 37 when his symptoms started to manifest with dizziness and hypertension. Currently, he suffers from occasional non-anginal chest pain, intermittent dyspnea on exertion and peripheral edema. He is in New York Heart Association (NYHA) class II. The last brother, who is 35 years old (III-11), was examined twice and found to have a normal left ventricular wall without any signs of LVNC. All affected siblings had late onset symptoms of LVNC that occurred around the third decade of life. One offspring (III-10) died at the age of 12 with LVNC phenotype (**Figure 1A** and **Table 1**).

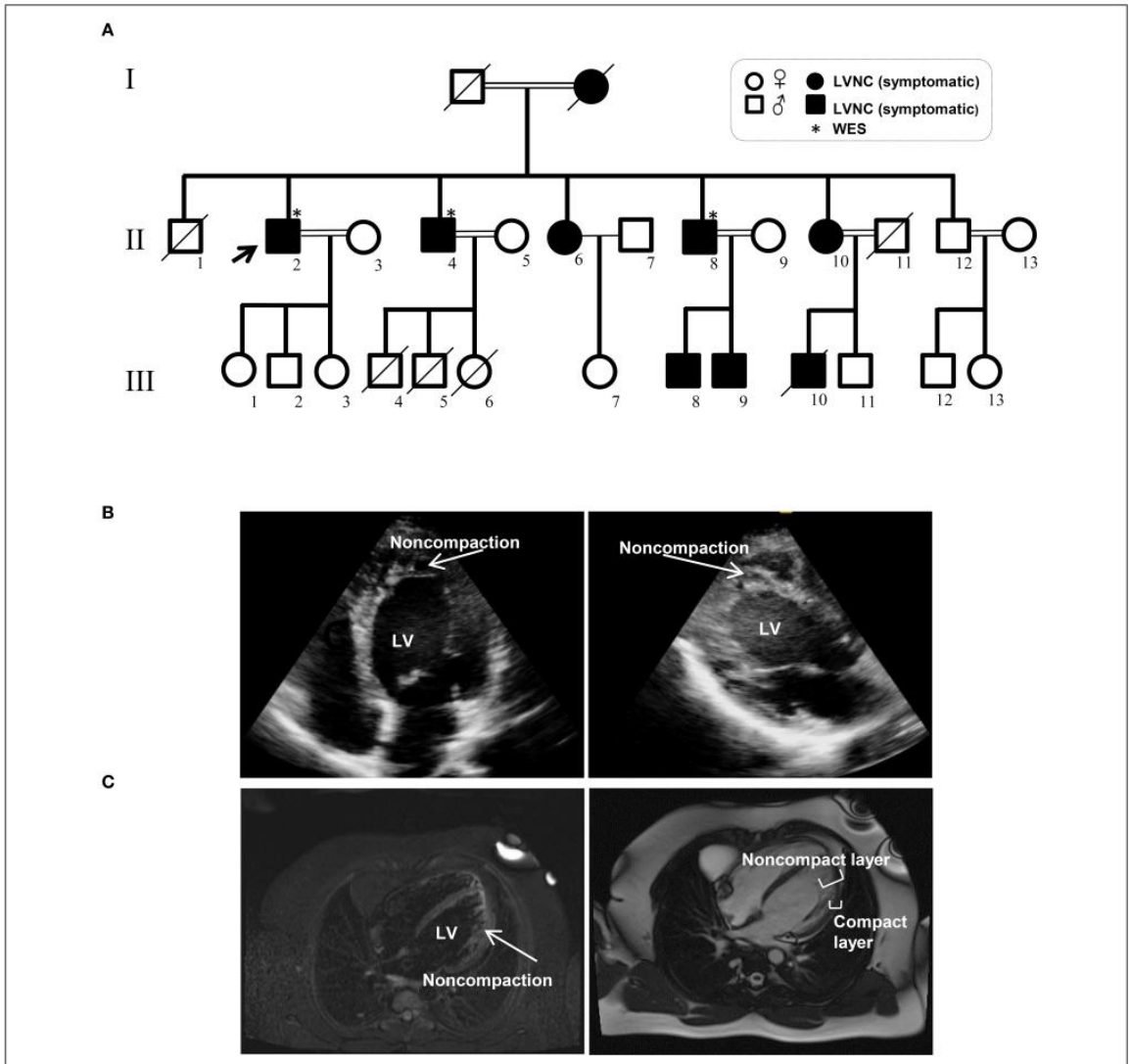

FIGURE 1 | Pedigree and clinical manifestation of the left ventricular non-compaction (LVNC) in the affected members included in this study. **(A)** A pedigree of the family shows the number of affected members (affected members: shaded, WT: unshaded). A black arrow indicates the proband. Genotypes for the proband and all other family members are shown. **(B)** Echocardiograph (ECG) images of affected individuals with LVNC of the myocardium. **(C)** Magnetic resonance imaging (MRI) of thin epicardial and trabeculated endocardial layers of the ventricular wall.

Variant in Myosin Heavy Chain 7 (*MYH7*) Identified as a Candidate for LVNC

WES was performed using the Illumina NovaSeq platform, which generated paired-end reads of 150 base pairs with an average coverage of 100X for the three affected, well-characterized brothers (II-2, II-4, and II-8) who had clinically proven disease (**Figures 1B,C** and **Table 1**).

A novel non-synonymous variant in *MYH7* was identified (c.1963C>A:p.Leu655Met, GenBank: NM_000257) (**Figure 2A**). Myosin heavy chain beta (MHC-β) or *MYH7* protein is encoded by the *MYH7* gene on chromosome 14. The identified variant was a pathogenic missense variation. All three affected individuals were heterozygotes, which was further confirmed by Sanger sequencing (**Figure 2B**). Other variations in this gene are

associated with HCM (13), DCM (28, 29) and LVNC (30–32). The resultant protein is composed of a myosin N-terminal SH3-like domain (residues 32–81), a myosin motor domain (residues 85–778) and an IQ domain (residues 781–810). *MYH7* is an actin based motor protein that exhibits ATPase activity (22, 24). On the other hand, this protein has two actin-binding regions (655–677 and 757–771) and one nucleotide-binding region (178–185) (22, 24).

Segregation analysis of all family members (20 members) confirmed the presence of heterozygous alleles ($MYH7^{W/M}$) in all seven affected members and wild type alleles ($MYH7^{W/W}$) within the healthy members (**Figure 2B**). *In silico* prediction tools were used for protein-protein interaction analysis to predict the functional consequences of p.Leu655Met at the structural level. Phylogenetically, this variant is located in a conserved region among mammalians, and zebrafish and belongs to the motor domain area of the *MYH7* protein (**Figure 2C**). Several prediction tools suggested this variant as a pathogenic one; MutationTaster2 predicted that it is a disease-causing mutation with a score of 0.489. SIFT showed a damaging score of 0.912 and Polymorphism Phenotyping v2 (PolyPhen-2) predicted a score of 0.971.

In preliminary studies, two boys in the third generation (III-8 and III-9) showed no specific clinical symptoms and appeared healthy at the initial consultation. However, after genotyping of all family members, it was found that III-8 and III-9 also carry this variation. To confirm the genotyping results, III-8 and III-9 were referred to a specialist, and they were diagnosed with mild LVNC symptoms.

MYH7 Expression Patterns

The expression patterns of all myosin heavy chain classes were explored using a bio GPS database in order to investigate the tissue specificity of this protein. The results revealed high *MYH7* protein expression levels in the heart, skeletal muscle, and fetal thyroid (**Supplementary Figure 1**). This result further confirmed the phenotypic presentations of the affected members, which was cardiac dysfunction and mild muscle weakness. These data suggested that *MYH7* protein might be one of the major myosin heavy chain classes in the heart and skeletal muscle, and thus its mutations could result in cardiac and skeletal manifestations. Comparison of RNA sequencing data from various developmental stages of mouse heart revealed that, while all myosin classes were expressed, *MYH7* had the highest expression level in all embryonic stages as well as in the adult and aged mouse hearts (GEO: GSE93271) (**Figure 3A**). Furthermore, the *in silico* analysis revealed that various myosin classes are expressed during different cardiac developmental stages of zebrafish [at 24, 48, and 72 h post fertilization (hpf)] (GEO: GSE120236). And *MYH7* expression pattern showed the highest level among all myosin heavy chain classes in every stage (**Supplementary Figure 2**).

Contractile machinery of cardiac muscle is mainly dependent on actin and myosin proteins and their function; thus, it is likely that any structural associated dysfunction of these proteins would greatly affect cardiac performance.

In silico Modeling for *MYH7*-Mutant Interactions With Actin

For evaluating the effect of the variation (p.Leu655Met) on *MYH7* function, the wild type and mutant minimized structures of *MYH7* were docked with actin through the HADDOCK2.2 web server. The most reliable complex conformation of the wild type and mutant *MYH7* interactions with actin were selected based on the HADDOCK2.2 results and presented here. Both complexes were aligned based on the *MYH7* structure and shown in surface (**Figure 3B**) and secondary structure cartoon (**Figure 3C**) representations. The averaged HADDOCK2.2 score over the top four members of the best cluster was -125.1 ± 13.7 for the wild type *MYH7*-actin complex, which increased for the mutant *MYH7*-actin complex (HADDOCK2.2 score $= -115.1 \pm 13.4$). This result revealed that the mutant complex was relatively more unstable than the wild type complex. In addition, a comparison of the actin protein position in interaction with the mutant *MYH7* (red in **Figures 3B–D**) and wild type (green in **Figures 3B–D**) showed a mean root mean square deviation (RMSD value) of 48.05 Å, which indicated rotation and transition of this protein. In the p.Leu655Met mutation, a leucine amino acid is changed to methionine, which is a longer hydrophobic amino acid with an S-methyl thioether side chain. As it can be seen in **Figure 3D**, the amino acid at position 655 tends to the inner side of the protein. The methionine in this position would stabilize the structure with its longer hydrophobic side chain and S/π interactions between the side chain sulfur atom and aromatic amino acids. Thus, we postulate that this conformational change leads to a weaker binding energy of the actin protein to the 655M residue and subsequent functional insufficiency.

Generation of *MYH7* Knockout Zebrafish

WES data revealed that p.Leu655Met point mutation in the *MYH7* gene is related with LVNC. Next, to investigate the role of *MYH7* in vertebrate heart development *in vivo*, we exploited clustered regularly interspaced short palindromic repeats/CRISPR associated protein 9 (CRISPR/Cas9) technology to generate a *MYH7* knockout (KO) zebrafish model (33, 34). We specifically designed a sgRNA to target exon 18, similar loci where the missense mutation occurred in patients. Following the microinjection of ribonucleoprotein (RNP) complex, we monitored the embryos daily under a stereomicroscope and observed a pronounced phenotype in majority of the embryos starting from 3 days post-fertilization (dpf). Next, we extracted genomic DNA from individual larvae at 5 dpf and proceeded with Sanger sequencing in order to determine insertions and deletions (indels). Sequencing results confirmed indels in *MYH7* gene with an efficiency of approximately 90% (data not shown). We further characterized *MYH7* KO zebrafish by using fluorescence microscopy to examine heart development and whole-mount *in situ* hybridization (WMISH) to detect mRNA expression of cardiac marker genes.

Daily observation of *MYH7* KO zebrafish larvae revealed cardiovascular defects such as pericardial edema, chamber formation at pericardial sac and misshapen heart that became

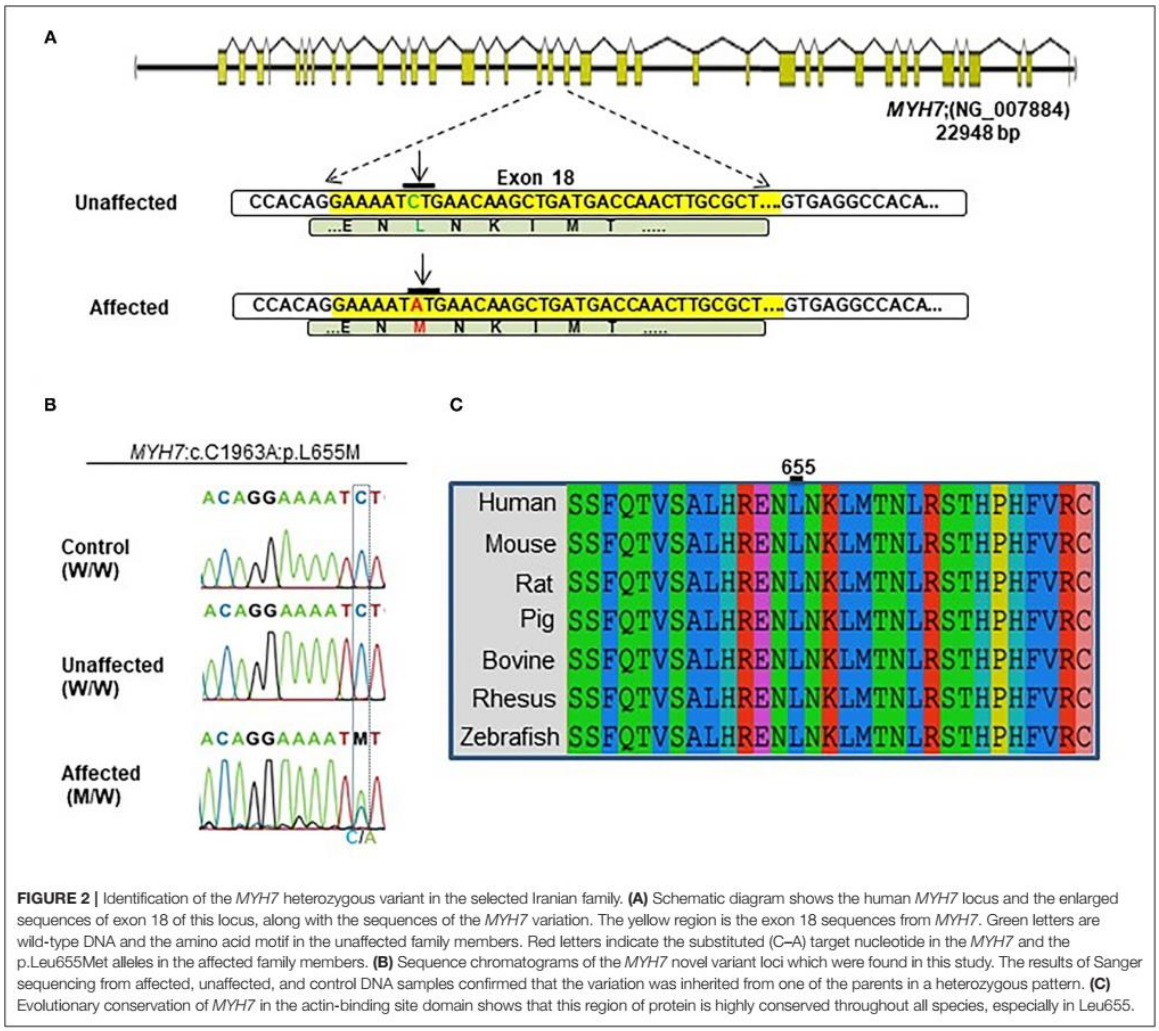

FIGURE 2 | Identification of the *MYH7* heterozygous variant in the selected Iranian family. **(A)** Schematic diagram shows the human *MYH7* locus and the enlarged sequences of exon 18 of this locus, along with the sequences of the *MYH7* variation. The yellow region is the exon 18 sequences from *MYH7*. Green letters are wild-type DNA and the amino acid motif in the unaffected family members. Red letters indicate the substituted (C–A) target nucleotide in the *MYH7* and the p.Leu655Met alleles in the affected family members. **(B)** Sequence chromatograms of the *MYH7* novel variant loci which were found in this study. The results of Sanger sequencing from affected, unaffected, and control DNA samples confirmed that the variation was inherited from one of the parents in a heterozygous pattern. **(C)** Evolutionary conservation of *MYH7* in the actin-binding site domain shows that this region of protein is highly conserved throughout all species, especially in Leu655.

visible starting 3 dpf compared to the control sgRNA injected larvae. We also observed hemorrhage at various parts of the body near the heart and the vasculature system (**Figure 4A**). Pericardial and yolk sac/abdominal edema continued to expand until 5 dpf. At day five post fertilization, *MYH7* KO fish showed thickened heart with abnormal development of atrial and ventricular chambers as well as disturbed S-looping process (13), resulting in nearly unified heart (**Figure 4A**). **Supplementary Video 1** shows a 5-dpf *MYH7* KO zebrafish larva with complications in heart contraction and blood flow, which are likely to be responsible for the hemorrhage. In addition, mutant fish exhibited reduced swimming ability and mobility (data not shown). Cardiac malformations advanced over time, where most of the larvae were dead at 7 dpf due to failure of proper cardiovascular system development. These data suggest that *MYH7* gene is essential for cardiovascular development.

The zebrafish heart has a tubular form at 1 dpf, later, it undergoes morphogenesis including looping and chamber ballooning at 2 dpf and forms the functional heart at 5 dpf (35). To understand how these processes are affected by *MYH7* loss-of-function, we injected *MYH7* sgRNA into the embryos of Tg(actb2:hyper3), a transgenic zebrafish reporter that contains the GFP driven by the *cmlc2* promoter (cmlc2:egfp) transgenesis marker within HyPer3 (36). The *MYH7* mutant zebrafish exhibited disorganized heart with enlarged atrium and ventricle along with abnormal looping at 3 dpf (**Figure 4B**). We observed several heart morphological defects in *MYH7* KO zebrafish. Majority of the larvae displayed elongated and granulated ventricle at 4 dpf (**Figure 4B**). At 5 dpf, loss of *MYH7*

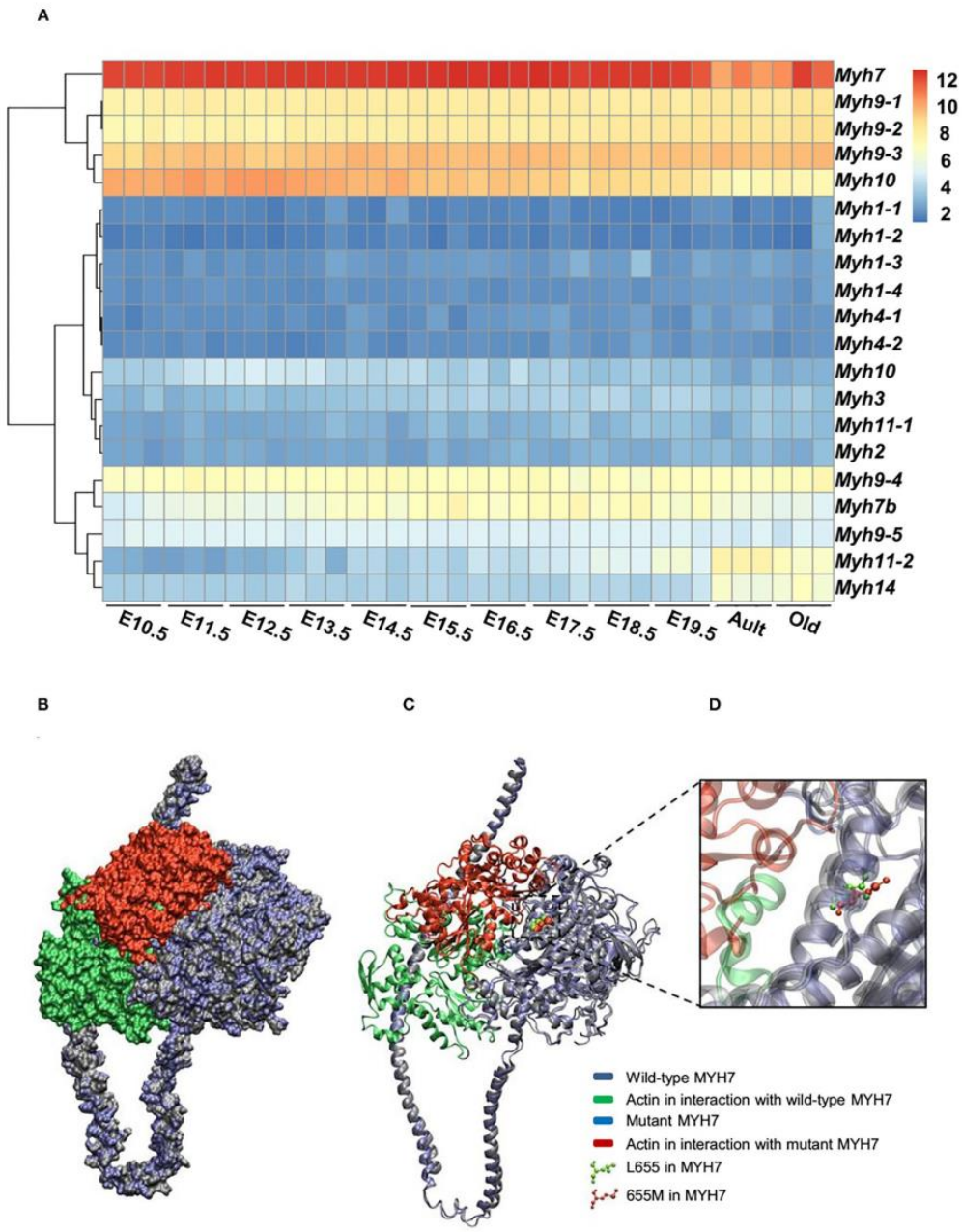

FIGURE 3 | Expression patterns of all *MYH* superfamily members during cardiac development. **(A)** Differential expression pattern of *MYH7* in the mouse heart during 12 stages of development indicates that the expression of this gene plays an important role in the mouse cardiogenesis, especially during embryonic life. **(B)** Modeling scheme of the protein-protein interaction between native *MYH7*/actin and *MYH7* p.Leu655Met/actin at the surface. Actin in the wild-type position is shown in green and in the mutant position, is shown in red. **(C)** Secondary structure cartoon representation. Actin in the wild-type position is shown in green, and in the mutant position, is shown in red. **(D)** The Leu655Met mutation is highlighted. Wild *MYH7* protein (Leu 655) is shown in green, and the protein that has the mutated residue (Met 655) is shown in red.

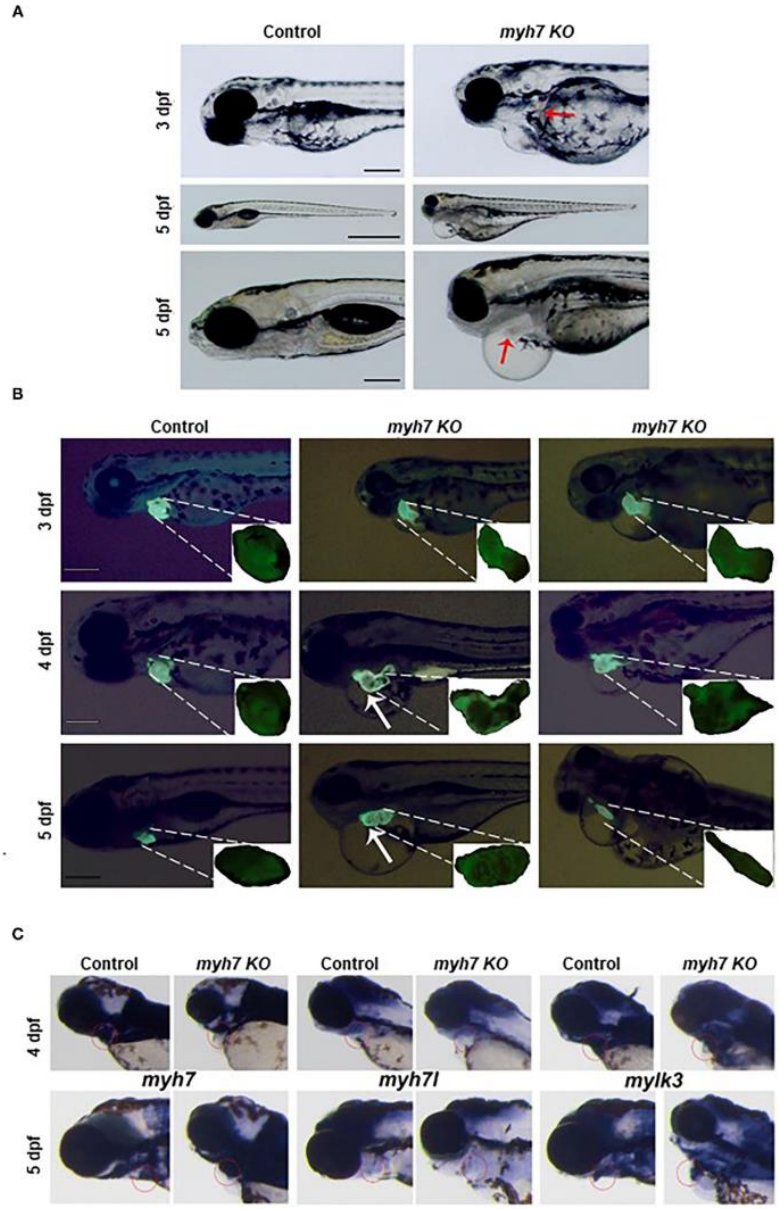

FIGURE 4 | The *MYH7* deficiency causes cardiovascular defects in zebrafish. **(A)** Loss of *MYH7* disrupts heart development. Lateral view of 3 and 5 dpf scramble gRNA injected control group and *MYH7* KO larvae. Cardiac edema is clearly noticeable. Arrow at 3 dpf shows hemorrhage near heart. Edema accumulated around heart and spread to the abdominal area at 5 dpf. Arrow at 5 dpf shows enlarged heart. Scale bars: 200 μm in 3 and 5 dpf, 1 mm in middle 5 dpf. **(B)** The *MYH7* knockout zebrafish has distorted cardiac chamber formation and looping as shown by fluorescence imaging of the Tg(*actb2:hyper3*) transgenic zebrafish reporter injected with scramble or *MYH7* sgRNA. Representative images of control and mutant zebrafish are shown at 3, 4, and 5 dpf. Two different *MYH7* KO fish at 3 dpf showed abnormal looping. Two different *MYH7* KO fish at 4 dpf displayed enlarged and deformed ventricles. At 5 dpf, *myh*7 KO fish showed enlarged and granulated ventricle. Furthermore, a *MYH7* mutant zebrafish with tubular heart is shown. Scale bars: 200 μm. **(C)** *MYH7* is essential for proper formation of the cardiac ventricle and the pericardial cavity as shown by WMISH. Expression of *MYH7, MYH7l, and mylk3* mRNAs is strongly reduced in *MYH7* KO zebrafish at 4 dpf. *MYH7* expression expands to the pericardial cavity and ventricular chamber in *MYH7* KO fish at 5 dpf. *MYH7l* expression is reduced in *MYH7* KO fish at 5 dpf. Expression of *mylk3* in the cardiac ventricle of *MYH7* KO larvae is disrupted at 5 dpf.

function was visible as bloated heart with thickened ventricle and altered S-looping formation (**Figure 4B**). Moreover, some larvae exhibited a tubular heart phenotype with visible separation between atrium and ventricle but no S-loop formation, resulting in a drastic reduction of the heart volume, ventricular contraction and blood flow rate (**Figure 4B** and **Supplementary Video 2**). These results indicate that *MYH7* is necessary for proper establishment of the heart at the morphological level and its contractile function.

Cardiac Ventricular Gene Expression Is Disturbed in *MYH7* KO Zebrafish

Next, to investigate how *MYH7* mutation affected cardiac ventricular-related gene expression, we exploited WMISH by using the antisense RNA probes for *MYH7* and two other cardiac genes *myosin heavy chain 7-like* (*MYH7l*) and *myosin light chain kinase 3* (*mylk3*) on control and *MYH7* KO zebrafish larvae at 3 and 5 dpf. In control larvae, *MYH7*, *MYH7l,* and *mylk3* were properly expressed at the cardiac ventricle at 3 and 5 dpf (**Figure 4C**). In contrast, their expression levels were significantly reduced in *MYH7* KO larvae at 3 dpf. At 5 dpf, *MYH7* expression appeared to expand in parallel to the widening pericardial cavity and ventricular chamber (**Figure 4C**). The *MYH7l* was hardly detectable in the mutant larvae at 5 dpf. Expression of *mylk3* was also severely distorted in the cardiac ventricle of *MYH7* KO larvae, in accordance with its key role in enhancement of contraction force via regulation of actin-myosin interaction (**Figure 4C**) (37). These results suggest the *MYH7* role in heart development, especially in proper formation of the cardiac ventricle and the pericardial cavity.

DISCUSSION

MYH7 or cardiac muscle beta isoform, the protein encoded by *MYH7,* is a member of the myosin superfamily of proteins expressed in muscle cells. *MYH7* contributes to movement and contraction, especially in cardiac cells, and plays a vital role in the sarcomere structure and heartbeat. Any mutation in *MHY7* can influence contractile properties and form-function relationship (32, 38) by affecting its binding to actin, MYBPC3, and TNNT2. The normal *MYH7* can also regulate ATP consumption and protein-protein interaction, and as a result, the binding regions of this protein and accompanying proteins are crucial to the function of myosin (39).

In this study, we used WES to elucidate the cause of LVNC in a highly affected Iranian family. WES analysis revealed a novel variation in the *MYH7* gene. Segregation analysis confirmed the variation in the affected members. In the next step, the expression pattern of myosin heavy chain classes was investigated in human tissues and in developmental stages of mice and zebrafish hearts. These analyses highlighted higher expression of *MYH7* in the heart and skeletal muscle, the entire mouse and zebrafish cardiogenesis, in addition to its presence in adult mice hearts. According to this finding, *MYH7* activity starts in the early embryonic stages of heart development. Due to its important role in the heart, its expression is distinct and excessive in this tissue. *MYH7* is also expressed differently from other myosin classes in the heart. A previous report also indicated higher expression levels of *MYH7* during the fetal stage of mice and its conditional depletion led to mild adulthood lethality (40, 41). The current RNAseq data analysis also suggested an important developmental role for myosins, especially for *MYH7*, as they are expressed ubiquistously during mouse cardiac organogenesis.

A novel missense variant was identified (c.1963C>A:p.Leu655Met) in the *MYH7* gene of a rare cardiomyopathy condition called LVNC by using WES analysis, a mutation that affected the *MYH7*-actin interaction. SIFT data showed that the region in which the new variant is located, is sensitive to amino acid changes and would impair *MYH7*-actin binding and its function. Thus, WES analysis provides great opportunity for researchers to find the correlation between the phenotype and genotype in inherited diseases. The results of *MYH7* protein alignment revealed that the original Leu655 is a conserved amino acid between several disciplines of vertebrates. These findings further highlight the importance of this protein's originality and the reason underlying its Leu655 conservation over the course of evolution. Although several researchers have investigated different variations in the vicinity of the actin-binding domain with the HCM phenotype (13, 42–44), This study suggested, for the first time, a novel variation of *MYH7* which might affect the actin-binding site that causes LVNC (45–47).

In mammalian muscles, actin-myosin machinery requires a regular cycle of ATP molecules and the frequent binding of two proteins, actin and myosin. This process is regulated by the myosin light chain protein (48, 49). Any malfunction of this regulator will reduce the contractile strength and loss of actin filament mobility (50, 51). The 3D analysis of myosin heavy chain classes by crystallography (52) and cryo-electron micrographs of actin-myosin complexes (53) provide platforms for studying this complex under different conditions (39). In the current study, we investigated the interaction between *MYH7* and actin at the new variation site. Three-dimensional modeling revealed that the *MYH7* mutant, which causes an amino acid exchange in the actin-binding site, resulted in a change in protein-protein interaction by actin rotation and transition. Interestingly, in other reports, similar variations near the actin-interacting domain were associated with different stages of HCM (13, 42, 54). However, in our affected family members, the pathogenicity is an LVNC phenotype, which is another type of cardiomyopathy. This difference between our clinical report and other studies needs to be investigated in more detail to find the appropriate correlation between these two phenotype manifestations.

An investigation to the effect of the uncovered variant(s) in terms of protein structure and function, may provide more information on the specific cellular events during an organ function as well as development. In the early stages of heart development, delamination of compact layer cardiomyocytes is the result of apical-basal polarization. Enrichment of the actomyosin network on the apical side of the delaminating cardiomyocytes has been reported (5). We

suggest that the current *MHY7* variation may have altered the delamination process by affecting the frequency of apical-basal polarization and excessive response to tension heterogeneity. As a result, this variation induces more delamination signaling or more proliferation in delaminating cardiomyocytes, which eventually leads to irregular trabecular structures and deep recesses.

Here, we have generated the zebrafish knockout model of *MYH7* by using CRISPR/Cas9 genome editing technology and examined the influence of *MYH7* on cardiac morphogenesis and ventricular contraction. Cardiomyopathies have been modeled by using a variety of genetic or chemical manipulation techniques. The most abundant phenotypic indicators for zebrafish cardiomyopathy are (i) edema in the heart and the pericardial sac (ii) disrupted S-looping morphogenesis, and (iii) deformation of the heart anatomy. These phenotypic characteristics are consistent with those observed in other cardiomyopathy models (13, 55, 56).

Genetic screening of LVNC patients has identified several variations in genes encoding for sarcomeric proteins including *MYH7*, α-cardiac actin, cardiac troponin T, tafazzin, α-dystrobrevin, lamin A/C and dystrophin (30, 57, 58). Most of these genes have been associated with contractile function. Moreover, a mouse model of LVNC generated by a missense variation in the cardiac muscle gene *dystrobrevin-α* shows multiple trabeculations, expanded left ventricle and cardiac contractile dysfunction (59). Our *MYH7* KO zebrafish displays abnormally developed heart with pericardial edema, severe hemorrhage, distorted chambers and contraction problems. The correlation of features between these models suggest the use of our KO zebrafish as a platform to investigate the molecular mechanisms of *MYH7*-related disorder such as non-compaction cardiomyopathies.

The *MYH7* is major sarcomeric protein that is mainly expressed in the zebrafish heart. There are nine zebrafish homologs of the human *MYH* gene and seven of them share more than 80% protein homology with human *MYH7* (60). Being a component of the myosin complex, zebrafish *MYH7* is expressed in a variety of structures, including the heart primordium, the pericardial region and the musculature system during embryogenesis. The cardiac ventricle is a prominent structure where we detected high levels of *MYH7* in zebrafish embryos. Thus, disrupted heart formation and ultimate death of *MYH7* KO larvae suggests its key role in cardiovascular system development.

CONCLUSION

In summary, this study introduced a novel genetic variation in *MYH7* (c.1963C>A:p.Leu655Met) and its corresponding clinical outcome was associated with LVNC. Data analysis and segregation study allowed us to predict new patients in the pedigree. Genotyping results combined with clinical phenotypes can confirm the function of any genetic variation and identify all affected, asymptomatic members in the pedigree for earlier and more effective treatment strategies. *In silico* and *in vivo* studies suggested actin-myosin binding changes as the underlying mechanism for *MYH7* variation phenotype.

DATA AVAILABILITY STATEMENT

The accession number for the variant c.C1963A reported in this paper is [ClinVar]: [SCV000886483.1]. The data presented in the study is available per request from corresponding author.

ETHICS STATEMENT

The studies involving human participants were reviewed and approved by Royan Institute, Tehran, Iran. Written informed consent to participate in this study was provided by the participants' legal guardian/next of kin. The animal study was reviewed and approved by the Animal Experiments Local Ethics Committee of Izmir Biomedicine and Genome Center (IBG-AELEC). Written informed consent was obtained from the individual(s), and minor(s)' legal guardian/next of kin, for the publication of any potentially identifiable images or data included in this article.

AUTHOR CONTRIBUTIONS

MH, UB, SP, MB, and HB contributed to the conception and design of the study. SAM, NS, and MH performed bioinformatics analysis and functional analysis. MH and SP wrote the first draft of the manuscript. SJR, MT, and GO revised the manuscript. All authors contributed to the revisions and approved the submitted manuscript.

FUNDING

This work was supported by a grant from Royan Institute, Tehran, Iran and the Scientific and Technological Research Council of Turkey (TUBITAK, grant no. 217Z123). GO Lab was funded by an EMBO Installation Grant (IG 3024).

ACKNOWLEDGMENTS

The authors thank the proband and his family members for participating in this study. They also thank Izmir Biomedicine and Genome Center Vivarium-Zebrafish Core Facility and Optical Imaging Core Facility for providing zebrafish care and microscope facility support, respectively.

SUPPLEMENTARY MATERIAL

The Supplementary Material for this article can be found online at: https://www.frontiersin.org/articles/10.3389/fcvm.2022.839862/full#supplementary-material

Supplementary Figure 1 | Expression patterns of *MYH7* in different human tissues. Comparison of *MYH7* expression patterns in different tissues shows that this protein has elevated expression in skeletal and heart muscles.

Supplementary Figure 2 | Expression patterns of *myh* superfamily members during zebrafish cardiac development in 24, 48, and 72 hpf.

Supplementary Table 1 | Primer sequences for *MYH7* targeting sgRNA, scrambled control RNA, *MYH7* sequencing and RNA probes.

Supplementary Video 1 | A 5 dpf *MYH7* KO zebrafish larva with complications in heart contraction and blood flow.

Supplementary Video 2 | The *MYH7* KO zebrafish heart contraction and blood flow rate.

REFERENCES

1. Bennett CE, Freudenberger R. The current approach to diagnosis and management of left ventricular noncompaction cardiomyopathy: review of the literature. *Cardiol Res Pract.* (2016) 2016:5172308. doi: 10.1155/2016/5172308
2. Sasse-Klaassen S, Gerull B, Oechslin E, Jenni R, Thierfelder L. Isolated noncompaction of the left ventricular myocardium in the adult is an autosomal dominant disorder in the majority of patients. *Am J Med Genet A.* (2003) 119A:162–7. doi: 10.1002/ajmg.a.20075
3. Postma AV, Van Engelen K, Van De Meerakker J, Rahman T, Probst S, Baars MJ, et al. Mutations in the sarcomere gene *MYH7* in Ebstein anomaly. *Circ Cardiovasc Genet.* (2011) 4:43–50. doi: 10.1161/CIRCGENETICS.110.957985
4. Gaertner A, Klauke B, Brodehl A, Milting H. RBM20 mutations in left ventricular non-compaction cardiomyopathy. *Pediatr Investig.* (2020) 4:61–3. doi: 10.1002/ped4.12184
5. Priya R, Allanki S, Gentile A, Mansingh S, Uribe V, Maischein HM, et al. Tension heterogeneity directs form and fate to pattern the myocardial wall. *Nature.* (2020) 588:130–4. doi: 10.1038/s41586-020-2946-9
6. Vasilescu C, Ojala TH, Brilhante V, Ojanen S, Hinterding HM, Palin E, et al. Genetic basis of severe childhood-onset cardiomyopathies. *J Am Coll Cardiol.* (2018) 72:2324–38. doi: 10.1016/j.jacc.2018.08.2171
7. Van Waning JI, Caliskan K, Hoedemaekers YM, Van Spaendonck-Zwarts KY, Baas AF, Boekholdt SM, et al. Clinical features, and long-term outcome of noncompaction cardiomyopathy. *J Am Coll Cardiol.* (2018) 71:711–22. doi: 10.1016/j.jacc.2017.12.019
8. Uribe V, Ramadass R, Dogra D, Rasouli SJ, Gunawan F, Nakajima H, et al. *In vivo* analysis of cardiomyocyte proliferation during trabeculation. *Development.* (2018) 145:dev164194. doi: 10.1242/dev.164194
9. Luxan G, Casanova JC, Martinez-Poveda B, Prados B, D'amato G, Macgrogan D, et al. Mutations in the NOTCH pathway regulator MIB1 cause left ventricular noncompaction cardiomyopathy. *Nat Med.* (2013) 19:193–201. doi: 10.1038/nm.3046
10. Van Der Velden J, Stienen GJ.M. Cardiac disorders and pathophysiology of sarcomeric proteins. *Physiol Rev.* (2019) 99:381–426. doi: 10.1152/physrev.00040.2017
11. Stuart CA, Stone WL, Howell ME, Brannon MF, Hall HK, Gibson AL, et al. Myosin content of individual human muscle fibers isolated by laser capture microdissection. *Am J Physiol Cell Physiol.* (2016) 310:C381–9. doi: 10.1152/ajpcell.00317.2015
12. Soetkamp D, Gallet R, Parker SJ, Holewinski R, Venkatraman V, Peck K, et al. Myofilament phosphorylation in stem cell treated diastolic heart failure. *Circ Res.* (2021) 129:1125–40. doi: 10.1161/CIRCRESAHA.119.316311
13. Cohn R, Thakar K, Lowe A, Ladha FA, Pettinato AM, Romano R, et al. A contraction stress model of hypertrophic cardiomyopathy due to sarcomere mutations. *Stem Cell Reports.* (2019) 12:71–83. doi: 10.1016/j.stemcr.2018.11.015
14. Li H, Durbin R. Fast and accurate short read alignment with Burrows–Wheeler transform. *Bioinformatics.* (2009) 25:1754–60. doi: 10.1093/bioinformatics/btp324
15. Wang K, Li M, Hakonarson H. ANNOVAR: functional annotation of genetic variants from high-throughput sequencing data. *Nucleic Acids Res.* (2010) 38:e164. doi: 10.1093/nar/gkq603
16. Chang X, Wang K. wANNOVAR: annotating genetic variants for personal genomes via the web. *J Med Genet.* (2012) 49:433–6. doi: 10.1136/jmedgenet-2012-100918
17. Sabour D, Machado RSR, Pinto JP, Rohani S, Sahito RGA, Hescheler J, et al. Parallel genome-wide profiling of coding and non-coding RNAs to identify novel regulatory elements in embryonic and maturated heart. *Mol Ther Nucleic Acids.* (2018) 12:158–73. doi: 10.1016/j.omtn.2018.04.018
18. Pawlak M, Kedzierska KZ, Migdal M, Nahia KA, Ramilowski JA, Bugajski L, et al. Dynamics of cardiomyocyte transcriptome and chromatin landscape demarcates key events of heart development. *Genome Res.* (2019) 29:506–19. doi: 10.1101/gr.244491.118
19. Humphrey W, Dalke A, Schulten K. VMD: visual molecular dynamics. *J Mol Graphics.* (1996) 14:33–8. doi: 10.1016/0263-7855(96)00018-5
20. Phillips JC, Braun R, Wang W, Gumbart J, Tajkhorshid E, Villa E, et al. Scalable molecular dynamics with NAMD. *J Comput Chem.* (2005) 26:1781–802. doi: 10.1002/jcc.20289
21. Mackerell Jr AD, Bashford D, Bellott M, Dunbrack Jr RL, Evanseck JD, Field MJ, et al. All-atom empirical potential for molecular modeling and dynamics studies of proteins. *J Phys Chem B.* (1998) 102:3586–616. doi: 10.1021/jp973084f
22. Dominguez C, Boelens R, Bonvin AM. HADDOCK: a protein– protein docking approach based on biochemical or biophysical information. *J Am Chem Soc.* (2003) 125:1731–7. doi: 10.1021/ja026939x
23. Van Zundert G, Rodrigues J, Trellet M, Schmitz C, Kastritis P, Karaca E, et al. The HADDOCK2. 2 web server: user-friendly integrative modeling of biomolecular complexes. *J Mol Biol.* (2016) 428:720–5. doi: 10.1016/j.jmb.2015.09.014
24. Dominguez R. A common binding site for actin-binding proteins on the actin surface. In: *Actin-Monomer-Binding Proteins.* Springer (2007). pp.107–15.
25. Jowett T, Lettice L. Whole-mount in situ hybridizations on zebrafish embryos using a mixture of digoxigenin- and fluorescein-labelled probes. *Trends Genet.* (1994) 10:73–4. doi: 10.1016/0168-9525(94)90220-8
26. Ozalp O, Cark O, Azbazdar Y, Haykir B, Cucun G, Kucukaylak I, et al. Nradd acts as a negative feedback regulator of wnt/beta-catenin signaling and promotes apoptosis. *Biomolecules.* (2021) 11:100. doi: 10.3390/biom11010100
27. Thisse C, Thisse B. High-resolution in situ hybridization to whole-mount zebrafish embryos. *Nat Protoc.* (2008) 3:59–69. doi: 10.1038/nprot.2007.514
28. Kamisago M, Sharma SD, Depalma SR, Solomon S, Sharma P, Mcdonough B, et al. Mutations in sarcomere protein genes as a cause of dilated cardiomyopathy. *N Engl J Med.* (2000) 343:1688–96. doi: 10.1056/NEJM200012073432304
29. Gifford CA, Ranade SS, Samarakoon R, Salunga HT, De Soysa TY, Huang Y, et al. Oligogenic inheritance of a human heart disease involving a genetic modifier. *Science.* (2019) 364:865–70. doi: 10.1126/science.aat5056
30. Klaassen S, Probst S, Oechslin E, Gerull B, Krings G, Schuler P, et al. Mutations in sarcomere protein genes in left ventricular noncompaction. *Circulation.* (2008) 117:2893–901. doi: 10.1161/CIRCULATIONAHA.107.746164
31. Probst S, Oechslin E, Schuler P, Greutmann M, Boye P, Knirsch W, et al. Sarcomere gene mutations in isolated left ventricular noncompaction cardiomyopathy do not predict clinical phenotype. *Circ Cardiovasc Genet.* (2011) 4:367–74. doi: 10.1161/CIRCGENETICS.110.959270
32. Kolokotronis K, Kuhnisch J, Klopocki E, Dartsch J, Rost S, Huculak C, et al. Biallelic mutation in *MYH7* and MYBPC3 leads to severe cardiomyopathy with left ventricular noncompaction phenotype. *Hum Mutat.* (2019) 40:1101–111. doi: 10.1002/humu.23757
33. Tessadori F, Roessler HI, Savelberg SMC, Chocron S, Kamel SM, Duran KJ, et al. Effective CRISPR/Cas9-based nucleotide editing in zebrafish to model human genetic cardiovascular disorders. *Dis Model Mech.* (2018) 11:dmm035469. doi: 10.1242/dmm.035469
34. Varshney GK, Carrington B, Pei W, Bishop K, Chen Z, Fan C, et al. A high-throughput functional genomics workflow based on CRISPR/Cas9-mediated targeted mutagenesis in zebrafish. *Nat Protoc.* (2016) 11:2357–75. doi: 10.1038/nprot.2016.141

35. Derrick CJ, Noel ES. The ECM as a driver of heart development and repair. *Development*. (2021) 148:dev191320. doi: 10.1242/dev.191320
36. Bilan DS, Pase L, Joosen L, Gorokhovatsky AY, Ermakova YG, Gadella TW, et al. HyPer-3: a genetically encoded H(2)O(2) probe with improved performance for ratiometric and fluorescence lifetime imaging. *ACS Chem Biol*. (2013) 8:535–42. doi: 10.1021/cb300625g
37. Tobita T, Nomura S, Morita H, Ko T, Fujita T, Toko H, et al. Identification of MYLK3 mutations in familial dilated cardiomyopathy. *Sci Rep*. (2017) 7:17495. doi: 10.1038/s41598-017-17769-1
38. Mori AA, Castro LR, Bortolin RH, Bastos GM, Oliveira VF, Ferreira GM, et al. Association of variants in *MYH7*, MYBPC3 and TNNT2 with sudden cardiac death-related risk factors in Brazilian patients with hypertrophic cardiomyopathy. *Forensic Sci Int Genet*. (2021) 52:102478. doi: 10.1016/j.fsigen.2021.102478
39. Guhathakurta P, Prochniewicz E, Thomas DD. Actin-myosin interaction: structure, function and drug discovery. *Int J Mol Sci*. (2018) 19:2628. doi: 10.3390/ijms19092628
40. Yue P, Xia S, Wu G, Liu L, Zhou K, Liao H, et al. Attenuation of cardiomyocyte hypertrophy via depletion *MYH7* using CASAAV. *Cardiovasc Toxicol*. (2021) 21:255–64. doi: 10.1007/s12012-020-09617-y
41. Guo Y, Pu WT. Cardiomyocyte maturation: new phase in development. *Circ Res*. (2020) 126:1086–106. doi: 10.1161/CIRCRESAHA.119.315862
42. Nag S, Sommese RF, Ujfalusi Z, Combs A, Langer S, Sutton S, et al. Contractility parameters of human beta-cardiac myosin with the hypertrophic cardiomyopathy mutation R403Q show loss of motor function. *Sci Adv*. (2015) 1:e1500511. doi: 10.1126/sciadv.1500511
43. Sommese RF, Sung J, Nag S, Sutton S, Deacon JC, Choe E, et al. Molecular consequences of the R453C hypertrophic cardiomyopathy mutation on human beta-cardiac myosin motor function. *Proc Natl Acad Sci USA*. (2013) 110:12607–12. doi: 10.1073/pnas.1309493110
44. Geisterfer-Lowrance AA, Kass S, Tanigawa G, Vosberg H-P, Mckenna W, Seidman CE, et al. A molecular basis for familial hypertrophic cardiomyopathy: a β cardiac myosin heavy chain gene missense mutation. *Cell*. (1990) 62:999–1006. doi: 10.1016/0092-8674(90)90274-I
45. Mohiddin SA, Begley DA, Mclam E, Cardoso JP, Winkler JB, Sellers JR, et al. Utility of genetic screening in hypertrophic cardiomyopathy: prevalence and significance of novel and double (homozygous and heterozygous) beta-myosin mutations. *Genet Test*. (2003) 7:21–7. doi: 10.1089/109065703321560895
46. Van Driest SL, Jaeger MA, Ommen SR, Will ML, Gersh BJ, Tajik AJ, et al. Comprehensive analysis of the beta-myosin heavy chain gene in 389 unrelated patients with hypertrophic cardiomyopathy. *J Am Coll Cardiol*. (2004) 44:602–10. doi: 10.1016/j.jacc.2004.04.039
47. Richard P, Charron P, Carrier L, Ledeuil C, Cheav T, Pichereau C, et al. Hypertrophic cardiomyopathy: distribution of disease genes, spectrum of mutations, and implications for a molecular diagnosis strategy. *Circulation*. (2003) 107:2227–32. doi: 10.1161/01.CIR.0000066323.15244.54
48. Guhathakurta P, Prochniewicz E, Roopnarine O, Rohde JA, Thomas DD. A cardiomyopathy mutation in the myosin essential light chain alters actomyosin structure. *Biophys J*. (2017) 113:91–100. doi: 10.1016/j.bpj.2017.05.027
49. Sweeney HL, Bowman BF, Stull JT. Myosin light chain phosphorylation in vertebrate striated muscle: regulation and function. *Am J Physiol*. (1993) 264:C1085–95. doi: 10.1152/ajpcell.1993.264.5.C1085
50. Lowey S, Waller GS, Trybus KM. Skeletal muscle myosin light chains are essential for physiological speeds of shortening. *Nature*. (1993) 365:454–6. doi: 10.1038/365454a0
51. Vanburen P, Waller GS, Harris DE, Trybus KM, Warshaw DM, Lowey S. The essential light chain is required for full force production by skeletal muscle myosin. *Proc Natl Acad Sci USA*. (1994) 91:12403–7. doi: 10.1073/pnas.91.26.12403
52. Sweeney HL, Houdusse A. Structural and functional insights into the myosin motor mechanism. *Ann Rev Biophys*. (2010) 39:539–57. doi: 10.1146/annurev.biophys.050708.133751
53. Wulf SF, Ropars V, Fujita-Becker S, Oster M, Hofhaus G, Trabuco LG, et al. Force-producing ADP state of myosin bound to actin. *Proc Natl Acad Sci USA*. (2016) 113:E1844–52. doi: 10.1073/pnas.1516598113
54. Chuan P, Sivaramakrishnan S, Ashley EA, Spudich JA. Cell-intrinsic functional effects of the alpha-cardiac myosin Arg-403-Gln mutation in familial hypertrophic cardiomyopathy. *Biophys J*. (2012) 102:2782–90. doi: 10.1016/j.bpj.2012.04.049
55. Lu S, Hu M, Wang Z, Liu H, Kou Y, Lyu Z, et al. Generation and application of the zebrafish heg1 mutant as a cardiovascular disease model. *Biomolecules*. (2020) 10:1542. doi: 10.3390/biom10111542
56. Kustermann M, Manta L, Paone C, Kustermann J, Lausser L, Wiesner C, et al. Loss of the novel Vcp (valosin containing protein) interactor Washc4 interferes with autophagy-mediated proteostasis in striated muscle and leads to myopathy *in vivo*. *Autophagy*. (2018) 14:1911–27. doi: 10.1080/15548627.2018.1491491
57. Xing Y, Ichida F, Matsuoka T, Isobe T, Ikemoto Y, Higaki T, et al. Genetic analysis in patients with left ventricular noncompaction and evidence for genetic heterogeneity. *Mol Genet Metab*. (2006) 88:71–7. doi: 10.1016/j.ymgme.2005.11.009
58. Zhang W, Chen H, Qu X, Chang CP, Shou W. Molecular mechanism of ventricular trabeculation/compaction and the pathogenesis of the left ventricular noncompaction cardiomyopathy (LVNC). *Am J Med Genet C Semin Med Genet*. (2013) 163C:144–56. doi: 10.1002/ajmg.c.31369
59. Cao Q, Shen Y, Liu X, Yu X, Yuan P, Wan R, et al. Phenotype and functional analyses in a transgenic mouse model of left ventricular noncompaction caused by a DTNA mutation. *Int Heart J*. (2017) 58:939–47. doi: 10.1536/ihj.16-019
60. Shih YH, Zhang Y, Ding Y, Ross CA, Li H, Olson TM, et al. Cardiac transcriptome and dilated cardiomyopathy genes in zebrafish. *Circ Cardiovasc Genet*. (2015) 8:261–9. doi: 10.1161/CIRCGENETICS.114.000702

Conflict of Interest: The authors declare that the research was conducted in the absence of any commercial or financial relationships that could be construed as a potential conflict of interest.